MONTHLY NOTICES

OF THE

ROYAL ASTRONOMICAL SOCIETY

COES MEMORIAL LIBRARY
NEW BEDFORD, MASS.

Volume 122 No. 3 1961

OHIO STATE UNIVERSITY
JUL 3 1961
LIBRARY

Published and Sold by the

ROYAL ASTRONOMICAL SOCIETY
BURLINGTON HOUSE
LONDON, W.1

Price £1 4*s.* 0*d.* (*US* $3.50)

Subscription for volume £6 (*US* $18)

ROYAL ASTRONOMICAL SOCIETY

Subscribers to *Monthly Notices* may like to note the publication by the Society of

The Earth Today

A collection of papers dedicated to

Sir Harold Jeffreys

by some of his students and colleagues on the occasion of his 70th birthday

This is an extra volume of the Society's *Geophysical Journal* (Vol. 4), which is now made available as a special publication, comprising over 400 pp., suitably bound in cloth boards. The Geophysical Editors have obtained the co-operation of many of Sir Harold's distinguished colleagues and pupils in the preparation of this volume and they believe that it contains the most advanced work in a number of fields in which Sir Harold has long been interested.

Price £4 (US$ 12)

Orders should be sent to the Society's distributors:

Messrs. Oliver & Boyd, Ltd., Tweeddale Court, 14 High Street, Edinburgh.

SPECIAL NOTICE TO FELLOWS

Fellows of the Society may obtain *The Earth Today* at a specially reduced price of £1 10*s*. 0*d*. (US$ 4.50). It is requested that Fellows wishing to receive a copy should send their orders, with remittance, as soon as possible to:

Assistant Secretary, Royal Astronomical Society, Burlington House, London, W.1

MONTHLY NOTICES
OF THE
ROYAL ASTRONOMICAL SOCIETY
Vol. 122 No. 3

PHOTOELECTRIC MEASUREMENTS OF THE λ5250A Fe I TRIPLET AND THE *D* LINES IN G AND K STARS

R. F. Griffin

(Communicated by the Director of the Cambridge Observatories)

(Received 1960 October 20)

Summary

A new spectrometer has been used at the coudé focus of the Cambridge 36-inch reflector to measure directly the integrated intensities of features in stellar spectra. The manner in which light is fed to the photomultipliers has required careful consideration owing to the irregular distribution of sensitivity of present-day photocathodes.

The intensity of the Fe I triplet near λ5250A in G5–K5 stars is shown to be strongly dependent upon stellar luminosity, and to be related to luminosity and spectral type with little or no intrinsic spread. It therefore forms a very favourable luminosity criterion.

The *D* lines are relatively insensitive to luminosity, at least until the late K types; they vary in strength rapidly with spectral type in the K stars, but their usefulness as a criterion of spectral type is limited by the large intrinsic scatter among individual objects. The scatter is not correlated with space motions.

Introduction.—Photoelectric photometry of stellar spectra in discrete bands of the order of 50A width, isolated by a diaphragm in the focal plane of a spectrometer, has been discussed in an earlier paper (1) to which we will refer as Paper I. It is demonstrated there that such photometry permits measurements of the intensity of spectral features rapidly and with considerable accuracy. Derivation of similar quantitative information from photographic spectrograms would involve not only very much longer observation and reduction times but also much greater liability to random and systematic errors.

Provided that the bands of wavelength isolated for measurement by the spectrometer are appropriately chosen, the parameter representing the strength of the spectral feature observed may be defined uniquely in terms of the distributions with wavelength of radiation from the star's surface and from a standard lamp within the dome. The parameter is practically independent of the characteristics of the instrumental equipment, and of the absorbing media in interstellar space and within the terrestrial atmosphere (unless indeed they superimpose a line-absorption spectrum upon that of the star); and it is extremely insensitive even to the characteristics of the standard lamp.

Many photometric measurements have been made through filters, and, especially during the last decade, through interference filters. These measurements are in general dependent upon the properties of the transmitting media and of the instrumentation. The properties of the transmitting media (particularly the Earth's atmosphere) are prone to change and are beyond the observer's control; while the characteristics of the instrumental equipment also vary with time owing to the ageing of filters, reflective coatings, etc., and are difficult if not impossible

XUM

to reproduce. Therefore, although measurements can be made of some parameter related to the strength of a spectral feature by means of what we may call "filter photometry", the dependence upon irreproducible factors inherent in this method implies that each season's observations with each individual instrument require the introduction of a fresh "system". There is already a formidable accumulation of such "systems". Measurements of slightly different spectral parameters are sometimes subjected to empirical "corrections" which are supposed to interrelate the different "systems" to which the measurements refer; but every such "correction" implies an assumption regarding the characteristics of the stellar spectrum, since a measurement of one spectral parameter cannot by itself give information about another. One of the important advantages of the spectrometer method over filter photometry is that the observational results can be duplicated or extended at any time, with different equipment if desired; so that the problem of an ever-increasing burden of irrecoverable "systems" does not arise.

At the conclusion of the work presented in Paper I, a new spectrometer was designed especially for narrow-band photoelectric measurements at the coudé focus of the 36-inch reflector at the Cambridge Observatories. The earlier instrument had not been designed for this purpose but for the isolation of 200A bands. After modification, it was successfully used to measure 30–50A bands, and considerable experience of the method was gained with it. Certain disadvantages were, however, associated with this modified equipment: its limited resolution (about 3A with a wide slit) precluded accurate observations in bands less than about 30A wide; there were difficulties in maintaining its wavelength setting accurate to better than 1A; its presence at the coudé focus hampered or prevented observations in an undesirably large region of the northern sky; and its controls were more scattered in the dome than one would have wished. Also the slit was horizontal, so that atmospheric dispersion tended to spread star images across it. These shortcomings have been to some extent avoided or reduced in the new and more specialised spectrometer, which was built in the Observatories' workshop and was brought into use in 1960 May.

2. *The spectrometer.*—The coudé focus of the 36-inch reflector is above and to the north of the declination axis, and lies within the skeleton upper tube of the telescope when the latter is pointed to declinations above 74°. By keeping the dimensions of the spectrometer in the vicinity of the entrance slit small, however, and by deflecting the collimator beam downwards through 90° in the meridian plane by a quartz prism immediately behind the slit, interference of the spectrometer with the free movement of the telescope is kept to a minimum. Indeed, the Pole itself is accessible, although the optical axis of the telescope passes through the spectrometer slit at this declination.

The slit lies in the plane of the meridian so that when stars are observed at small hour angles the atmospheric dispersion is along the slit.

The collimator is a 6-inch Wildey mirror of 9 feet focus, and feeds a 6 × 8-inch Bausch and Lomb grating blazed in the first order red; the camera is a 7-inch doublet lens of focal length 103 inches. The axis of the camera beam is vertical. The principal structural elements of the spectrometer are tubes of rectangular cross-section welded from 1/8-inch steel sheet; each of the optical components is kinematically mounted upon three supports disposed in a right-angled triangle. A diagrammatic vertical section through the instrument appears in Fig. 1.

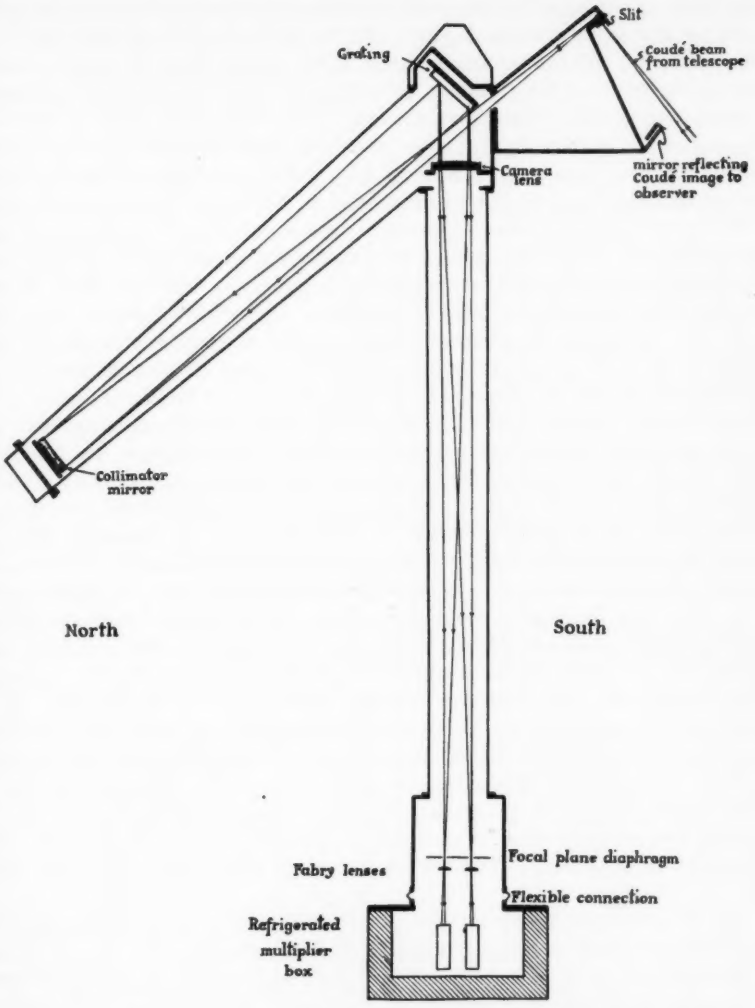

FIG. 1.—*Vertical section through the coudé spectrometer of the 36-inch Cambridge reflector.*

Focal plane assembly.—The dispersion at the focus of the spectrometer is approximately 5A/mm in the first order. The focal plane diaphragm is formed from a 10 × 1-inch metal strip and fits into a removable, kinematically located holder to facilitate changing from one programme of measurements to another. In the work described below, three bands were isolated: the central one embraced the spectral feature whose intensity was required, while the others, symmetrically spaced and of equal width, served as comparison bands. By virtue of the small spectrophotometric gradient in the green region of the spectra of G and K type stars, and the symmetrical choice of the bands, the amount of light in the two comparison regions was approximately the same; in these circumstances,

there exists the possibility (mentioned in Paper I) of measuring the comparison bands by the same photomultiplier. In the present case, an EMI type 9558 cell received the light in the two bands. Fabry images from them were made to coincide upon the photocathode by using as Fabry lenses two rectangular portions appropriately cut from a single lens. The major axis of the Fabry image upon the 9558 photomultiplier measured approximately 1 cm; the photocathode diameter is 5 cm. A 2 mm Fabry image was formed from the light in the central band upon the 9 mm cathode of an EMI type 9502 photomultiplier.

The photomultipliers are supported in a thermally insulated box well below the focal plane. The box is cooled to $-15°$C by a commerical refrigerator unit; experiments have shown that negligible further reduction in dark count is obtained by more intense cooling of the cells. The refrigerated box also houses amplifiers adjacent to the photomultipliers whose outputs they receive. Pulse-counting channels similar in principle to those used in conjunction with the earlier spectrometer are employed: the counts are read from a dekatron panel. Thanks to the efforts of Mr D. W. Beggs, however, the circuits have been greatly improved in detail since 1958, and their characteristics are completely stable despite the extraordinarily adverse microclimate of the dome. Repeated counts upon the standard lamp, whose purpose—to calibrate the overall sensitivities of the photometric channels—is fully described in Paper I, show only the fluctuations to be expected statistically from the finite count. The response is linear within the errors of measurement up to counting rates of at least 10^4/sec.

In observing bands 50A wide, it is convenient to ignore Doppler shifts due to stellar radial motions. Where much narrower bands (of the order of 5–15A) are concerned, neglect of this problem may lead to gross errors; for example, a radial velocity of 100 km/sec displaces the spectrum by 2A at λ6000A. In the spectrometer described, the whole focal plane assembly (including the Fabry lenses and photomultipliers) is kinematically constrained with one degree of freedom so that the diaphragm may be correctly sited with respect to the features of the displaced stellar spectrum. The adjustment is made by a screw and naturally has to be effected for each star individually; a knowledge of the radial velocity is presupposed. Tabular correction is made for the Earth's orbital motion.

Wavelength stability.—It is necessary to maintain the focal plane diaphragm in its nominal position (subject to radial velocity corrections) within a fraction of an Ångstrom at all times. Since periodic checks would be necessary even if the spectrometer were thermostatically controlled, and in view of the difficulty of applying such control to the present instrument, it was decided to rely entirely upon adjusting the wavelength setting as often as necessary. To monitor this adjustment, each focal plane diaphragm is provided with a glass insert upon which crossed lines are ruled in such a position that, when the spectrometer is correctly adjusted, their intersection is coincident with an emission line from a gas discharge lamp. The time interval between successive adjustments is many times longer than the counting time, which is normally 54 seconds.

Controls.—All the controls of the new equipment are grouped next to the setting console of the telescope, and the observer need leave his chair only when it is necessary to move the dome. The entrance slit of the spectrometer has reflecting jaws, and the coudé field of the telescope is re-imaged at an eyepiece

near the observer. A second eyepiece provides a view of the crossed lines in the focal plane diaphragm of the spectrometer. Corrections to the adjustment of the spectrometer are made by slow-motion controls of the attitude of the diffraction grating in both coordinates, operated via long rods fitted with universal joints. The standard lamp and gas discharge tube are presented before the entrance slit, when needed, by solenoids; and solenoid-operated filters in the collimator beam permit the flux of light from bright stars to be reduced by factors of 2 up to 2^7 to prevent the counting rate from exceeding the limit of linear photometric response.

The Fabry image test.—Although statistical reproducibility of lamp counts has been achieved, the r.m.s. errors of star counts are 50–75 per cent greater than is demanded by the count statistics. There are two possible sources of error which may affect observations of stars but not of the lamp:

(i) Indefiniteness of the bands of wavelength isolated by the spectrometer owing to the finite resolution and to errors of wavelength setting; and

(ii) Irregular sensitivity of the photomultiplier cathodes.

When, as in the programmes described below, the wavelengths of the band ends can be sited in almost featureless regions of the spectrum, the first of these possibilities is obviated. With regard to the second, the reasons why irregular photocathode sensitivity can adversely affect the accuracy of the spectrometer observations have been indicated in Paper I. In the absence of photomultipliers having spatially uniform photocathode sensitivities, one has to attempt to utilise only a portion of each cathode surface over which the sensitivity variation is small. Laboratory tests of type 9558 tubes show reasonably uniform ($\pm$ 10–20 per cent)

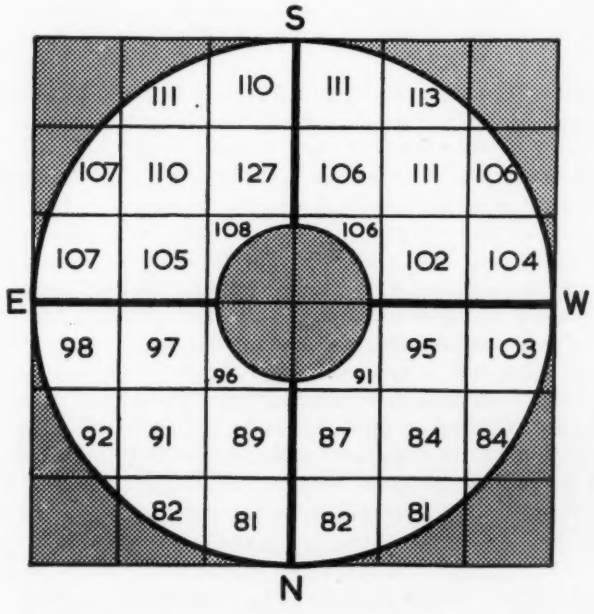

FIG. 2.—*Relative response pattern (arbitrary units), 9558: 9502 cells, during D-line programme.*

areas up to 1 cm across, although the total range of variation of the whole cathode is something like tenfold.

The uniformity of relative response of the two multipliers used in the investigations reported below, to light focussed at different parts of the Fabry images, was checked directly, with the cells *in situ*. A diffuse light source six inches square was scanned over the telescope aperture, counts being taken at each position of the source; a map of the relative sensitivities of those parts of the photocathode receiving corresponding parts of the two Fabry images was thereby built up. Fig. 2 shows such a map made during the *D*-line observations.

It is seen that, at the time the observations used in constructing Fig. 2 were made, the relative sensitivity variations reached ± 15–20 per cent; and it is to these variations that the increase of standard error of star counts over the statistically expected value is attributed. Other experiments have suggested that variations as great as ± 50 per cent (*i.e.* 3 to 1) introduce severe errors (~ 5 per cent) into star measurements. These errors have both random and systematic components, which correspond to the random and systematic components of non-uniformity in illumination of the Fabry images. The random component is due to the normal scintillation in the star image. Systematic components may be caused by allowing part of an imperfectly focussed image or of a comatic image, etc., to overlap a slit jaw.

To secure theoretical accuracy in observations of stars, uniformity of relative sensitivity between the several cathodes better than ± 5 per cent is probably necessary. With the present photomultipliers, smaller Fabry images would probably be an advantage; alternatives to the Fabry method of feeding light to the photocathodes which have so far been tried at other observatories (**2**), (**3**) do not appear very promising to the writer; but the possible alternatives have by no means been fully explored, and the subject is under active review at Cambridge.

Observations.—The observing routine described in Paper I has been retained. The wavelength setting of the spectrometer has been maintained at its nominal value, corrected for stellar radial motions, within $\pm 0{\cdot}25$A. Direct experiments with the setting purposely maladjusted showed that such an error had an undetectable effect upon the measured intensity ratios.

The Fe I *triplet near* $\lambda 5250A$.—The Fe I triplet with wavelengths 5247·1, 5250·2 and 5254·9A has been shown by Thackeray (**4**) to possess considerable sensitivity to stellar luminosity. In the programme here reported, a band 11A in width, including all three lines, was measured. Although other lines occur within this as well as within the comparison bands, in this part of the spectrum the continuum is reached or approached in numerous regions 1A or more wide in α Bootis and presumably therefore in most other stars of G and K types. The band ends were sited in such regions to avoid any errors associated with uncertainty as to the form and exact location of the instrumental cut off. The wavelengths of the bands observed were

$$\begin{aligned} A\ & 5190{\cdot}0 - 5224{\cdot}0\text{A} \\ B\ & 5245{\cdot}5 - 5256{\cdot}5\text{A} \\ C\ & 5278{\cdot}0 - 5312{\cdot}0\text{A} \end{aligned}$$

for an object without radial motion. The wavelengths quoted are correct to 0·1A. The width of the entrance slit of the spectrometer was 0·16 mm, equivalent to 0·8A in the spectrum and to 2″ of arc in the star field.

Seven hundred and eighty measurements of Fe I intensity were made on 111 stars on nine nights during the period 1960 May 16–31. The programme was chosen principally from stars of integral luminosity class and of types G5 – K5, and was designed to contain adequate representation of all luminosity classes within this range of spectral type. The results, given in Table I, are quoted as " Fe I ratios ": the ratio is defined as

$$\frac{A_S + C_S}{A_L + C_L} \Big/ \frac{B_S}{B_L}$$

where the suffices S and L refer to photometric counts from the star and lamp respectively. The ratio rises with increasing absorption in the central band; ratios less than unity imply that the absorption is more intense in the comparison regions, or possibly that the Fe lines are in emission.

TABLE I—*Fe I and D-line intensities.*

Column 1 gives the star's name; 2, the visual magnitude; 3, the spectral type; 4, the number of Fe I observations; 5, the Fe ratio; 6, Thackeray's Fe central intensity in units 100 log ΔI; 7, the number of D-line observations; 8, the D-line ratio; 9, Thackeray's D-line equivalent width in Ångstroms. The Cambridge observations were usually made in pairs.

γ^1	And	2·3	K3	II	2	1·085	15			
η	Per	3·9	K3	Ib	4	1·138	22			
α	UMa	1·9	Ko	III	8	1·045	11	6	1·176	2·3
ψ	UMa	3·1	K1	III	6	1·055	12	6	1·198	2·5
ν	UMa	3·7	K3	III	8	1·070	15	6	1·294	3·4
56	UMa	5·1	G8	II	8	1·063		6	1·163	
2	Dra	5·4	Ko	III	4	1·034				
HD	101013	6·0	Ko		11	1·038		5	1·152	
92	Leo	5·4	Ko	III	9	1·036		5	1·176	
61	UMa	5·5	G8	V	6	1·000		5	1·162	
χ	UMa	3·8	Ko	III	8	1·054	11	6	1·148	2·7
HR	4550	6·5	G8	Vp	6	0·990		6	1·101	
o	Vir	4·2	G8	III	10	1·034	8	6	1·132	2·2
HR	4668	5·1	K1	III	9	1·059		6	1·191	
16	Vir	5·1	Ko	III	10	1·076		5	1·172	
11	Com	4·9	G8	III	6	1·046		7	1·174	
5	CVn	5·0	G7	III	10	1·031		6	1·133	
γ	Com	4·6	K1	III–IV	8	1·049		6	1·271	
33	Vir	5·9	K1	IV	16	1·026		5	1·204	
31	Com	5·1	Go	III	6	1·010		7	1·104	
37	Com	5·1	K1	p	10	1·070		7	1·264	
41	Com	4·9	K5	III	7	1·074		6	1·369	
HR	4997	5·0	Ko	III	6	1·057		6	1·170	
70	Vir	5·2	G5	V	10	1·007		8	1·135	
84	Vir	5·0	K2	III	6	1·061		7	1·292	
υ	Boo	4·3	K5	III	8	1·068		4	1·433	
6	Boo	5·1	K4	III	10	1·066		4	1·277	
η	Boo	2·8	Go	IV	6	1·005		4	1·117	
4	UMi	5·0	K3	III	8	1·067		6	1·291	
α	Boo	−0·1	K2	III	10	1·049	12	6	1·147	2·4
A	Boo	4·8	K1	III	7	1·051		6	1·190	
20	Boo	5·0	K3	III	2	1·047		3	1·299	
ρ	Boo	3·8	K3	III	9	1·060	16	4	1·229	2·7

TABLE I—*continued*

5	UMi	4·4	K4	III	12	1·076		6	1·306	
HR	5464	5·9	K4	III	8	1·080		6	1·186	
31	Boo	5·0	G8	III	8	1·046		6	1·181	
32	Boo	5·6	G8	III	9	1·035		7	1·153	
ϵ^1	Boo	2·7	Ko		4	1·050	13	6	1·183	2·2:
o	Boo	4·7	Ko	III	4	1·029	9	4	1·139	2·0
ξ^1	Boo	4·6	G8	V	6	0·995	5	8	1·163	2·3
HR	5552	5·5	K4	III	12	1·065		6	1·300	
β	UMi	2·2	K4	III	13	1·060	17	6	1·274	3·4
ω	Boo	4·9	K4	III	4	1·058		4	1·392	
β	Boo	3·6	G8	II–III	2	1·038	9	4	1·135	2·0
ψ	Boo	4·7	K2	III	2	1·045		4	1·217	
δ	Boo	3·5	G8	III	6	1·028	9	6	1·126	2·7
ι	Dra	3·5	K2	III	10	1·052	12	6	1·255	3·3
θ	UMi	5·3	K5	III	8	1·118		6	1·576	
16	Ser	5·4	Ko	p	10	1·031		10	1·178	
ϕ	Boo	5·4	G8	IV	12	1·017		6	1·122	
α	Ser	2·7	K2	III	10	1·048	13	6	1·314	4·0
ρ	Ser	4·9	K5	III	8	1·066		6	1·402	
κ	CrB	4·8	Ko	III–IV	2	1·020	9	4	1·210	3·0
ϵ	CrB	4·2	K3	III	4	1·051	12	4	1·194	2·9
HR	6014	6·0	Ko	IV	12	1·008		12	1·28	
τ	CrB	4·9	Ko	III	4	1·021		4	1·192	
ξ	CrB	4·7	Ko	III	4	1·022		4	1·186	
η	Dra	2·9	G8	III	10	1·026	9	6	1·155	2·2
β	Her	2·3	G8	III	8	1·037		7	1·138	
HR	6152	5·3	G8	p	12	1·051		7	1·117	
HR	6199	5·4	K1	III	15	1·045		6	1·191	
ϵ	UMi	4·4	G5	III	6	1·036		4	1·154	
κ	Oph	3·4	K2	III	8	1·044	11	6	1·204	3·5
π	Her	3·4	K3	II	6	1·092	16	6	1·322	4·4
σ	Oph	4·4	K3	II	6	1·103		5	1·275	
β	Dra	3·0	G2	Ib	6	1·033		6	1·120	
θ	Her	4·0	K1	II	7	1·100	21	6	1·242	3·2
γ	Dra	2·4	K5	III	6	1·063	19	6	1·423	4·9
70	Oph A	4·3	Ko	V	6	0·995	7	6	1·227	4·0
HR	6791	5·1	Ko	p	12	1·040		4	1·183	
HR	6806	6·4	K2	V	7	0·984		9	1·29	
κ	Lyr	4·3	K2	III	6	1·045	12	6	1·239	3·0
108	Her	5·5	F9	Ib	6	0·986		4	1·077	
109	Her	3·9	K2	III	6	1·036	12:	4	1·205	3·4:
45	Dra	4·9	F7	Ib	6	1·001		4	1·106	
ϵ	Aql	4·2	K2	III	6	1·052		4	1·225	
λ	Lyr	5·1	K3	II	6	1·092		5	1·303	
δ	Dra	3·2	G9	III	6	1·030	9	4	1·143	1·9
θ	Lyr	4·5	Ko	II	6	1·098	16	6	1·229	3·6
κ	Cyg	4·0	Ko	III	4	1·023		5	1·148	
τ	Dra	4·6	K3	III	2	1·056				
31	Aql	5·2	G8	IV	4	1·203		4	1·180	
β	Cyg A	3·2	K1	p	2	1·045				
σ	Dra	4·8	Ko	V	4	0·984		4	1·198	
β	Sge	4·4	G8	II	6	1·066		4	1·184	

TABLE I—*continued*

γ Aql	2·8	K3	II	5	1·113	17	4	1·320	4·7
HR 7542	6·4	Go	Ib	11	1·033		9	1·16	
ϵ Dra	4·0	G8	III	2	1·030				
ρ Dra	4·7	K3	III	2	1·064				
27 Cyg	5·5	Ko	IV	4	1·025		4	1·188	
θ Del	6·1	K3	Ib	11	1·148		5	1·350	
η Cep	3·6	Ko	IV	4	1·007	7:	4	1·123	1·9
ϵ Cyg	2·6	Ko	III	6	1·036	9	4	1·145	2·4
ξ Cyg	3·9	K5	Ib	10	1·149	23	6	1·429	5·4
61 Cyg A	5·6	K5	V	8	0·959		7	1·706	
61 Cyg B	6·3	K7	V				3	1·91	
63 Cyg	4·9	K4	II	6	1·141		7	1·464	
ζ Cyg	3·4	G8	II	4	1·035	9	4	1·157	2·3
HR 8248	6·6	K1	Ib	8	1·179		5	1·464	
ϵ Peg	2·5	K2	Ib	6	1·160	22	6	1·320	4·6
9 Peg	4·5	G5	Ib	4	1·083		4	1·181	
12 Peg	5·4	Go	Ib	8	1·114		7	1·275	
HR 8374	6·2	G8	Ib	7	1·128		8	1·222	
ζ Cep	3·6	K1	Ib	6	1·160	22	4	1·313	4·0
RW Cep	var.		Iap	10	1·27		9	1·54	
β Lac	4·6	G9	III	4	1·030		4	1·125	
5 Lac	4·6	Mo	Iab	4	1·160	23	4	1·451	4·7
11 Lac	4·6	K3	III	4	1·070		4	1·216	
ι Cep	3·7	K1	III	4	1·040	12			
HR 8726	5·1	K5	Ib	8	1·178		6	1·469	
ψ And	5·1	G5	Ib	4	1·076				
ρ Cas	var		Iap	4	1·027				
WZ Cas	var	N					5	8·2	

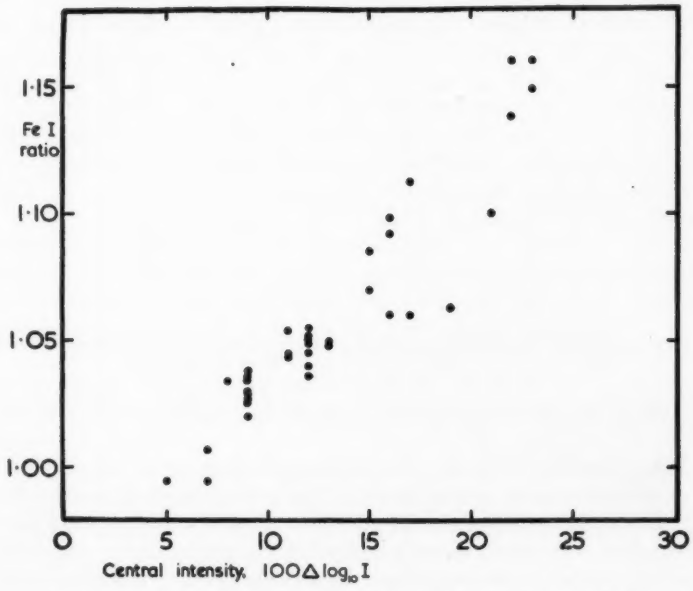

FIG. 3.—*Comparison of Fe I ratios with central intensities measured by Thackeray.*

The r.m.s. deviation of a single determination of the Fe I ratio from the mean value derived for the star to which it refers is 0·013, which corresponds to a standard error for one observation of 1·4 per cent. Although this is considerably better than was achieved in the measurements discussed in Paper I, the statistical error for all but the faintest stars in the present programme should be 1 per cent or less.

A comparison of the mean Fe I ratios given in Table I with the central intensities measured by Thackeray (4) is shown in Fig. 3.

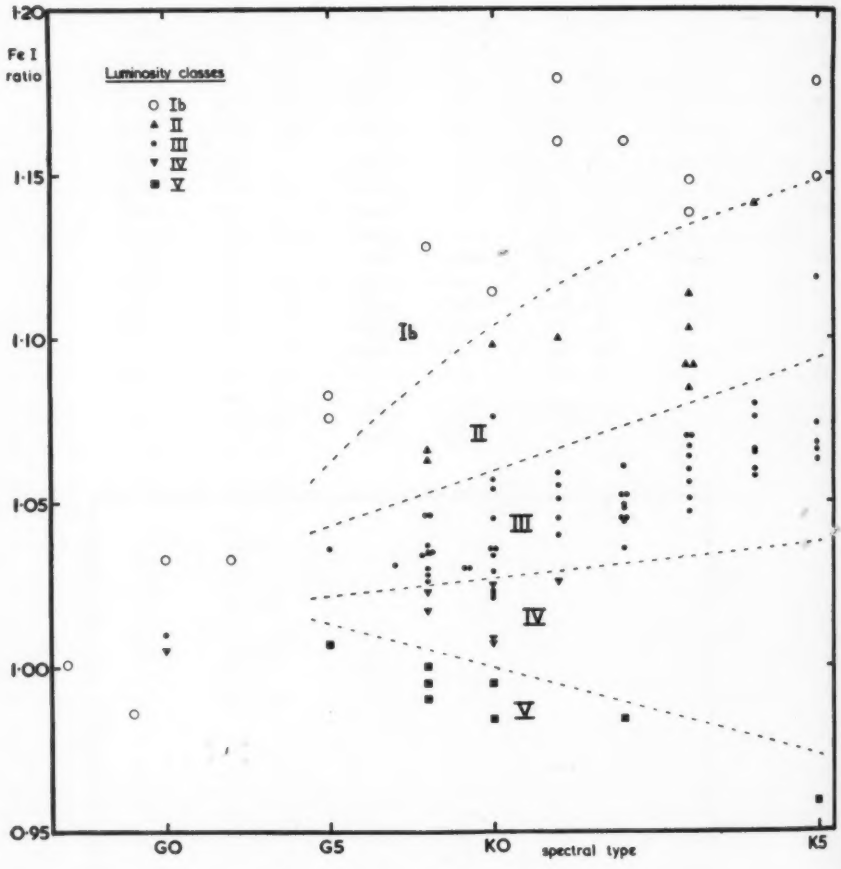

FIG. 4.—*Fe I ratios as a function of spectral type at each luminosity class.*

In Fig. 4 the Fe I ratios for the 98 programme stars of integral luminosity class are plotted against spectral type. The dotted lines are arbitrarily drawn to divide the diagram, for spectral types later than G5, into five regions which are intended to correspond to the principal luminosity classes. It is clear that, in types G5–K5, the Fe I ratio is a remarkably good criterion of luminosity. Of 92 G5–K5 stars, 86 fall in the region of the diagram appropriate to their

respective luminosities. Of the other six stars, three (the Ko III stars τ CrB, ξ CrB and κ Cyg) show only marginal discrepancies which may well be ascribed to observational error. The remaining three (16 Vir, θ UMi and ζ Cyg) exhibit definitely anomalous Fe I ratios. It is not impossible that these stars have been misclassified. The hypothesis that 16 Vir is of luminosity class II rather than III is lent support by the circumstance that, although it has been classified as a "weak-CN" star (**5**), its CN intensity is above the average for a class III star of its spectral type (**1**); while the *D*-line ratio (see below) of θ UMi is extraordinary for a class III star but plausible for class II.

If 16 Vir and θ UMi are excluded, the r.m.s. deviation of the class III stars about a mean straight line drawn through Fe I ratios of 1·040 at Ko and 1·070 at K5 is only 0·0088. This is very little greater than would be expected on account of observational errors alone. It is not possible from the presently available material to determine whether or not the small additional scatter is due to slight luminosity differences between individual stars and to errors of spectral type. There is no correlation between the "Fe I anomalies", which we may define as the deviations of Fe I ratios for individual class III stars from the mean line referred to above, and space motions; nor is there any detectable systematic differences between stars belonging to Miss Roman's so-called "strong-line" and "weak-line" divisions (**5**).

The major result of the Fe I programme is that, in stars of known spectral type between G5 and K5, the luminosity class may be determined with a certainty approaching 100 per cent by measurement of the strength of the λ 5250A triplet. The error involved in assigning absolute magnitudes on the basis of such measurements is less than is detectable using the present observations and current luminosity estimates. If another feature of the spectrum can be found whose intensity is a comparably good criterion of spectral type, it should be possible to make two-dimensional spectral classifications with exceptional speed and precision; it has been shown (**1**) that the *G* band is a suitable criterion in type G5 – K1, provided the ambiguity with late K and M stars can be resolved. Stars at least as faint as $m_V = 8{\cdot}0$ can be reached with the Cambridge equipment in a one-minute integrating time.

The D lines.—This programme was undertaken principally to discover whether the strength of the *D* lines may be used as an accurate guide to spectral type, and whether measurements of the *D* lines in conjunction with those of Fe I can reproduce MK types and luminosities without ambiguity.

A year ago T. J. Deeming made a first series of photoelectric measurements of the *D* lines in G8 – K5 stars, using the earlier spectrometer. His work is as yet incomplete and unpublished, but his preliminary conclusions were that the *D* lines are not good as criteria of spectral type or absolute luminosity, within the range of spectral types examined, and show no clear promise of being population indicators. As will be seen, Deeming's results are now fully confirmed.

The equipment and procedure used to observe the *D* lines were in all respects similar to those described for the Fe I programme, expect that the focal plane diaphragm was replaced by one which isolated the following bands:

A 5818·8 – 5850·0A
B 5885·0 – 5900·6A
C 5935·6 – 5966·8A

In nine nights' observing during the period 1960 June 1–13 inclusive, 581 observations were made of 103 stars. The *D*-line ratios for these stars, defined in an analogous manner to the Fe I ratios, are given in Table I.

Owing to the poor state of the aluminium coats of the telescope mirrors, the anticyclonic haze which persisted during most of the period of observation, and the low quantum efficiency of the type 9502 photomultiplier at λ 5900A, some difficulty was experienced in reaching stars fainter than $6^{m}{\cdot}0$. The standard error of observations on stars brighter than this limit, which numbered over 80 per cent of the total, was 1·5 per cent; for fainter stars, except WZ Cas (a carbon star with such intense *D*-line absorption that there was practically no residual light in the band measured), the standard error was 2·8 per cent.

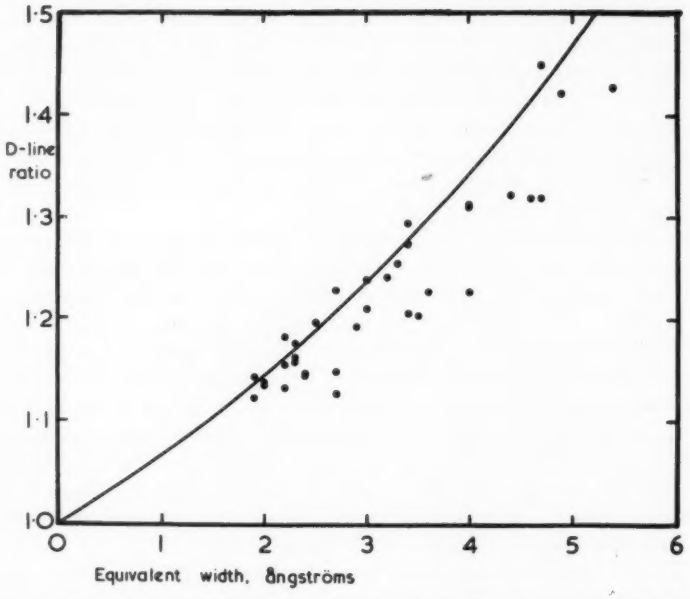

FIG. 5.—*Comparison of D-line ratios with equivalent widths measured by Thackeray.*

Fig. 5 shows a comparison of the *D*-line ratios with equivalent widths determined by Thackeray (4). In so far as the *D* lines may be regarded as constituting an isolated feature of the spectrum, a quantitative comparison between the two series of measurements is possible. Suppose that one measures an isolated feature wholly contained within the central channel observed with the spectrometer, and that an intensity ratio R is obtained. The mean light intensity within the band is $1/R$ times the mean intensity of the continuum on either side, and the mean fractional absorption is $1-1/R$. If the width of the band is A angstroms, the equivalent width W of the feature is given by

$$W = A(1-1/R)$$

The line corresponding to this equation is drawn in Fig. 5. There is a tendency for the *D*-line equivalent widths derived from the spectrometer measurements to be somewhat lower than those quoted by Thackeray. An effect of this sign would be expected if there were appreciable absorption in the comparison regions.

The *D*-line ratios of class III stars are plotted against spectral type in Fig. 6, and the other luminosity classes are shown in Fig. 7. An approximate mean line for class III is drawn on both diagrams. It is seen that the *D* lines have a minimum intensity at luminosity class III or IV, and increase both towards the dwarfs and towards the supergiants somewhat in the manner shown by Thackeray. A striking feature of the behaviour of the *D* lines is their rapid increase in intensity in late K types, especially at luminosity class V, if the two components of 61 Cyg are typical.

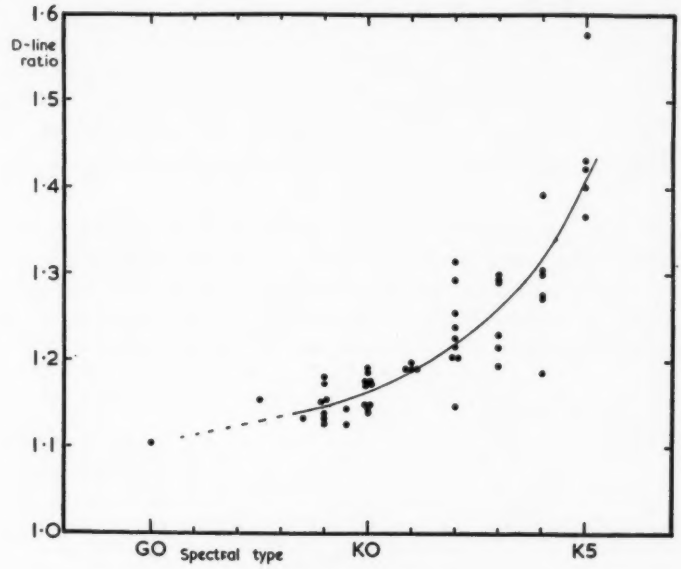

FIG. 6.—*D-line ratios as a function of spectral type for class III stars.*

It is quite clear from Figs. 6 and 7 that the strength of the *D* lines is not a very good criterion of spectral type. In G types the change of intensity with spectral type is slow, and the scatter of individual stars—even those of similar luminosities—is too great. In K types the enhanced sensitivity to spectral type is offset by a large increase in the scatter. For class III stars in the range of spectral type G7 – K1 the r.m.s. spread in *D*-line ratio is 0·017, which is much greater than the error of measurement. The sensitivity of the ratio to spectral type and luminosity is altogether too low for classification errors to contribute significantly to the spread, which is therefore to be regarded as intrinsic. The same situation exists for the K2 – K5 stars, but for these the r.m.s. scatter is as much as 0·049, even if θ UMi is omitted from consideration. The strength of the *D* lines, as of the Fe I triplet, is much greater in θ UMi than in any other star classified as a K giant.

In Fig. 8 the "*D*-line anomalies" of class III stars are plotted against space motions. It is evident that no significant correlation exists between these quantities. The difference between the mean anomalies of the " weak-line " and " strong-line " stars is $0{\cdot}0042 \pm 0{\cdot}0075$: again it is without significance.

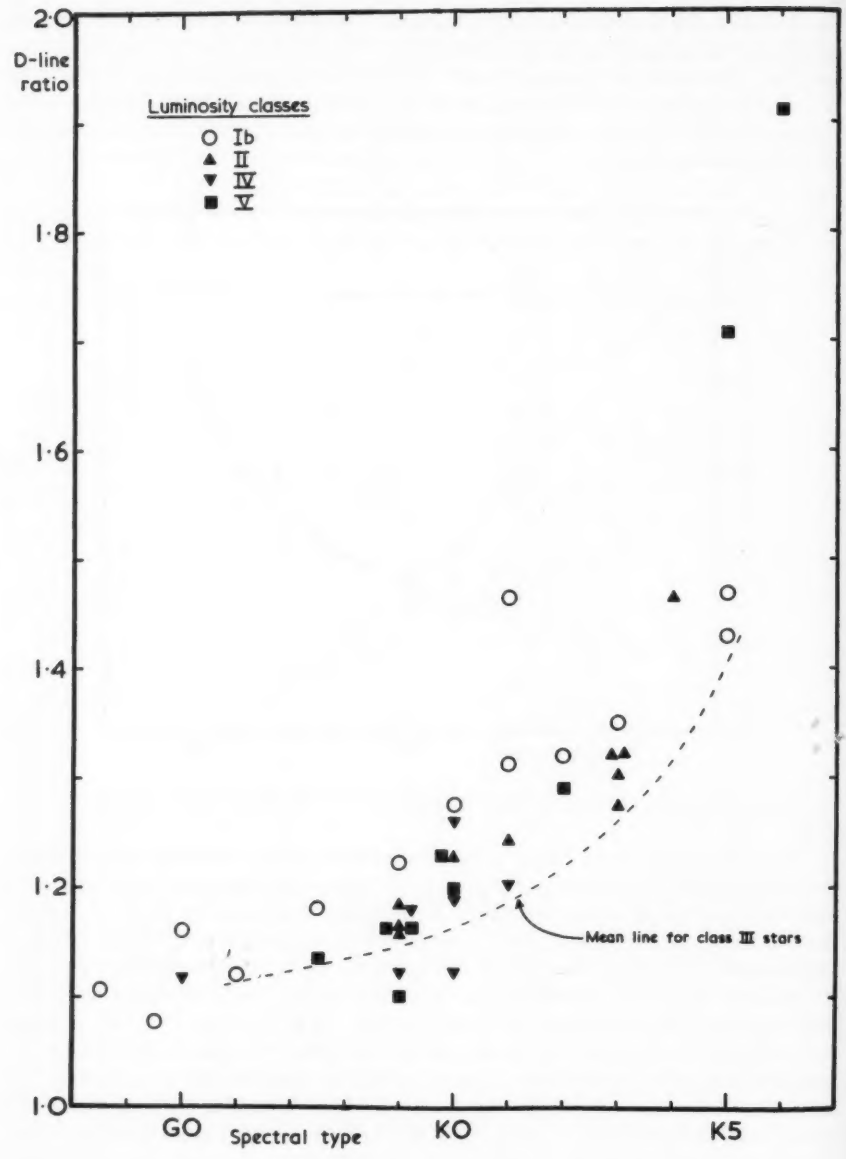

FIG. 7.—*D-line ratios as a function of spectral type at each luminosity class.*

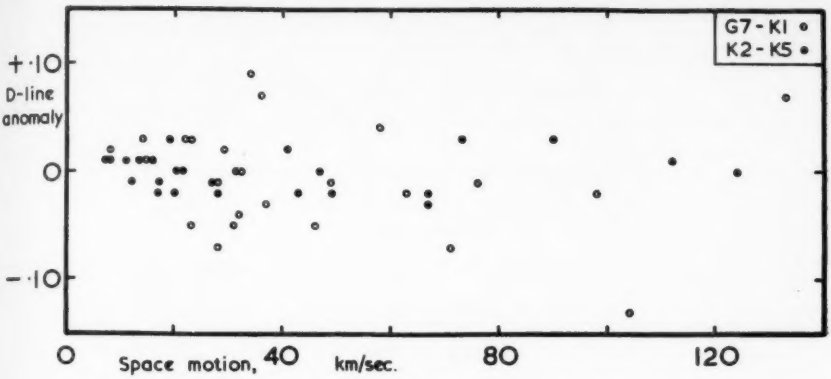

FIG. 8.—*D-line anomalies as a function of space motion for class III stars.*

Acknowledgments.—My best thanks are due to Professor R. O. Redman for his continued assistance and encouragement in this project; and to Mr D. W. Beggs for his skill in maintaining and greatly improving the electronic equipment involved. I am much indebted to the Dominion Astrophysical Observatory, Victoria, British Columbia, for the use of an excellent high-resolution spectrogram of α Bootis.

The Observatories,
Madingley Road,
Cambridge:
1960 *October* 12.

References

(1) R. F. Griffin and R. O. Redman, *M.N.*, **120**, 287, 1960.
(2) P. Guérin, *Ann. d'Astr.*, **22**, 611, 1959.
(3) J. E. Geake and W. L. Wilcock, *M.N.*, **116**, 561, 1956.
(4) A. D. Thackeray, *M.N.*, **109**, 436, 1949.
(5) N. G. Roman, *Ap. J.*, **116**, 122, 1952.

PHOTOGRAPHIC PHOTOMETRY WITH THE CAMBRIDGE SCHMIDT TELESCOPE

I. Three-Colour Survey of the Praesepe Region

A. N. Argue

(Communicated by the Director of the Cambridge Observatories)

(Received 1960 October 21)

Summary

An experimental photometric survey of the Praesepe region has been made, using W. Becker's *RGU* system. The instruments were the Cambridge 17-inch Schmidt telescope, Sartorius and Becker iris photometers, and the EDSAC I and II computers. A theoretical assessment of the performance of the telescope indicates the tolerances in various adjustments and shows that the most critical is focus adjustment, which must be maintained within $\pm 0{\cdot}05$ mm, if local field variations are to be kept below $\pm 0^{m}{\cdot}036$ pg. In certain tests, local variations, to which irregularities of the photographic emulsion also contribute, averaged $0^{m}{\cdot}050$ in *R*, $0^{m}{\cdot}007$ in *G* and $0^{m}{\cdot}020$ in *U*. Those in *R* showed strong correlation with background density of the panchromatic emulsion; those in *U* appear to be due mainly to mechanical causes, associated with the naturally smaller photographic star images in *U*. Standard errors for single measurements, for stars brighter than 11^{m}, were $0^{m}{\cdot}059$ in *R*, $0^{m}{\cdot}035$ in *G* and $0^{m}{\cdot}047$ in *U*. Near the plate limit, about 15^{m}, they were greater by a factor about 2.

Satisfactory calibration of the plates (by photoelectric measures) requires a good selection of stars with regard to colour, magnitude and position in field and it is necessary also to calibrate in spectral regions closely similar to those used in the photography. Not less than 10 stars are needed per magnitude range. These requirements are not yet met in the Praesepe region, where *UBV* magnitudes had to be supplemented by the photoelectric *R* magnitudes of Kron *et al.*, pieced out by corrections based on the Planck radiation formula.

Results beyond $14^{m}{\cdot}0$ are too uncertain for detailed discussion. In the two-colour diagrams *K* but not *G* giants were distinguishable from field dwarfs. A and F stars were prominent and the method shows promise in finding stars with ultra-violet excess. The chief limitation at present is lack of calibration stars, a defect difficult to remedy in a poor climate.

---

1. *Introduction.*—The problems in mind when this work was undertaken were:

(i) Can satisfactory accuracy be obtained in in-focus photometry with a Schmidt telescope?

(ii) Can techniques be developed which ultimately will permit handling even a moderate sample of the total amount of information on a Schmidt photograph? (The Cambridge telescope may record 10^{5} star images in a half-hour exposure on a Milky Way field).

XUM

(iii) Does W. Becker's three-colour *RGU* system permit one to distinguish satisfactorily between class III and class V stars of spectral types G and K?

Measurements were made on nearly 1000 stars situated within a rectangular area extending over 80′ in RA and 90′ in declination and centred on the Praesepe cluster. Observations were made in three colours as near as practicable to those of the Becker *RGU* system (**13**). Nine plates were used for *R*, six for *G* and eight for *U*, and altogether about 20 000 images were measured. The limiting magnitude is about $G = 16^{m}$ but the survey is complete only to $G = 15^{m}{\cdot}0$.

The general conclusions are:

(i) Provided certain necessary precautions are observed, the photometric accuracy given by Schmidt star images is about the same as that given by a refractor. With the Schmidt telescope there is, however, a substantial increase in random error, up to about $0^{m}{\cdot}1$ r.m.s., as one approaches the plate limit, primarily owing to the diminishing number of photographic grains in the image. It is important to note that the limiting magnitude of the Schmidt is fainter than that of the refractor because of this same property, the smaller image diameter. The effect of image diameter on random errors is demonstrated very clearly in Haffner's comparison of the large and small Schmidt telescopes at Hamburg (**2**). The faint threshold magnitude combined with wide field isoplanatism should make the Schmidt telescope a very powerful instrument in photometric survey work. In the present study no attempt has been made to examine the performance of the telescope over its entire field of diameter 5°, but rather to examine intensively a small number of sample regions almost to the limit of the plates.

(ii) A first step towards mechanization has been taken by punching the Becker photometer readings directly on to paper tape in a form suitable for reduction by digital computer, and a substantial economy in labour can be achieved. This apparatus has been described elsewhere (**4**). It was only ready in time for the last three plates of this programme. The remaining plates were measured on a Sartorius photometer, the settings of which were written down and later punched on tape for reduction by the computer.

(iii) The *RGU* system permits one to segregate some, but not all, class III stars of late type from class V.

A further point to be examined was in connection with establishing scales in *R* and *G*. Photoelectric calibrations were not available and it was considered impracticable to provide them in view of past experience of sky conditions at Cambridge. On the other hand *UBV* magnitudes are available in the Praesepe region and in some other areas too, and part of this work was to examine the possibility of transforming from this system to *R* and *G*. In passing we may note that a similar problem arises in the National Geographic–Palomar Sky Survey in which the *E* plates are similar in colour system to *R*.

Praesepe was a convenient choice because, as well as *UBV* magnitudes by Johnson (**5**), there are available proper motions by Klein Wassink (**6**) and a spectrophotometric survey by Ramberg (**7**). This last has been of particular value in identifying 24 G and K giants in the general field, to test the *RGU* system. Field stars are more suitable for this purpose than cluster members. Apart from their small numbers and narrow selection, the cluster giants are 5^{m}

brighter than the dwarfs, making their comparison sensitive to photographic scale errors.

The region is situated in Hubble's region of normal distribution and may be almost completely free from interstellar absorption. The galactic latitude (old) is 34°, almost in the anticentral direction. The total absorption given by the Oort cosecant formula (**8**) is $A_v = 0^m{\cdot}42$ but Johnson (**5**) has found A_v to be very low in front of and within the cluster, and it probably does not exceed $0^m{\cdot}045$ according to Sandage and Eggen (**9**). We assume that there is negligible absorption beyond the cluster, which is itself over 100 pc away from the galactic plane.

2. *Optical considerations.*—The Cambridge Schmidt telescope has been described elsewhere (**1, 10**). It is a 17/24-inch classical Schmidt, with focal ratio $f/3{\cdot}8$ and plate scale 8μ per second or arc. The circular plates cover a 5° diameter field, of which 3°·3 is unvignetted. These are cut from thin (1 mm) glass and are deformed by the plateholder to coincide with the Petzval surface. An objective grating spectrogram, for which I am grateful to Mr I. G. van Breda, shows that the transmission cut-off in the ultra-violet is at about λ 3500 A.

As is well known, a Schmidt telescope shows out-of-focus ghost images of bright stars, situated symmetrically and equidistant in the field opposite the parent star. The ghosts are caused by reflection of the original image from the photographic emulsion by way of the mirror, back to the corrector and thence back again to the focal surface. In this telescope the ghost intensity is reduced by making the corrector a mensicus, convex to the mirror, to spread out the ghost image, and by blooming both corrector surfaces. The figuring is on the rear surface of the corrector plate.

Another drawback of a Schmidt telescope, when used quantitatively, is that different parts of the star field use different parts of the telescope mirror. Two factors are involved: the mechanical and thermal stability of the mirror disk and the reflectivity of its surface. With regard to the first, the mirror is of Pilkington low expansion glass. It is supported around its edge by six counterbalance levers acting on a band surrounding the disk, and located by two fixed stops and a spring plunger. The back is supported by 18 fluon disks dynamically mounted. The reflectivity was measured photoelectrically and found uniform to ±1 per cent two years after realuminizing. On this point it may be noted that a Schmidt mirror is much more easily kept in good condition than the mirror of an ordinary reflector, because of the closed tube.

The plateholder is supported by four fins, ridged so as to give constant obstruction over the field. The system of ties attaching the fins to the telescope tube permit a small axial displacement, allowing the distance of plateholder from mirror to be controlled by four brass–invar compensators. For slow changes of temperature this compensation has been found accurate to within ±0·025 mm.

For an image situated on the principal axis of the corrector the spherical aberration of the mirror is corrected and the image is error-free. For an off-axis image the rays traverse the corrector obliquely, introducing a small amount of lateral spherical aberration and higher astigmatism into the image (**11**). The resulting radial image spread is approximately:

$$\pm 0{\cdot}021 \left(\frac{D}{f}\right)^3 \sin^2\phi \text{ radians} \qquad (1)$$

where ϕ is the angular off-axis distance. The maximum value of (1) is at the edge of the field ($\phi = 2^\circ{\cdot}5$), where substituting $D/f = 1/3{\cdot}8$, we obtain $\pm 0''{\cdot}15$ or $\pm 1{\cdot}2\,\mu$.

The corrector is not achromatic; it gives overcorrection in the ultra-violet and undercorrection in the infra-red. The spherochromatic aberration spread at a given wave-length is:

$$\pm \frac{1}{64}\frac{\Delta n}{n-1}\left(\frac{D}{f}\right)^3 \quad \text{radians} \tag{2}$$

where n is the refractive index of the corrector at the wave-length where correction is complete, and $n+\Delta n$ the value at any other given wave-length. For example if the corrector be figured for λ4861 A(F), the spread given by (2) for λ6563 A(C) is $\pm 1{\cdot}9\,\mu$, assuming

$$\frac{n_F - n_C}{n_F - 1} = \frac{1}{60}.$$

The total spread due to (1) and (2) together is small compared with the combined seeing and photographic turbidity spreads, the minimum image diameter being about $25\,\mu$ for the usual astro emulsion. On this basis the whole field of a correctly adjusted Schmidt telescope may be regarded as isoplanatic. These results are well known, expressions (1) and (2) following directly from the treatment in E. H. Linfoot's *Recent Advances in Optics* (**11**).

We should consider also the question of maladjustment of the corrector. There are three adjustments: lateral, axial and tilt, and we shall estimate the accuracy with which these must be maintained for in-focus photometry. A general treatment of effects of decentring on plate–mirror systems has been given by Linfoot (**12**). Expressions (3) and (4) below were derived using the optical aberration function (**11**) and, like (1) and (2), are for geometric image spreads and refer to the colour optimized case ($r_0 = \sqrt{3}/2$).

(i) Lateral maladjustment introduces (to third-order approximation) coma, uniform over the field and of amount:

$$\frac{3}{32}\left(\frac{D}{f}\right)^2 \Delta l \tag{3}$$

where Δl is the lateral displacement of the centre of the corrector from the centre of curvature of the mirror. Because of flexure, Δl is a function of zenith distance. With the telescope tube horizontal $\Delta l = 0{\cdot}4$ mm and the coma spread given by (3) is $2{\cdot}6\,\mu$. This is a maximum Δl, not attained in practice, so that the coma spread from this cause is negligible.

(ii) Axial maladjustment introduces secondary spherical aberration spread:

$$\pm \frac{9}{2^{14}}\left(\frac{D}{f}\right)^5 \Delta z \tag{4}$$

where Δz is the distance between the centre of the corrector and the centre of curvature of the mirror, measured along the principal axis of the corrector. For $\Delta z = 1$ cm, a higher value than is likely to be attained, the spread is $\pm 0{\cdot}01\,\mu$ which is quite negligible. The off-axis coma spread is

$$\frac{3}{32}\left(\frac{D}{f}\right)^2 \tan\phi\,\Delta z,$$

or $2{\cdot}8\,\mu$ at the edge of the field for $\Delta z = 1$ cm.

(iii) The effect of an error in tilt of the corrector follows from (1). For example an error of 1° causes an increase in ϕ from $2\frac{1}{2}°$ to $3\frac{1}{2}°$ at a certain point at the edge of the working field, and the spread given by (1) increases from $\pm 1{\cdot}2\,\mu$ to $\pm 2{\cdot}3\,\mu$. However an error of this magnitude is inconceivable. The tilt may be adjusted using the ghost images referred to above. The principal axis of the corrector intersects the photographic emulsion surface midway between an in-focus image and its ghost, and this point of intersection may be brought into coincidence with the centre of the photographic plate to $\pm 0°{\cdot}1$. The maximum off-axis image spread is then $\pm 1{\cdot}3\,\mu$ by (1).

Given proper care, none of the effects so far considered, taken alone, is likely to be of any serious practical importance. On the other hand an error of 0·025 mm in focus setting causes an increase in geometric image spread of $\pm 3{\cdot}3\,\mu$. Tests have shown that the error in measured magnitude for focus shift Δf is approximately:

$$m = \alpha(\Delta f)^2. \qquad (5)$$

For *pg* magnitudes the error is $0^m{\cdot}018$ for $\Delta f = 0{\cdot}025$ mm (**10**). In the present programme each plate contains only one exposure, so that a small error in focus which is uniform over the measured region would affect programme and calibration stars alike, and have no systematic effect on the photometry. It would, however, make a measurement more sensitive to local, accidental variation in emulsion profile or filter thickness as can be seen from (5). Experience has shown that such variations do not normally exceed $\pm 0{\cdot}013$ mm, except within 1 cm of the edge of the plate, a region which the measurer usually avoids. Apart from this, the effect of a shift in mean focus, in either direction, of 0·050 mm combined with local variations of $\pm 0{\cdot}013$ mm will be to give, by (5), magnitude variations of $\pm 0^m{\cdot}036$ in *pg*. Now a focus shift of 0·013 mm gives rise approximately to a change in image spread of $\pm 2\mu$ and this is comparable to the off-axis spreads arising from lateral spherical aberration and higher astigmatism (1) and from coma due to the filter (to be described). If the magnitude effect of any given spread is equal to that for a focus shift giving the same spread, at any rate to a rough approximation, it follows from (5) that the off-axis aberrations may become perceptible, of order a few hundredths of a magnitude, in presence of an overall focus shift of 0·050 mm. The general conclusion is that the mean focus should be maintained to better than $\pm 0{\cdot}050$ mm. This tolerance may be slightly less stringent in *RGU* photometry (**10**). As we have seen, there is adequate correction for temperature changes, provided these are slow.

The effect of tilting the plateholder may be examined using (5). The plateholder is designed to hold the photographic emulsion on a sphere concentric with the telescope mirror. Tests have shown that on turning the telescope tube from zenith to horizontal the two centres separate laterally by 0·1 mm. Supposing correct focus to be maintained at the centre of the field, the greatest photometric error at the edge of the field would be less than $0^m{\cdot}001$ which is quite negligible. If the centre is out of focus by 0·050 mm on the other hand, the edge effect is $0^m{\cdot}011$ relative to the centre, by (5). The effect of mechanical elongation of the images in long exposure will be considered further below, in Section 6.

Lastly we may consider the filters used for the *RGU* work. These are of optical glass, plane parallel and mounted just in front of the emulsion surface.

When the principal ray is normal to the filter ($\phi = 0$) the circle of least confusion has diameter:

$$d = \frac{t}{32n}\left(1 - \frac{1}{n^2}\right)\left(\frac{D}{f}\right)^3 \qquad (6)$$

where t and n are the filter thickness and refractive index respectively. The greatest t is 3 mm, so that the maximum d is $0{\cdot}6\,\mu$. At the edge of the field the principle ray passes obliquely through the filter, introducing comatic spread of about $1{\cdot}6\,\mu$.

Vignetting in this telescope begins at field diameter $2\phi = 3^\circ{\cdot}3$ and increases to $0^m{\cdot}14$ at the edge of the field. In this paper we shall be concerned only with the unvignetted region, and the magnitude effect given by (1) is below $0^m{\cdot}006$ for focus tolerance $\pm 0{\cdot}025$ mm.

The most dangerous situation appears to be when an attempt is made to compare two fields widely separated in the sky, when the effects of telescope flexure are important. However, the errors likely to be introduced are much below those expected from variations in sky transparency or seeing.

3. *Observations.*—The following plate/filter combinations were used:

R: Kodak OaE/Chance OR1 3 mm ($\lambda\lambda$ 6100–6700 A);
G: Ilford Zenith/Chance OY8 3 mm ($\lambda\lambda$ 4400–5200 A);
U: Ilford Zenith/Schott UG2 1 mm ($\lambda\lambda$ 3500–3900 A).

These are similar to but, for *R* and *G*, not identical with W. Becker's system (**13**).

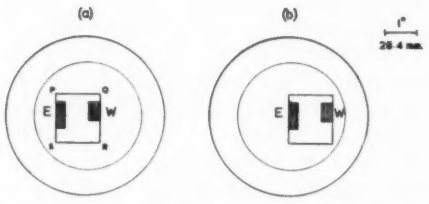

FIG. 1.—*Location of measured region (PQRS) on plates. The outer circle denotes the edge of the field ($\phi = 2^\circ{\cdot}5$). Vignetting occurs between inner and outer circles ($\phi \geqslant 1^\circ{\cdot}7$).*

Twenty plates were selected from the 1957 observations and three from 1959. Each plate consisted of a single exposure, the time varying from 5 to 30 minutes for *R* and *G*, and from 5 to 60 minutes for *U*. On about half the plates the measured region was situated almost centrally (*PQRS* in Fig. 1 (*a*)). On the remainder it was displaced westerly more nearly to the edge of the unvignetted field (Fig. 1 (*b*)). For most plates the hour angle at mid-exposure was less than one hour, but for one *G* and one *R* plate it was as much as two hours which is regarded as undesirably large. Eight plates were accepted for which the sky transparency was low although not visibly patchy. Since these were of long exposure it is hoped that no serious error was introduced. In the climate of Cambridge the setting of much tighter tolerances with regard to either hour angle or transparency would have slowed down the programme considerably.

Kodak D19b developer was used with continuous brushing, followed immediately by an acetic acid stop bath.

For measurement the stars were identified from a marked chart divided into twenty strips covering each 4′ in declination. Measurement proceeded systematically along each strip but in opposite directions for alternate strips, and with the strips taken in random order. In addition fourteen stars were repeatedly measured throughout the runs, sometimes twenty times per plate, for drift control. Both photometers showed some systematic drift apparently originating mainly in changes in room temperature, with contribution from heat from the main lamp and, for the Sartorius, from the chopper motor.

The earliest measurements, from the Sartorius photometer, were subsequently punched on paper tape, and for convenience the drift corrections were applied by hand at that stage, although they could have been made by the digital computer at the cost of a slightly more elaborate programme. Corrections were normally small, $<0^{m}\cdot03$, and independent of stellar brightness.

The consistency of measurement was examined by repeating an *R* plate, where the centring error is larger than in *G* or *U* on account of coarser photographic grain. Down to 14^{m}, 2^{m} above the plate limit, the standard deviation was $0^{m}\cdot017$ increasing slightly towards the limit. This figure is small compared with the standard error of a single magnitude measurement (Section 6). The effect of photometer drift had been corrected. The comparison beam of the photometer had been adjusted to optimize the signal-to-noise ratio as described elsewhere (**10**).

4. *Reduction.*—The process of reduction of the photometer readings to magnitudes is essentially analogous to constructing a smooth curve from the calibration data and reading off the unknown stars. The first reductions were of the *U* measurements, using the EDSAC 1 computer at the Cambridge University Mathematical Laboratory. This machine was within a few months of the end of its existence and the reduction programme was made as simple as possible. It consisted of second-order interpolation by Neville's method, using tabular values read from a hand plot of iris settings against photoelectric *U* magnitudes. I am grateful to Mr H. P. F. Swinnerton-Dyer of the University Mathematical Laboratory for writing this programme.

When EDSAC 2 came into use the programme was reorganized to eliminate hand preparation, with the trivial exception of drift correction. Essentially the method followed standard practice in data-fitting with digital computers. Iris setting θ and star magnitude m are related by an interpolation formula of the form:

$$m_l(\theta) = a_0 + a_1\theta + a_2\theta^2 + \ldots + a_l\theta^l \qquad (7)$$

where the coefficients a_i are fitted to the calibration data by least squares. The solution involved expressing (7) as an expansion in orthogonal polynomials, generated by the recurrence relationships given by Forsythe (**14**). This was employed in preference to the classical solution where the normal equations are ill-conditioned and lead to a rapid accumulation of machine rounding error with increasing l, culminating ultimately in complete failure of the solution usually, in practice, around $l=10$ (**14**).

In applying the Gauss–Markoff theorem to the estimation of the a_i's, a necessary condition is that θ be known with negligible inaccuracy and the observational error concentrated in m. Violation of this condition results in biased estimates

of the coefficients a_i (**15**) because the errors in θ are carried into the normal equations through the sums of their even powers, and distort the solution. In the present case the standard stars have catalogue errors, and the standard magnitudes in general are likely to be on a colour system differing somewhat from the natural instrumental system in which the measures were actually made. There must inevitably be accidental errors in θ, from errors of the photometer and photographic granularity. In fact the errors in θ and m are of the same order of magnitude, and the instrumental magnitudes derived from (7) will thus be subject to bias. An empirical study of this was made by carrying out reductions on synthetic data with known scatter in both variables. The data were obtained using a subroutine in the EDSAC library for generating random normal deviates. It was concluded that the effect under normal conditions is of order $\pm 0^{m}{\cdot}01$ and is not serious in photographic photometry. This is confirmed by comparison between observed and catalogue magnitudes (Figs. 2, 4 and 5), where any systematic effect exceeding $\pm 0^{m}{\cdot}01$ would have shown up. These comparisons, subdivided into magnitude classes, may be used to correct for bias (to a first approximation) as well as for colour equation.

Biased estimates cannot be avoided simply by increasing the number of calibration stars, however many are added (**15**). When the scatter in θ is large there may be an advantage in averaging θ for each star over a number of similar plates and using a mean calibration. For the present programme however a separate calibration for each plate was preferable since we wish, firstly, to examine local variations among the plates. In comparing the two regions of a given plate in which the stars measured have nearly the same mean brightness, the bias tends to cancel. This situation holds for Figs. 8 and 9 below. Secondly, in comparing classes III and V of comparable brightness the effect of bias is again very small (Fig. 11 (*a*)).

TABLE I

Comparison of machine with graphically determined magnitudes for one plate. Number of calibration points $N=119$.

Iris	Magnitude (graphical)	Δm (machine *minus* graphical) $l=3$	4	6	8	12
56	13·90	0·01:	0·06:	0·01:	−0·05:	0·07:
60	12·97	0·10	0·04	−0·06	−0·05	−0·04
64	12·23	0·07	0·00	−0·01	0·04	0·03
68	11·63	−0·03	−0·06	0·01	0·01	0·00
72	11·02	−0·04	−0·04	0·03	−0·01	0·00
76	10·44	−0·07	−0·01	0·01	−0·01	−0·01
80	9·87	−0·05	0·04	−0·01	0·00	0.00
84	9·33	−0·02	0·05	−0·03	0·01	0·01
88	8·82	0·00	0·03	−0·03	0·00	−0·01
92	8·31	0·05	0·01	0·01	0·00	−0·01
96	7·85	0·05	−0·04	0·02	−0·02	−0·01
100	7·40	0·05	−0·08	0·02	−0·01	0·01
104	6·99	0·00	−0·09	−0·03	0·00	−0·02
108	6·57	−0·04	0·01	−0·03	0·00	0·01

Results obtained from an expression of the form (7) are compared with a graphical reduction in Table I. Iris settings and graphically derived magnitudes are in the first two columns. Succeeding columns give differences (machine

minus graphical magnitude) for $l=3, \ldots 12$. There were 119 calibration points but only one was below $\theta=56$, so that differences in the first row are uncertain. Otherwise the results for $l \geqslant 6$ are satisfactory, and even for 3 and 4 are fair.

TABLE II

Mean square residual and variance for one plate $N=144$

l	1	2	3	4
S_l/N (mag.^{2})	0·247	0·0101	0·00642	0·00639
$S_l/(N-l-1)$	0·250	0·0103	0·00632	0·00662
l	5	6	7	8
S_l/N (mag.^{2})	0·00600	0·00524	0·00504	0·00501
$S_l/(N-l-1)$	0·00626	0·00551	0·00534	0·00534

It is not intended to imply that graphical reduction represents some ideal or "best fit" which the computer programme ought to reproduce. A criterion of goodness of fit is given by the mean square residual:

$$\frac{S_l}{N} = \frac{1}{N}\sum_{i=1}^{N} \{m_i - m_l(\theta_i)\}^2 \qquad (8)$$

where summation is over N calibration points. For illustration, values of S/N for another plate with $N=144$ are given in Table II for $l \leqslant 8$. The last row gives the variance $S_l/(N-l-1)$ which is seen to decrease rather slowly for $l \geqslant 3$. This raises the question of what is the best choice of l for such work as this. The S_r $(r=0, \ldots l)$ are generated by a very simple recurrence relationship, so that, as Forsythe (**14**) has pointed out, a routine which is economical in computer time may be devised for increasing l until the variance shows no further significant decrease. (This has no counterpart in the classical solution.) In our existing routines however where all data for a given observing programme are reduced in a single run (up to 20 plates) we have taken the simpler course of fixing l in advance. The 1957 plates were reduced using $l=8$, the 1959 with $l=4$. No systematic difference was found between the two. A higher l gives better interpolation in the sense of lower variance, but at higher cost in machine time. Lower values of l favour extrapolation beyond the range of calibration. There is no point in seeking greater refinement than is demanded by the precision of the measurements; in most cases it should be sufficient to take $l=4$.

5. *Calibration.*—The general opinion today is that all photographic stellar photometry should be based on standard stars set up by photoelectric photometry. Despite all the publicity given to photoelectric photometry during the past 15 years there are remarkably few areas of the northern sky where photoelectric measurements in three colours and really suitable for this purpose are available down to, say, 16^m. One of the reasons why the Praesepe region was chosen for this work is that photoelectric measurements by H. L. Johnson (**5**) on the *UBV* system are available, mainly for cluster members. Of these, the photoelectric U magnitudes have colour properties close to those of the corresponding photographic U magnitudes, and can be used for calibration immediately. But the photoelectric B and V systems are too dissimilar to the photographic G and R

systems to permit this. In attempting to evade this difficulty, the photoelectric R measurements of Kron, Gascoigne and White have been used, as described below.

Although photoelectric U and our photographic U magnitudes are similar in their colour characteristics, they are not identical. Differences must be expected, particularly in the short-wave region of the spectrum band used, arising from differences in light receiver, in the climates, and in the telescopes. However, luminosity effects are not conspicuous, perhaps because we are not dealing with stars covering a wide range of intrinsic brightness. Fig. 2 shows $U_{pg}-U_{pe}$ plotted against $(U-G)$ for different ranges of apparent magnitude. Different symbols are used for cluster members, field stars, metallic line stars, etc.

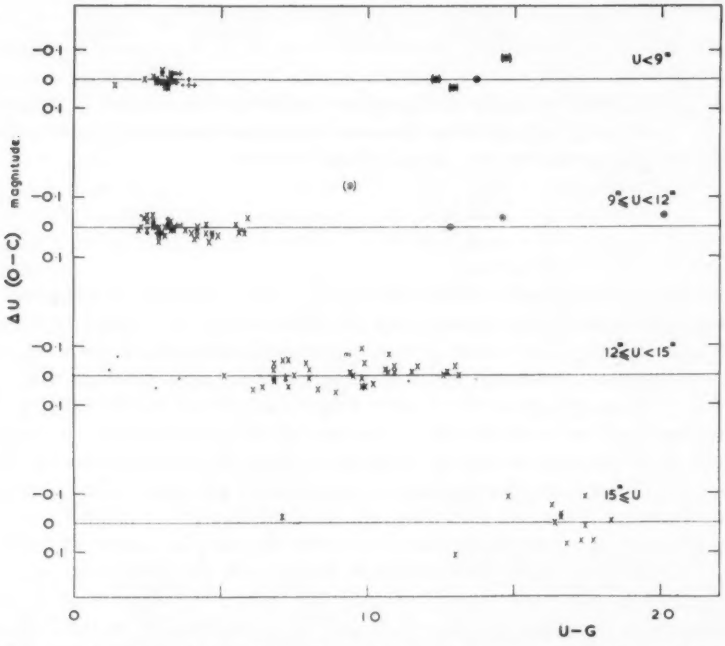

FIG. 2.—*Comparison of pg. with pe. U magnitudes. Means for all eight plates for* $U<14^{m}$, *otherwise for four* 1^{h} *exposures. Diagonal crosses represent cluster members, circled for giants; dots: field dwarfs; circles and dots: field giants. Upright crosses: metallic line stars. Diagonal crosses with vertical bar: suspected subdwarfs* (**5**). *Brackets indicate unsatisfactory measurement, usually due to disturbance from neighbouring image.*

Despite a relatively lavish supply of standard stars there are not enough for an ideal transformation between U_{pg} and U_{pe} systems. For example, there is only one standard star with $(U-G)<1^{m}\cdot0$ and fainter than $U=15^{m}$, although a large number of programme stars falls in this region (cf. Fig. 11 (*d*)). This is a well-known difficulty when the standard stars are members of one cluster. Brighter than $U=15^{m}$, however, the U_{pg} scale is unlikely to deviate from U_{pe} by more than $\pm0^{m}\cdot05$ for main sequence and giant stars. In the subsequent discussion we use the U_{pg} magnitudes as they stand, believing they are on the U_{pe} scale within the limits just quoted.

We cannot apply the same straightforward procedure to G and R because these are too dissimilar to B and V. The B scale response extends from λ 3900 to 5500 A with equivalent wave-length about 4300 A. The V scale extends from 4900 to 6500 A with equivalent wave-length about 5500 A. Comparing these with G and R in Section 3 we find G about midway (in $1/\lambda$) between B and V, and V about midway between R and G. To establish a Pogson scale in R from B and V involves therefore extrapolation over a large interval of $1/\lambda$, and would require *either* (i) detailed knowledge of the spectral distribution of a sufficient number of calibration stars over the ranges B, V and R together with the overall wave-length response of the photometers in these ranges, or (ii) a sufficient number of calibration stars of about the same spectral distribution but extending over the whole interval of calibration magnitude. Neither of these requirements is fulfilled. We can, however, make a close approximation to a Pogson scale by transforming B, V to the photoelectric R scale of Kron *et al.* (**17**) in the following way.

A selection of stars in the solar neighbourhood has been measured for R by Kron, Gascoigne and White (**18**), and in B, V by Johnson and Morgan (**19**) or Johnson and Harris (**20**). From these observations we obtain for each luminosity class, the relationship between $R_{\text{Kron}}-V$ and $B-V$. These are plotted in Fig. 3. With these relationships the B, V observations in Praesepe were transformed to R_{Kron} and then used as calibration for the R plates. The resulting magnitudes are compared with R_{Kron} in Fig. 4 (*a*). For $R<12^{\text{m}}\cdot4$ there is fair agreement, but fainter than this the indications are that the

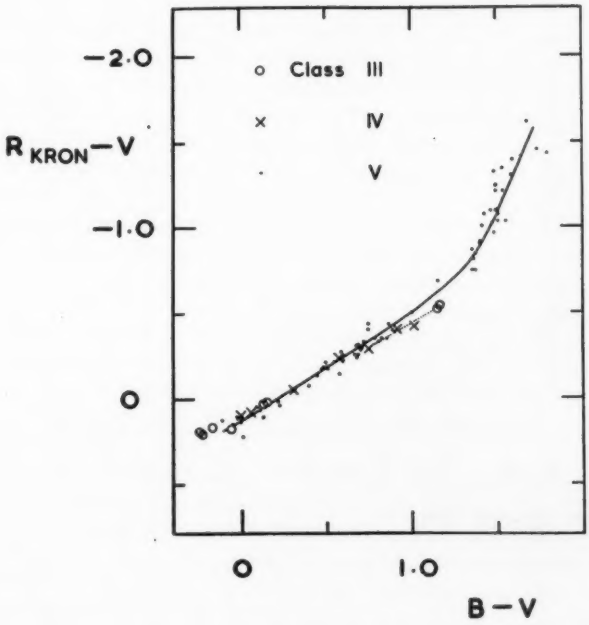

FIG. 3.—*Relationship between $R_{\text{Kron}}-V$ and $B-V$ based on R_{Kron} measured by Kron, Gascoigne and White* (**18**), *and B, V by Johnson, Morgan and Harris* (**19, 20**).

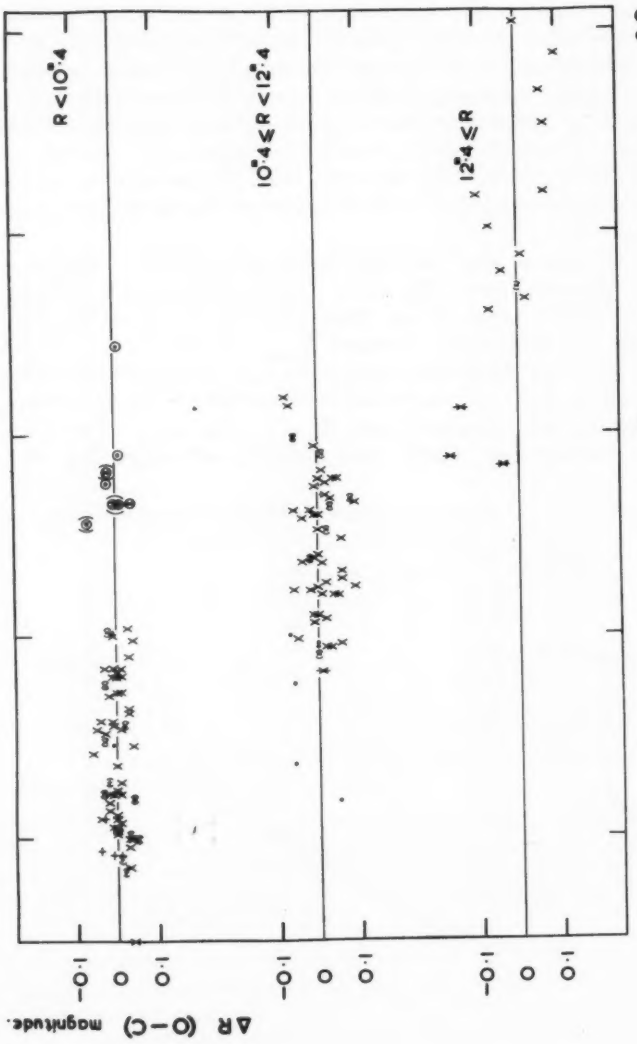

FIG. 4 (*a*).—*Comparison of $R_{(Krom)}$ with provisional R based on calibration from $R_{(Krom)}$. Mean for six plates for $R < 13^m$, otherwise over four with exposure exceeding 5 min. Notation as for Fig. 2.*

photographic measures are too faint for redder stars. The reason lies in the fundamental difference between the two systems. The R_{Kron} system has an overall response $\lambda\lambda$ 5000 to 9000 A (OG1 + BG21 + GB17) with equivalent wave-length about 6800 A, whereas our photographic system has a narrower response and an equivalent wave-length shorter by about 400 A. This difference will result in the R scale not being Pogsonian, because the fainter calibration stars are systematically redder than the brighter calibration stars.

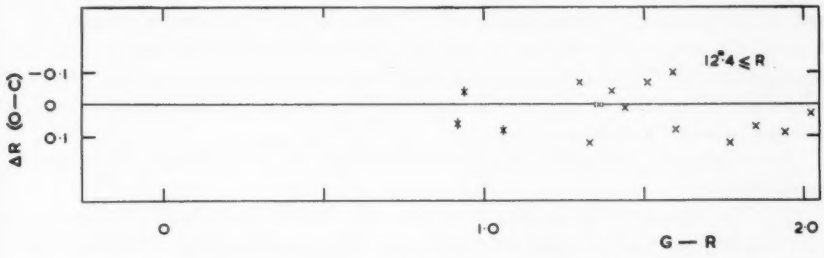

FIG. 4 (*b*).—*Comparison of $R_{Computed}$ with R based on calibration from $R_{Computed}$. $R_{Computed}$ is derived from $R_{(Kron)}$ using the Planck distribution formula.*

It is not possible to attempt an empirical transformation of our measurements to R_{Kron} because of the inadequate distribution of calibration stars with regard to luminosity class. Transformation from our narrow band to Kron's wide band system might be expected to show luminosity effects for cooler stars due to molecular absorption (although we cannot say how great these effects would be). The data of Fig. 4 (*a*) are completely inadequate for such transformation, e.g. there are no calibration giants fainter than $10^{m}\cdot4$, yet about half the field giants are fainter than this limit. To extend a colour equation from bright to faint giants involves extrapolation of the colour response of the photographic system which at present is not justified. Furthermore the restricted sample of calibration stars may not be generally applicable to the field. In three-colour photometry it is just these luminosity effects that play a crucial role, and it is important to avoid introducing an uncertain transformation. We therefore adopt the alternative procedure of expressing our measurements on the instrumental scale. This of course has the objection of making our measurements not directly comparable with those of other workers without transformation. In this present work, however, we are concerned mainly with making consistent comparisons of intensity, and are not at this stage concerned with intrinsic colours, etc., from other workers.

To set up the instrumental scale we must transform R_{Kron} to our photographic R. Suitable spectral intensity data over this range ($\lambda\lambda$ 5000–9000 A) were not available, so the assumption of black body distribution was resorted to. The results were effectively in the form of scale corrections to our original R. These were negligible for stars brighter than 10^{m}, then increased progressively and with increasing rapidity, being $0^{m}\cdot1$ at $12^{m}\cdot4$ and $0^{m}\cdot3$ at $14^{m}\cdot0$. This behaviour is found because the calibration depends mainly on the cluster members, of which the faintest are also the reddest. With decreasing colour temperature the

maximum of the Planck curve moves progressively towards the infra-red, and magnitudes on the Kron scale become relatively brighter. The scale corrections applied to Fig. 4 (*a*), produce appreciable change only for R fainter than $12^m{\cdot}4$. This last interval is replotted in Fig. 4 (*b*) where it is seen that the colour difference has been largely eliminated.

The computations were made on EDSAC 2 and comprised integrations over the whole range of response of each photometer, no simplifying assumptions about equivalent wave-lengths or constant spectrophotometric gradients being necessary. R_{Kron} was computed from the published response of (OG1 + BG21 + BG17) (**17**) and the atmospheric transmission for Mt Wilson from Smithsonian Annals (**21**); R from the measured response of the OR1 filter, the published response of OaE emulsion and the Washington transmission (**21**) which was assumed to be identical with Cambridge, and V from the photometer response (**22**) and assuming reduction to outside the atmosphere.

In conclusion, calibration of R is by two stages, each involving a questionable assumption:

(i) The relationships in Fig. 3 are for stars in the solar neighbourhood and may not be applicable to the standards. For instance Bidelman (**16**) has found the A1 to A5 cluster members to be abnormal. However, if the scatter in Fig. 3 is predominantly cosmic in origin and due to real differences between stars, and, further, if the calibration sample is included within the range of these differences, then the error involved in applying Fig. 3 will not exceed the peak scatter in this diagram, i.e. $\pm 0^m{\cdot}1$ over the interval $0^m{\cdot}3 \leqslant B-V < 1^m{\cdot}3$, where the lower limi corresponds to A5 and the upper to the turn-up in the diagram where the scatter increases. The corresponding limits of R are 9^m and 13^m.

(ii) The assumption of black body distribution, to transform from broad to relatively narrow band receiver, is likely to introduce serious error for cooler stars, on which the faint end of the scale depends ($R \geqslant 12^m{\cdot}4$). There is no satisfactory way to estimate this error. Existing spectrophotometric measurements for bright stars distributed over the sky may not be applicable to the cluster, and the danger of applying them is evident from the discussion of their measurements given by Kron, Gascoigne and White (**18**). Justification for our procedure is mainly Fig. 4 (*b*), although this is not satisfactory.

Calibration magnitudes for the G scale were computed from R_{Kron} and V, again assuming black body distribution. In this case the regions are broader in wave-length so that the influence of absorption lines and bands is less, and an estimate may be made of the errors using the six colour photometry of Stebbins and Kron (**24**). Assuming negligible error in R_{Kron} and V, the error due to black body approximation has a maximum of $-0^m{\cdot}06$ at early K dwarfs which affect the calibration near $G = 12^m{\cdot}5$.

The comparison of measured with computed G is given in Fig. 5. Again the distribution with $G-R$ is unsatisfactory, but there is evidence of systematic effects for metallic line stars and field dwarfs. These have little effect on calibration, being few in number. For $14^m \leqslant G$ there are no calibration stars with $G-R$ appreciably below $1^m{\cdot}0$ (Fig. 5) so that lack of control in this region may have contributed to the apparent ultra-violet excess shown by the two-colour plots in Fig. 11 (*c*) and (*d*), which are discussed later. Evidence that measurements in this region are influenced by a photographic Purkinje effect was provided by comparing results for faint programme stars on short and long exposure plates.

These indicate that the sensitivity of R plates moves towards the blue for fainter photographic images. This would cause faint blue stars to be measured too

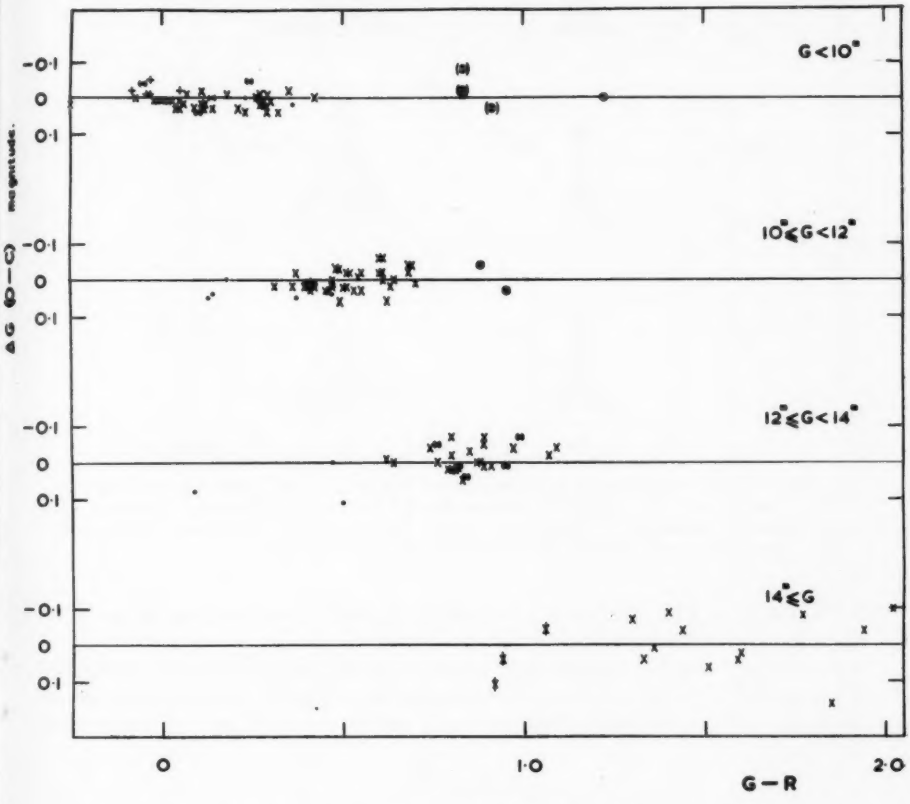

FIG. 5.—*Comparison of measured with computed G derived from $R_{(Kron)}$ and V, assuming black body distribution. Notation as for Fig. 2.*

bright on R plates, i.e. they would be moved to the right in the two-colour plots. Such a displacement is certainly present for the upper points in Fig. 11 (*c*) and (*d*), but how much of it is due to a real $U-G$ excess and how much to the photographic effect cannot be determined with the present data.

The most important conclusion from this discussion is that if one is to utilize to the full the potentialities of in-focus stellar photometry it is essential to have calibration stars well-distributed in colour and apparent brightness and also measured in very nearly the same spectral region as are used in the photography. Ideally one should not have less than 100 calibration stars per region. Since one cannot expect other observers to set up calibrations in these numbers in every region where Schmidt photometry happens to be contemplated, the photoelectric calibration must normally be regarded as part of the programme.

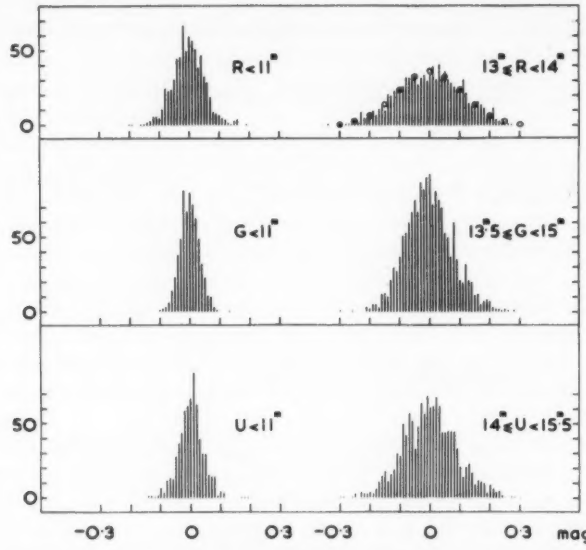

FIG. 6.—*Error histograms for individual magnitude determinations. An error is the difference Δm between an individual magnitude measurement and the mean for that star. Ordinates are the number of determinations having error between Δm−0·005 and Δm+0·005; abscissae are Δm. Open circles are for normal distribution with the sample variance.*

6. *Errors.*—The distribution of individual magnitude determinations about their respective means are given by the histograms in Fig. 6. Open circles for $13^m \leqslant R < 14^m$ are for normal distribution with the sample variance, computed from tables of erf (x). The measurements are affected systematically as we shall see, and a normal distribution would not be expected, but for the present

TABLE III

Standard error of individual magnitude measurement.

Colour	Magnitude range	No. of plates N	No. of observations	Standard deviation s	Standard error of single measurement
	m			m	m
R	<11·0	6	727	0·0535	0·059
	13·0–14·0	5	998	0·1090	0·122
G	<11·0	6	629	0·0320	0 035
	13·5–15·0	5	1612	0·0792	0·089
U	<11·0	8	652	0·0438	0·047
	14·0–15·5	4	1324	0·0905	0·105

purpose it will be sufficiently accurate to specify their distribution by the standard deviation s. This is given in Table III. Since each mean is derived from the individual observations themselves, N in number where there are N plates, the standard error of an individual measurement is approximately $s(1-1/N)^{-1/2}$.

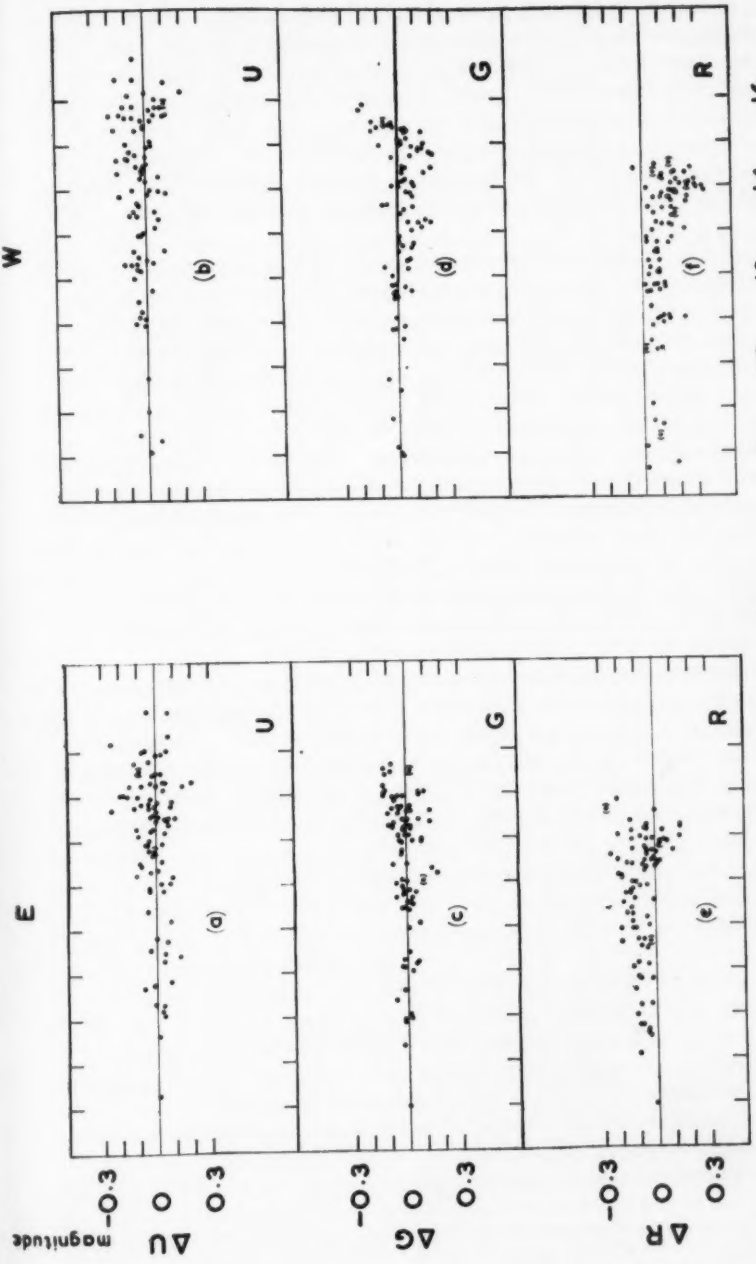

FIG. 7.—*Comparison of measured magnitudes on A plates (Fig. 1 (a)) with B (Fig. 1(b)). Ordinates are magnitude difference B minus A; abscissae mean magnitude A, B. Plots a, c and e are for the E region in Fig. 1; b, d and f for the W.*

To study systematic effects, the plates had been arranged in two groups according to the situation of the region measured. These are shown in Fig. 1 (*a*) and (*b*) and will be referred to as *A* and *B* respectively. We now consider measurements made within the two shaded rectangles *E* and *W*, each enclosing about 100 measured stars. These are compared in Fig. 7. For example in (*a*) is plotted, for each star in *E* rectangle, the measured *U* averaged over two *B* plates *minus* measured *U* averaged over four *A* plates. Fig. 7 (*a*) therefore gives the change in positional effect at *E* on passing from *B* to *A* in the ultra-violet, and Fig. 7 (*b*) the same for *W*, and so on for the other colours. The changes are averaged over the respective plates. Later we shall consider the individual plates.

Except over the last two magnitudes, the changes in positional effect in Fig. 7 may be regarded mainly as zero point changes, and these are barely significant in *G* and *U* with the possible exception of *W*(*U*), but very significant for *R*. Their values, expressed as zero point differences (*B*−*A*) and ignoring the final 2^m interval, are $0^m{\cdot}003$ and $-0^m{\cdot}005$ in *G* for *E* and *W* respectively with s.e. $0^m{\cdot}007$ in both cases; $0^m{\cdot}006$ and $-0^m{\cdot}017$ in *U* with s.e. $0^m{\cdot}009$; and $-0^m{\cdot}082$ and $0^m{\cdot}082$ in *R* with p.e. $0^m{\cdot}009$ and $0^m{\cdot}010$ respectively. These cannot have originated either in measurement or reduction. The measurements were made across the plates along narrow strips and in alternate directions so that a special drift pattern in the photometer would have been required to produce a systematic difference between *E* and *W*. A poor fit to the calibration data would also introduce no differential effect. Finally the large difference in *R* cannot be accounted for by variations in the filter, either in transparency or cut-off, nor by tilt of the plateholder which would have to be 0·08 mm between the *E* and *W* regions, an inconceivably large amount.

The disturbances in *R* were found to be mainly photographic effects. Microphotometer scans across *R* plates show considerable variation in background density which in extreme cases can be detected visually. These extend out into regions masked by the plateholder and cannot have been caused only by uneven sky brightness or scattered light. A correlation between measured magnitude and background density is shown in Fig. 8 where for each *R* plate

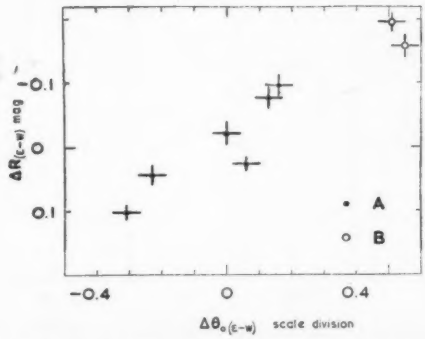

FIG. 8.—*Correlation of measured magnitude with photographic background density on R plates. Ordinates are zero point difference between E and W regions (Fig. 1). Abscisssae are correponding differences in background density between these regions, expressed as a change in irisphotometer reading. Crosses give ± internal s.e. in each ordinate.*

the difference in zero point between *E* and *W* regions (relative to the mean for the *A* plates) is plotted against the difference in background density between the same regions. This density was measured using the iris photometer, and expressed as an iris scale reading which increases with density. Eighty settings were made per region on each plate. The correlation in Fig. 8 is in the sense of bright measurement with high density. The effect in Fig. 7 (*e*) and (*f*) is now explicable by a steep density gradient across the *B* plates (open circles in Fig. 8). Although these *B* plates had been exposed for 30 minutes, the sky brightness is barely perceptible above chemical fog on visual inspection. It is probably accidental that the gradients are in the same sense on the *B* plates because considerable background variation was found among the *A* plates.

Precautions taken to give even development consisted of brushing and a stop bath, and the variations may be due mainly to dye sensitization. Uneven sensitivity is frequently experienced with panchromatic emulsions: e.g. Dr H. E. Butler of Edinburgh Observatory in a private communication described fluctuations in red sensitivity but not in blue on the same plates. Where an adequate distribution of standard stars is not available to control this effect over the regions measured, it may be desirable to make a few microphotometer scans before accepting a plate for measurement. Alternatively, corrections could be derived from Fig. 8, but this has not been attempted here.

All *R* plates in position *B* were rejected. They make no contribution to the standard errors in Table III.

For the *G* plates the individual variations in zero point are considerably smaller than for *R*, their numerical means being $0^{m}\cdot006$ for *E* and $0^{m}\cdot008$ for *W* with s.e. of each individual zero point of the same order, based on about 40 stars. There is no systematic difference between *A* and *B*.

Larger variation is found among *U* plates. The mean zero point difference without regard to sign is $0^{m}\cdot015$ for *E*, $0^{m}\cdot021$ for *W* with s.e. of each difference $0^{m}\cdot012$ based on 35 stars so that the differences may be significant. In this case the images are perceptibly elongated, and the following attempt is made to correlate this with the zero point differences. Elongation is more noticeable on visual inspection for *U* plates since the exposure times are on average longer while the image size arising from photographic turbidity is smaller than at longer wave-lengths. The maximum elongation observed has been 20 μ but considerable variation in amplitude is found, not only from one plate to another but even over individual plates. The most probable cause is mechanical disturbance of the plateholder supporting system (**10**).

If elongation be considered as due to motion perpendicular to the principal ray with one degree of freedom, a quantitative measure of the amplitude of elongation is given by $(a-b)$, where a and b are the major and minor axes of the photographic image. In Fig. 9 the difference in zero point between the two regions *E* and *W* (relative to the mean for the *A* plates) is plotted for individual plates against the difference in elongation between the two regions.

Measurements of a and b were rather crude as they relied on visual estimates of the edge of the image. In each region 20 images were measured by projection on the screen of the Becker irisphotometer, and the internal p.e. of the mean $a-b$ is about 0·7 μ. Furthermore the quantity $(a-b)$ does not give a complete description of image disturbance: e.g. for a small focus shift $(a-b)$ would be almost unaltered. Nevertheless there is evidence of a correlation in Fig. 9 in

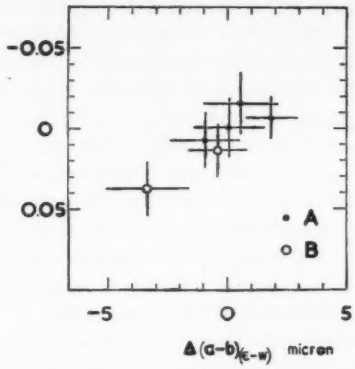

FIG. 9.—*Correlation of measured magnitude with elongation of photographic image on U plates. Ordinates are zero point difference between E and W regions (Fig. 1). Abscissae are corresponding difference in amplitude of elongation. Crosses give ±internal s.e. in each ordinate.*

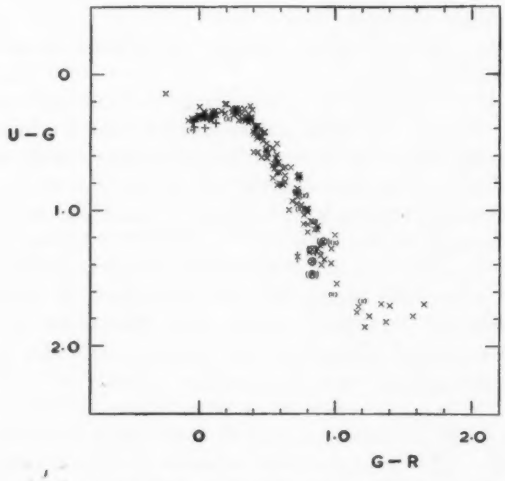

FIG. 10.—*Two colour plot for Praesepe cluster. Notation as for Fig. 2.*

the sense of measured brightness increasing with increasing elongation, as would be expected for an image in which the photographic density is approaching saturation. The magnitude of this effect appears to be about $0^{m}\cdot01$ per micron.

7. *Giant–dwarf distinction.*—The two-colour plots for the survey are given in Fig. 10 for cluster stars and Fig. 11 for field stars. These were derived from the same photometric data as Fig. 6 and Table III, i.e. all except the three rejected *R* plates in position *B*. No attempt has been made to correct individual measurements for background density or elongation of the image, it being assumed that the effects of these are randomly distributed with on the whole zero expectation. Internal standard errors were computed for the colours from Table III and

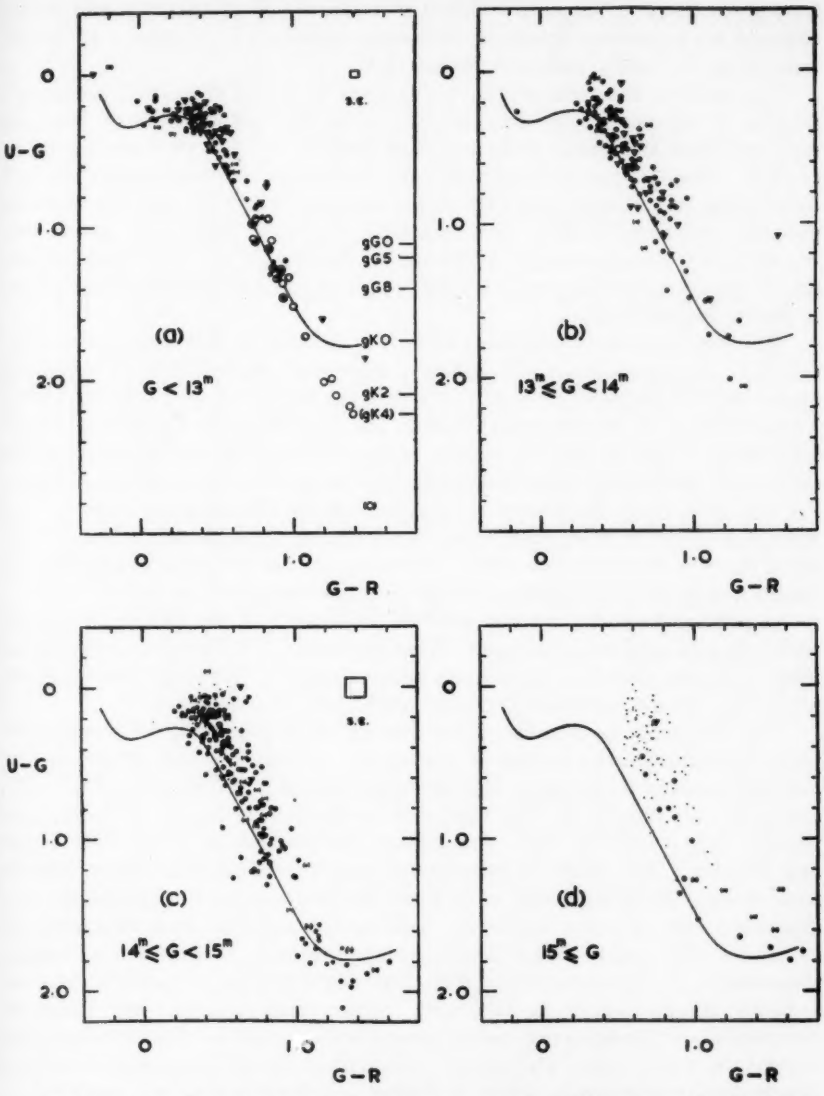

FIG. 11.—*Two colour plots for field stars in Praesepe region. Solid curves are for the cluster main sequence, from Fig.* 10. *Triangles: annual p.m.* $\geqslant 0''{\cdot}020$ *according to Klein Wassink* (6), *encircled for giants. Small dots: scale extrapolation* $R > 14^{m}$.

plotted as rectangles in Fig. 11 (*a*) and (*c*). Cluster membership was according to Klein Wassink (**6**) or Haffner and Heckmann (**25**). The curves in Fig. 11 are for the Praesepe cluster main sequence.

Field stars classified as giants by Ramberg (**7**) are plotted as circles in Fig. 11. All but one fall in Fig. 11 (*a*) which is the only plot for which Ramberg's survey is complete and the one mainly considered in this section. The standard error

for a given star is $0^m{\cdot}02$ in $U-G$ and $0^m{\cdot}03$ in $G-R$ (Table III), and superimposed are systematic errors of calibration estimated in Section 5 to be less than $0^m{\cdot}05$ in U and of order $0^m{\cdot}1$ in G and R.

The scale on the right of Fig. 11 (*a*) gives the mean $U-G$ for Ramberg's *g*-types as represented in this sample. The field giant sequence has just separated from the cluster main sequence curve at $U-G=1^m{\cdot}7$ corresponding to gKo. Now this part of the cluster curve is likely to represent closely the field dwarfs also, as is evident from Figs. 11 (*b*) and (*c*) in which the majority of points probably represent dwarfs. We conclude, therefore, that field giants with $U-G \geqslant 1^m{\cdot}7$, corresponding on average to Ramberg's gKo and later classes, are, in the absence of strong interstellar reddening, distinguishable from dwarfs in the two-colour diagram.

We consider now two regions of Fig. 11 (*a*) where *g*- and *d*-types are intermingled. Data on colours and cyanogen absorption are in Table IV where the upper block is for $0^m{\cdot}8 \leqslant U-G < 1^m{\cdot}0$ and the lower for $1^m{\cdot}2 \leqslant U-G < 1^m{\cdot}4$. The *d*-types are in the left-hand columns, the *g*- in the right. Within the upper block there is fair mixture as regards apparent magnitude and situation of the stars in the field, so that systematic errors in photometry should not be significant. For the lower block the *d*-types are fainter than the faintest *g*- by about 1^m but again the effects of systematic errors are probably insignificant. Within each block there is therefore real failure to resolve, in the two-colour diagram, two classes distinguished by cyanogen equivalent and designated *g*- and *d*-.

In passing, however, we may note the dKo star KW 161 (Table IV, upper) with high p.m. and weak cyanogen. This has excess $U-G$ relative to the cluster main sequence of $0^m{\cdot}2$, i.e. it occupies a special region in the two-colour diagram. Unfortunately the photometry was influenced by a nearby star.

The absence of segregation earlier than gKo was confirmed from two-colour plots derived from the six-colour photometry of Stebbins and Whitford (**26**) and Stebbins and Kron (**24**). The same result was obtained from the $(UV-BG)$ and $(BG-R)$ indices of Tifft (**27**), but conflicts with results of Becker and Steinlin (**13**). Of these three comparisons the most valid is that with Becker and Steinlin. The Stebbins photometry uses spectral regions rather different from those of *RGU*, especially in *R*, where the response is still about 90 per cent at λ7000 A and 5 per cent at 9000 A. Tifft made his photoelectric measurements in his *UV*, *BG* and *O* scales, the last being essentially at shorter wave-lengths than 6000 A. He then plotted his $(BG-O)$ index with change of scale to represent a linear transformation to $(BG-R)$. This transformation was based on comparison of photoelectric and photographic magnitudes for standard stars in NGC 6910 and 6913. The only photometry based on an instrumental response closely similar to our own is that of Becker and Steinlin and our results differ considerably from theirs with regard to the separation of *G* giants from the main sequence. The Becker and Steinlin two-colour diagram resembles our Fig. 10 more nearly than Fig. 11 (*a*), but we regard the position of the giants in Fig. 10 as unreliable on account of their brightness. The discrepancy between Fig. 11 (*a*) and the Becker and Steinlin results cannot be due to photometric errors in the former. A contributing factor may be selection; for instance the Praesepe cluster giants have abnormally strong cyanogen absorption as Ramberg (**7**) has pointed out, and this may contribute to their $(U-G)$ deficiency in Fig. 10. The material of the present programme is not extensive enough for a discussion of this question.

TABLE IV

Data for two groups classified by Ramberg (7) *as g- and d- and occupying the same regions of Fig.* 11(*a*). *Upper block:* $0^{m}.8 \leqslant U-G < 1^{m}.0$; *lower* $1^{m}.2 \leqslant U-G < 1^{m}.4$. *KW denotes catalogue no. from Klein Wassink* (6) *with colon for image slightly blended with nearby star.* μ *is the annual p.m. if* $\geqslant 0''.020$ *from Klein Wassink* (6). *Rm denotes catalogue no. and spectrum from Ramberg* (7).

KW	*Rm*		*G*	*c*	*U–G*	*G–R*	μ	*KW*	*Rm*	*G*	*c*	*U–G*	*G–R*	μ
281	461	dG8	12·59	0·08	0·85	0·76	—	440	604 gG5	12·38	0·25	0·94	0·84	—
310	480	dKo	12·80	0·10	0·87	0·75	—	134	302 gGo	10·47	0·23	0·94	0·75	—
356	521	dG5	11·43	0·13	0·93	0·75	—	105:	268 gG5	12·44	0·18	0·97:	0·73:	$0''.020$
373	536	dG8	12·60	0·13	0·93	0·80	—							
484	656	dG8	11·99	0·13	0·94	0·78	—							
161:	335	dKo	11·80	0·02	0·84:	0·79	$0''.085$							
469	639	dKo	12·72	0·16	1·21	0·95	—	248:	421 gG8	11·52	0·30	1·26:	0·87:	$0''.022$
28	171	d-gGo	12·79	0·17	1·22	0·87	—	108	272 gGo	10·52	0·25	1·28	0·92	—
								109	274 gG5	9·67	0·18	1·29	0·92	$0''.029$
								36	188 gG8	11·81	0·23	1·32	0·97	—
								99	264 gG5	11·85	0·26:	1·33	0·89	—
								480	651 gG8	11·53	0·35	1·36	0·93	—

8. *Praesepe field stars.*—It would not be profitable to attempt an exhaustive statistical analysis of the photometric results with the present uncertainty of the colour scales. Faint blue programme stars are without colour control, and in addition the faintest of these had to be extrapolated beyond the limit of the R calibration at $14^{m}\cdot0$, to a maximum of $15^{m}\cdot1$. Members of the latter group are plotted as small dots in Fig. 11. For these reasons the possibility cannot be excluded that the ultra-violet excesses in Fig. 11 (*c*) and (*d*) may be largely instrumental. Nevertheless the diagrams provide some interesting material.

(i) Fig. 11 (*a*) shows field stars with $G-R<0^{m}\cdot3$ and spectra A2 to F2 in Ramberg's classification (**7**). This region of the two-colour diagram is almost entirely unpopulated by the fainter stars. These stars are members of the galactic disk, and their distances were estimated from the colour magnitude diagram of the cluster corrected to the nearby stars as described by Bidelman (**16**). The A2–A5 stars were found to extend to a maximum distance of 800 pc in the line of sight; the F0–F2 to 500 pc. The corresponding distances from the galactic plane are about 400 and 250 pc respectively. These stars are included in Ramberg's survey but I have not found a subsequent discussion of their spatial distribution. Relative to them the cluster members show a deficiency in $U-G$ of $0^{m}\cdot05$. This is a real effect which has been noted by Bidelman (**16**).

(ii) Just to the right of the above group in Fig. 11 (*a*), at $G-R=0^{m}\cdot3$, there is a sharp increase in the number of stars, the number per unit interval of $G-R$ having increased about fourfold on passing this limit. This is due to the more numerous F dwarfs near the Sun. The limit $G-R=0^{m}\cdot3$ corresponds to $B-V=0^{m}\cdot46$ and is the the region of the HR diagram where the subgiant branch turns off the main sequence, for stars within 15 pc of the Sun (Sandage (**23**)). Such stars, if still present in Fig. 11 (*d*), would be at distances exceeding 2 kpc in the line of sight ($M_V=3^{m}\cdot5$) or 1 kpc above the galactic plane, but the photometry is too uncertain to decide whether Fig. 11 (*d*) represents such a population, or alternatively one more closely resembling M3 (Eggen (**10a**); Johnson and Sandage (**29**)) and showing ultra-violet excess. The similarity between Fig. 11 (*a*) and (*b*) and corresponding diagrams for the N galactic pole to the limit $G=13^{m}\cdot7$ given by Becker and Steinlin (**13**) is very marked.

(iii) Stars with annual p.m. $>0''\cdot020$ according to Klein Wassink (**6**) are plotted as filled triangles in Fig. 11. In the range $13^{m}\leqslant G<14^{m}$ there is a suggestion that two sequences are present, one coinciding with the cluster main sequence over the interval $0^{m}\cdot6<U-G\leqslant1^{m}\cdot2$ and the other displaced above this by about $0^{m}\cdot3$ in $U-G$. This is unlikely to be an instrumental effect because no correlation could be found between $U-G$ excess and either apparent brightness or position in the field. Proper motions for about 80 per cent of the stars plotted in this diagram were available.

The photometric and p.m. data are in Table V. The "sequence" with normal $U-G$ is in the left-hand columns. It probably comprises ordinary, background dwarfs of types G and early K, not far beyond the cluster. The "sequence" with excess $U-G$ in the right-hand columns may be related to the high velocity stars described by Miss Roman (**30**). The first star in Table V, KW 394, gives under approximate transformation $B-V=0^{m}\cdot67$ and hence, from the HR diagram of M3 given by Johnson and Sandage (**29**), $M_V=5^{m}\cdot0$. Then the distance modulus $V-M_V=8^{m}\cdot0$ and the peculiar tangential velocity 180 km/sec. The proper motion is such that the velocity vector in the Bottlinger

diagram (**31**) corresponds to an orbit of high eccentricity. This star has been classified dGo (**7**) and may be similar to Miss Roman's high velocity F stars (**30**).

TABLE V

Photometric and proper motion data for stars having annual p.m. $\geqslant 0''\cdot020$ *plotted in Fig.* 11(*b*). *KW and* μ *denote catalogue number and p.m. from Klein Wassink* (**6**). *The left-hand columns are for normal two-colour relationship, the right-hand for U–G excess* $0^{m}\cdot3$.

KW	*G*	*G–R*	*U–G*	μ	*KW*	*G*	*G–R*	*U–G*	μ
211	14·03	0·51	0·61	$0''\cdot036$	394	13·34	0·53	0·08	$0''\cdot105$
191	13·19:	0·56:	0·67:	33	364	13·74	0·53	0·32	25
41	13·57	0·69	0·80	164	65	13·54	0·55	0·41	23
228	13·74	0·59	0·89	21	312	13·22	0·66	0·43	26
479	13·43	0·64	0·90	34	247	13·11	0·61:	0·44:	55
137	13·34	0·75	1·00	41	131	13·13	0·62	0·47	26
355	13·60	0·81	1·08	34	188	13·79:	0·66	0·49	33
308	13·39	0·85	1·20	57	210	13·96	0·62	0·53	31
262	13·53	1·11	1·49	21	381	13·91	0·71	0·71	23
					46	13·74	0·80	0·80	24
					239a	13·94	0·90	1·01	48

Proper motion vectors for the two "sequences" are plotted in Fig. 12, that with normal $U-G$ in (*a*) and that with excess $U-G$ in (*b*). The vector for the cluster is also included in (*a*) and is quite separate. Proper rather than peculiar motions have been plotted to avoid estimates of absolute magnitude. For main sequence objects the difference is not large enough to influence the following discussion, as may be seen from values of parallactic *minus* mean relative proper motion given by Klein Wassink ((**6**), Table 7). The position angle of the p.m. vector gives a rough indication of the inclination of the orbit to the galactic plane. In Fig. 12 there is an indication of greater dispersion in inclination for (*b*), i.e. for excess $U-G$: We must be careful not to over-discuss this rather meagre material, but the results are consistent with present knowledge of high velocity stars, except that the concept of just two "sequences" is probably an

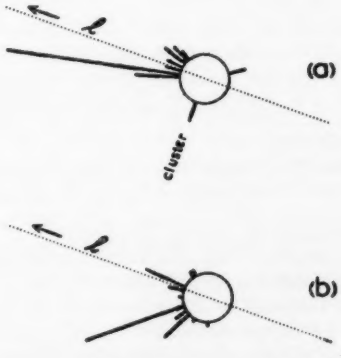

FIG. 12.—*Proper motion vectors* $\geqslant 0''\cdot020$ *for stars in Fig.* 11 (*b*). (*a*) *having the same two-colour relationship as the Praesepe cluster, including mean vector for cluster itself;* (*b*) *having* $U-G$ *excess of about* $0^{m}\cdot3$. *The dotted line is parallel to the galactic plane. Radius of circle corresponds to* $0''\cdot020$.

oversimplification forced on us by the small sample in Fig. 11 (*b*). However they confirm the value of three-colour photographic surveys with wide field optical systems extending beyond 13^m, in the study of stellar populations.

Acknowledgments.—It is a pleasure to express my gratitude to the Director of the Cambridge Observatories, Professor R. O. Redman, for his advice and support; to H.M. Astronomer Royal, Dr R. v. d. R. Woolley, for loan of the Greenwich Sartorius Iris Diaphragm Photometer; to the Director of the University Mathematical Laboratory, Cambridge, Dr M. V. Wilkes, for generous provision of time on the EDSAC computers, and to members of his staff, particularly Mr E. N. Mutch and Mr H. P. F. Swinnerton-Dyer, for their cooperation; and lastly to Dr P. B. Fellgett, now of the Royal Observatory, Edinburgh, for valuable discussion in connection with many aspects of the photometry and reductions.

The Observatories,
Cambridge:
1960 *October.*

References

(1) R. O. Redman, *Obs.*, **73**, 180, 1953.
(2) H. Haffner, *Mitt. Sternwarte Hamburg-Bergedorf*, **23**, Nr. 255, 1956.
(3) W. Becker and C. Biber, *Zeits. f. Ap.*, **41**, 52, 1956.
(4) A. N. Argue, *Obs.*, **80**, 73, 1960.
(5) H. L. Johnson, *Ap. J.*, **116**, 640, 1952.
(6) W. J. Klein Wassink, *Groningen Pub.*, Nr. 41, 1927.
(7) J. M. Ramberg, *Stockholm Obs. Ann.*, **13**, Nr. 9, 1941.
(8) J. H. Oort, *B.A.N.*, **8**, 233, 1938.
(9) A. Sandage and O. J. Eggen, *M.N.*, **119**, 294, 1959.
(10) A. N. Argue, *Vistas in Astronomy*, p. 184, Ed. A. Beer (Pergamon, London, 1960).
(10a) O. J. Eggen, *Ibid.*, p. 258, Fig. 31.
(11) E. H. Linfoot, *Recent Advances in Optics* (Oxford, 1955).
(12) E. H. Linfoot, *Proc. Phys. Soc.*, **58**, 65, 1946.
(13) W. Becker and U. Steinlin, *Zeits. f. Ap.*, **39**, 188, 1956.
(14) G. E. Forsythe, *J. Soc. Indust. Applied Math.*, **5**, 74, 1957.
(15) F. H. Seares, *Ap. J.*, **102**, 366, 1945.
(16) W. P. Bidelman, *P.A.S.P.*, **68**, 318, 1956.
(17) G. E. Kron and J. L. Smith, *Ap. J.*, **113**, 324, 1951.
(18) G. E. Kron, S. C. B. Gascoigne and H. S. White, *A.J.*, **62**, 205, 1957.
(19) H. L. Johnson and W. W. Morgan, *Ap. J.*, **117**, 313, 1953.
(20) H. L. Johnson and D. L. Harris III, *Ap. J.*, **120**, 196, 1954.
(21) *Smithsonian Annals*, III, **198**, 1913.
(22) H. L. Johnson and W. W. Morgan, *Ap. J.*, **114**, 522, 1951.
(23) A. Sandage, *Stellar Populations*, p. 287, Ed. D. J. K. O'Connell, S.J., (Vatican Obs., 1958).
(24) J. Stebbins and G. E. Kron, *Ap. J.*, **123**, 440, 1956.
(25) H. Haffner and O. Heckmann, *Veroff. Gottingen*, Nr. 55, 1937, *Ibid.*, Nr. 66, 67, 1940.
(26) J. Stebbins and A. E. Whitford, *Ap. J.*, **102**, 318, 1945.
(27) W. G. Tifft, *A.J.*, **63**, 127, 1958.
(28) H. L. Johnson, *Ap. J.*, **126**, 121, 1957.
(29) H. L. Johnson and A. Sandage, *Ap. J.*, **124**, 379, 1956.
(30) N. Roman, *Ap. J.*, Supp. **2**, 198, 1955.
——*A.J.*, **59**, 307, 1954.
——*Trans. I.A.U.*, **10**, 528, 1958.
(31) K. F. Bottlinger, *Veroff Berlin-Babelsberg*, **10**, Nr. 2, 1933.

INTERFEROMETRIC INVESTIGATION OF EMISSION LINES OF THE SOLAR CORONA DURING THE TOTAL SOLAR ECLIPSE OF 1958 OCTOBER 12

A. H. Jarrett and H. von Klüber

(Received 1960 November 4)

Summary

The total solar eclipse of 1958 October 12 was observed by a Cambridge Observatories expedition on the coral atoll Atafu, in the Tokelau Islands of the South Pacific. The solar corona was photographed through a Fabry–Perot interferometer, with a 0·35 mm spacer, using narrow-band interference filters for the green (λ 5303 A) and red (λ 6374 A) corona lines respectively. Several good photographs were obtained, standardized photometrically and showing very good interference fringes over the whole corona, in some position angles to more than 1·8 solar radii from the Sun's centre. Immediately before and after the eclipse, interference fringes were photographed in the light of the 5461 A line from a water-cooled mercury 198 isotope lamp, to check the instrumental adjustment and to provide an instrumental fringe profile. Many line profiles and half-widths, corrected for instrumental broadening, were determined for both the corona lines and temperatures derived from them. The mean temperature from the green line was about $3{\cdot}2 \times 10^6$ deg. K and from the red line $3{\cdot}5 \times 10^6$ deg. K, with an error of about 10 per cent in each case.

After many earlier attempts by other observers had failed, the present authors at last succeeded (**1, 2**) in obtaining Fabry–Perot interference fringes from the green corona line during the total solar eclipse of 1954. From this first attempt it became clear that with modern interference filters and with a suitable optical arrangement it is quite possible to obtain Fabry–Perot interference fringes of the brightest emission lines of the corona during a total eclipse, out to a distance from the Sun's centre which cannot be reached by the usual technique of daytime observations with coronagraphs. Line profiles of λ 5302·86 taken during an eclipse have also the advantage of being unaffected by the very disturbing iron absorption line λ 5302·309 which is present in the scattered skylight of all daytime observations and happens to be superimposed on to the violet wing of the corona line (**3**). The interferometric technique, when applied photographically, furthermore allows one to obtain line profiles with a fairly high resolving power over a considerable area of the corona simultaneously.

With the experience gained at the 1954 eclipse it seemed desirable to repeat interferometric observation of the solar corona during the total solar eclipse of 1958 October 12. This eclipse came near to the maximum (Epoch 1957·9) of the highest solar activity ever observed so far and also fell within the International Geophysical Year so that such observations could be assumed to be of special interest. The track of the 1958 total eclipse passed over the whole length of the Pacific Ocean and only eight tiny low coral atolls lay inside the belt of totality (**4**). Atafu, 172°30′W and 8°33′S, one of the Tokelau Islands, was chosen for the Cambridge Observatories eclipse expedition, mainly because flying boats could land

right on the lagoon of the island (**5**) and could be used for the transport of instruments and scientists to and from the station. The coral reefs lying outside the island are a serious obstacle for ordinary landing operations and the island is seldom approached by vessels. The members of the expedition and most of the optical, photographic and electric equipment were flown by a Sunderland flying boat direct to the lagoon. The expedition lived in army tents on the outskirts of the small village of Atafu. The concrete pillars for the instrument and a temporary shelter of wooden planks and coconut mats over the coelostat and the optical equipment were erected, with the most efficient help of the Tokelau Islands Administration and of the local population, on the east shore of the lagoon in front of the small village hospital. In spite of the fact that the width of the heavily wooded island between the ocean shore and the lagoon was only about 300 metres, sea spray and wind gave little trouble during the seven weeks the expedition stayed on the island. The surfaces of the aluminium coated mirrors, the interferometer and the interference filters actually kept very well and so did the relative adjustment of the interference plates. Shade temperatures were remarkably uniform and were seldom higher than 30 °C.

Instruments.—The optical arrangement was a much improved version of the instrument used successfully in 1954 and of the one prepared for the 1955 eclipse in Ceylon which unfortunately was clouded out (**1, 6**).

In the new design fringes from the green and from the red corona lines respectively could be obtained on successive photographs during totality, merely by changing the interference filters. The Sun's image now had a diameter of 13 mm, compared with only 6 mm in 1954. Special 5 × 5 cm plates were used instead of 36 mm film, in a precision holder specially designed for a very rapid change of plates. Fig. 1 gives a general sketch of the optical arrangement. Using

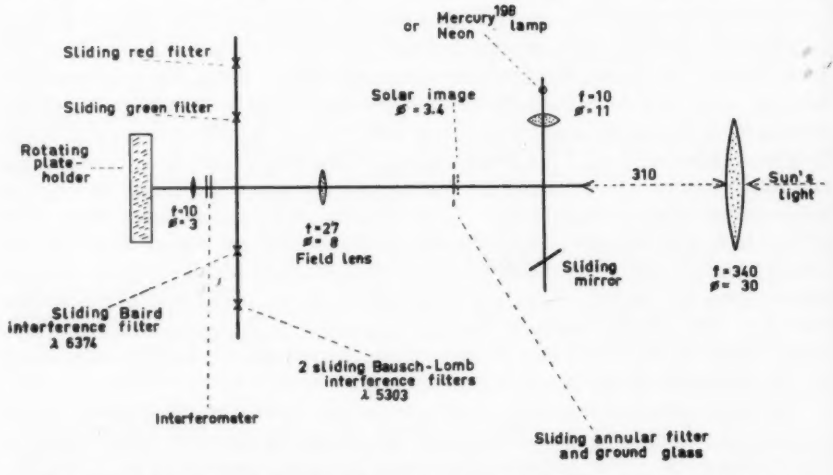

FIG. 1.—*General sketch of the optical arrangement. The symbol f gives the focal length and ϕ the aperture in cm.*

a coelostat and an auxiliary mirror, each having an aperture of 40 cm, the Sun's light was reflected on to an astrographic lens of 30 cm aperture and of 340 cm focal length. This lens formed a solar image of 34 mm diameter in the focal plane of a field lens of 27 cm focal length which, in turn, imaged the aperture of the

30 cm objective into the aperture of the interferometer, itself placed in a telecentric beam with respect to the Sun's image. A high quality Zeiss-Tessar camera lens of 10 cm focal length imaged the fringes of the interferometer as well as the corona, superimposed on each other, on the photographic plate. The image of the corona thereby was reduced in the proportion 10 : 27, i.e. the diameter of the solar image became now 13 mm. The plate holder was specially precision-made in the workshop of the Observatories so that by simply moving a handle from one mark to the next six plates 5 × 5 cm could be exposed in succession. The movement was controlled by precision ball bearings rotating against a large machined plate which itself was adjustable with respect to the optical axis by three push-pull screws. In this way all plates could be exposed within less than ± 0·05 mm of the best focus, a necessary requirement for obtaining good line profiles. The camera lens could be focussed by means of a special helical Zeiss mounting with equal accuracy. One interference filter for the green corona line λ 5303 and another one for the red line λ 6374 were arranged sliding on an optical rail perpendicular to the main optical axis in front of the interferometer. The change-over from the one to the other during totality controlled by pre-set stops, took about one second only. For adjustment and test purposes other ordinary glass filters could be moved into the main optical beam in the same way. Another short optical rail, again perpendicular to the main optical axis, was fixed a small distance in front of the primary image of the Sun. It carried the comparison light source, a condenser lens and a mirror which, when slid into the optical axis, reflected the comparison light on to a ground glass screen placed near the focal plane of the main objective. In this way, with the mirror inserted, comparison fringes could be imaged on the photographic plate in exactly the same way as were the fringes of the corona. The ground glass screen, resting against adjustable stops, had also the important function of providing a means of adjusting precisely the Sun's image and the fringe system on to each other. The mirror had, of course, to be shifted out of the optical beam during the actual eclipse observations.

It was to be expected that photometry of the interference fringes, superimposed on the background image of the corona, would be somewhat complicated by the well known steep intensity gradient of the corona near the limb of the Sun. With this in mind an annular filter had been prepared of dimensions and absorption gradient such that, when brought during the exposure of the corona near to the primary focal plane and adjusted concentrically with the corona, it would smooth out most of this unwanted steep intensity gradient. The filter was made according to given specifications by Messrs. Barr and Stroud, and worked very well during all tests before the eclipse. But obviously it had to absorb a certain amount of light and the feeling was that it should be used for the actual eclipse exposures only if the general circumstances and the transparency of the sky were such that this loss of light would be tolerable. Since some high cirri were still visible shortly before totality we eventually decided not to use this annular filter, for fear of under-exposure. Later, when the plated obtained during the eclipse were inspected, this decision was seen to err on the side of pessimism, for quite sufficient light had been available in the green line fully to justify use of the filter. But fortunately only some inconvenience, and no serious trouble was later encountered during the photometry from the steeper gradient thus obtained. For the long exposure (60 s) of the red line use of the annular filter would have given a more convenient gradient, whilst for the shorter exposure (20 s) of the red line, only a slight and

probably tolerable loss in density in the inner corona would have occurred. The final verdict is that use of such an annular filter, in this and in other photometric problems dealing with the corona, might prove very helpful.

Interferometer.—We used the same interferometer as in 1954 (1), consisting of two flats of crystalline quartz figured by Messrs. Hilger and Watts to $1/40\lambda$. For spacer we again used balls from the Miniature Ball Bearing Co., in Switzerland, of 0·35 mm diameter, giving a range of 4·04 A which seemed well suited for our problem. But this time use of multi-coated dielectric layers on the plates seemed inadvisable because having only one interferometer we wanted to use it for the green as well as for the red corona lines. Both flats, therefore, were coated by Messrs. Hilger and Watts with an aluminium surface and we had to make a compromise between reflectivity which, once the spacer was fixed by the circumstances of the problem, controls the resolving power, and between the transparency which for increasing reflectivity decreases rather quickly. The resolving power actually used on this occasion was about 10,000. Since the actual instrumental profile could be measured very accurately with the help of the green Hg^{198} isotope line, 5461 A, and remembering that the corona lines have a half width of the order of 1 A, this resolution was considered quite sufficient. As will be seen below, the observed half widths of the corona lines could be corrected very reliably for the instrumental profile.

Filter.—For isolating the λ 5303 line we used two combined Bausch and Lomb interference filters manufactured in 1954. Each had a size of 5×5 cm, a half width of about 38 A and a peak transmission of about 75 per cent. The transparency curve of this combination, as used during the eclipse, is shown in Fig. 2,

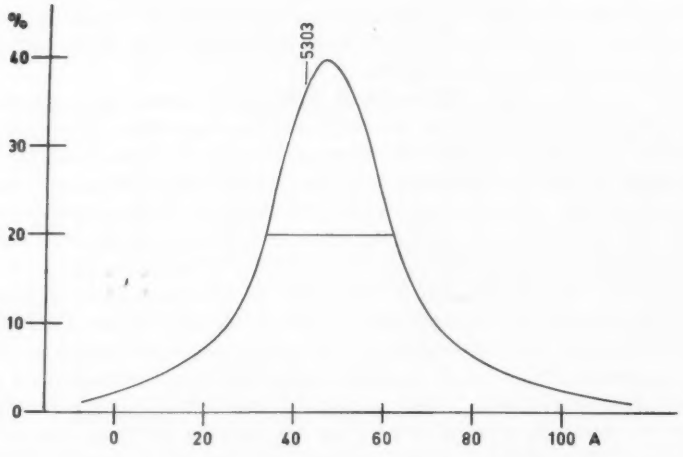

FIG. 2.—*Transmission of the two combined Bausch and Lomb interference filters used for observing the coronal emission* λ 5303.

from which we deduce that the effective half width was about 28 A. The peak transmission of about 40 per cent was found for perpendicular incidence to lie only 3 A to the red side of λ 5303 and could be brought right on to λ 5303 by tilting the

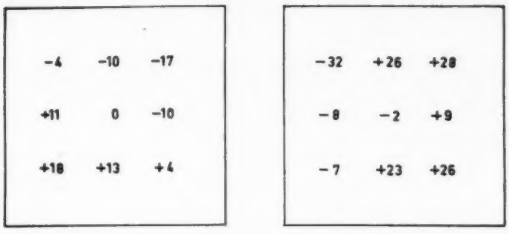

FIG. 3.—*Deviations from λ 5303 of the wavelengths of peak transmission at different parts of the Bausch and Lomb interference filters, in Angstrom units.*

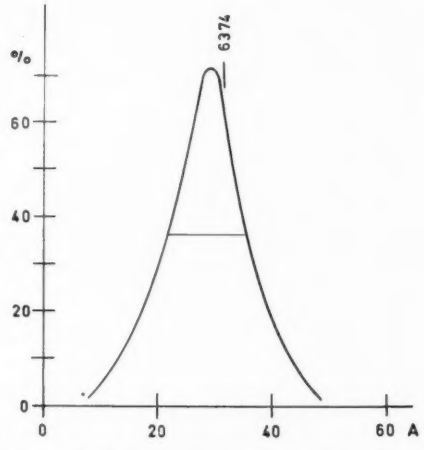

FIG. 4.—*Transmission of the Baird interference filter used for observing the coronal emission λ 6374.*

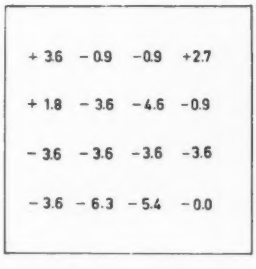

FIG. 5.—*Deviations from λ 6374 of the wavelengths of peak transmission at different parts of the Baird interference filter, in Angstrom units.*

FIG. 6.—*The corona with superimposed interference fringes in the light of λ 5303. (plate 2). Exposure time 20 seconds, range of the interferometer 4·0 Å.*

A. H. Jarrett and H. von Klüber, Interferometric investigation of emission lines of the solar corona during the total solar eclipse of 1958 October 12.

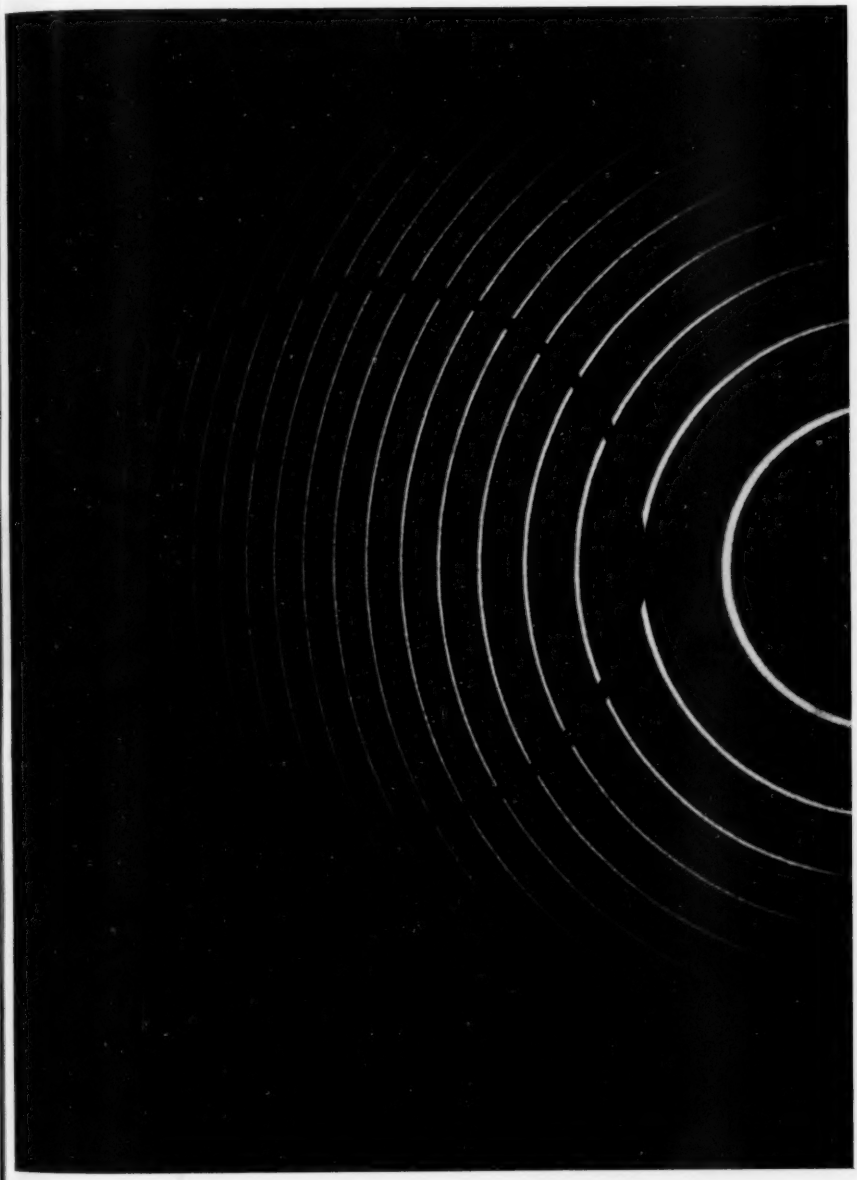

FIG. 7.—*Fabry-Perot test fringes at λ 5461 from a mercury 198 water-cooled isotope lamp, photographed a few minutes after totality (plate 5). Exposure time 15 seconds, range 4·04A.*

FIG. 6.—*The corona with superimposed interference fringes in the light of λ 5303. (plate 2). Exposure time 20 seconds, range of the interferometer 4·04A.*

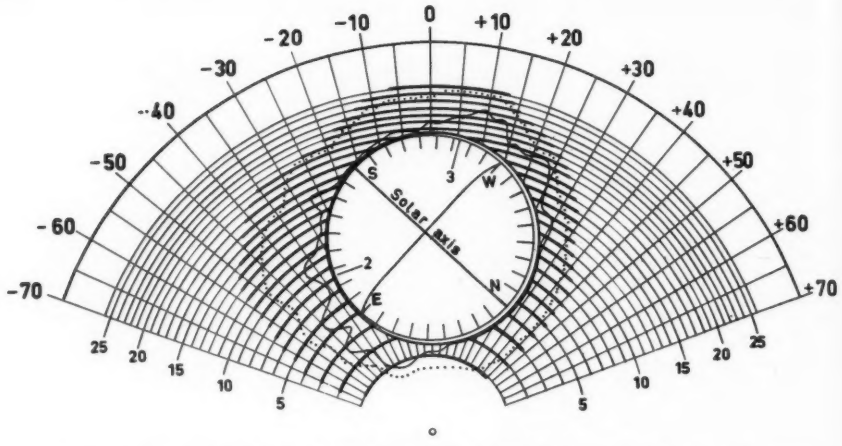

FIG. 8.—*Sketch showing the system of interference fringes of λ 5303, on plate 2, with respect to the solar coordinates. The Nos. 2 and 3 denote the second and third contact. The Sun's position is inserted into the circle of the moon for about the middle of exposures of plate 2. The heavily drawn parts of the concentric circles indicate all interference fringes clearly visible on the original plate. The dotted line indicates the contour of the corona background as visible on the plate and the thinly drawn curve the intensity estimations for λ 5303 carried out with the Climax coronagraph about one hour after the eclipse. The system of straight lines, originating from the centre of the fringe system but otherwise arbitrarily orientated, indicates the lines along which as far as possible photometry has been carried out.*

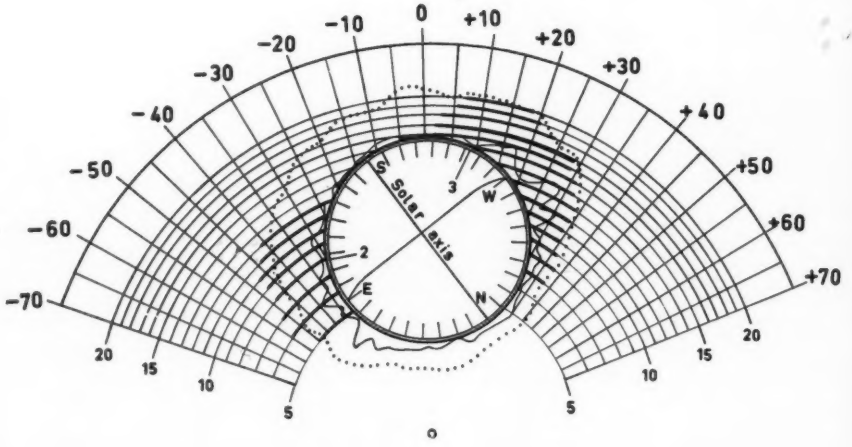

FIG. 9.—*Same as Fig. 8 but for λ 6374 on plates 3 and 4. The system of straight lines along which photometry has been carried out and originating in the centre of the fringe system is, for technical reasons, again arbitrary and not quite identical with the similar system in Fig. 8.*

filters slightly. This combination possessed another broad maximum around λ4400 which could be removed by an additional OY6 Chance glass filter. Another very weak maximum near λ6300 was placed well beyond the colour sensitivity of the photographic plates. The homogeneity of the two filters was satisfactory as one can see from Fig. 3.

For the red line λ6374, a specially excellent filter was made by Baird Atomic Inc., Cambridge (Mass.). Its properties, as measured photometrically with the large Cambridge spectrograph, are shown in Fig. 4. It had a half width of only 14 A and a peak transmission of well over 70 per cent. Unfortunately its maximum transparency was displaced about 3 A to the violet beyond λ6374 and could therefore not be corrected by tilting the filter, so that a slight loss of transparency and therefore of contrast had to be taken into account. With such a small band-width the uniformity of the filter over its surface is quite important and very often not well attained. This particular filter was found to be very uniform over its whole area, as can be seen from Fig. 5. The filter was cemented together with a coloured cover glass to remove the other unwanted transmission maxima. A weak transmission on the violet side of the main peak was easily removed by an OR2 Schott filter.

Photographic plates.—For the green line a Kodak emulsion similar to Kodak IIa J but specially prepared for this purpose (Code V 1008 on 5 × 5 cm plates), was used, while for the red corona line the Kodak emulsion IIaE was found very suitable (7). Both emulsions are only of moderate speed but were chosen after a long set of tests as giving a good compromise between resolving power, contrast, colour sensitivity and speed. We are obliged to the research laboratories of Kodak Ltd., Wealdstone, Harrow, for preparing several test emulsions according to our specifications and for supplying eventually all the plates used by us during the eclipse.

Observations.—The weather, somewhat doubtful in the early morning, became quite good during eclipse. Local time of mid-totality was $8^h 7^m{\cdot}5$. Soon after first contact, apart from a few drifting cumuli clouds, there was only faint irregular high cirrus disappearing slowly in the neighbourhood of the Sun, and, if present during totality, seems not to have interfered at all with the observations. But, as mentioned above, the cirrus was the reason for not using the annular filter, an unnecessary precaution as appeared later. The observations were carried out in the following sequence:

1: about 5 minutes before second contact test fringes of the green Hg 198 line were taken with 15 seconds exposure time.
2: the green mercury filter was then replaced by the Bausch and Lomb interference filters for the green corona line. This change took only about 2 seconds and no other part of the instrument was touched.
3: a few seconds after second contact the fringes of the green corona line were exposed for 20 seconds (Fig. 6).
4: the green interference filters were then replaced by the Baird λ6374 interference filter and 2 exposures of 60 and 20 seconds respectively were taken of the red fringes.
5: about 2 minutes after third contact another test exposure of the green Hg 198 line was taken in exactly the same manner as at the beginning (Fig. 7).

XUM

The change of plates with the rotating plate holder operated by the observer inside the hut required about 1 or 2 seconds. The actual exposures were made by a shutter operated by Mrs von Klüber in front of the 30 cm lens near the coelostat, so that the instrument was never touched during these operations.

After the eclipse a set of intensity marks from a Hilger rhodium step filter was printed on separate 5 × 5 cm plates which came out of the same boxes which had provided the eclipse plates. The exposure times were in each case identical with the exposure times of the eclipse plates with which they were to be combined. These exposures were made in a separate, small, electric standardising equipment through filters which separated the λ 5303 or the λ 6374 region in the same way as during the eclipse. Each eclipse photograph was developed together with its standardised companion, in a specially made plexi frame, ensuring that the whole sequence of processing was carried out for both plates absolutely identically. In this way the fundamental condition of photographic photometry, *viz*, equality of emulsion, exposure time, wavelength and processing could be easily and strictly fulfilled.

Since temperatures often reached, and sometimes surpassed, the 30°C limit, Kodak tropical developer DK 15 and a Kodak tropical hardening stop bath SB4 containing potassium chromalum were used for all photographic processing, and proved very satisfactory (**8**). There was a plentiful supply of rainwater for all solutions and for washing purposes.

The fringes of λ 5303 came out with remarkable contrast and quality all over the corona, as can be seen from Fig. 6. The intensity ratio of corona background to the fringes is on the average about 1 : 1·6. This contrast is much higher than found in 1954 and doubtless to a great extent is due to the much greater intensity of the green line during this eclipse. Solar activity had its highest maximum on record (**9**) in 1957 December, while the Zürich relative number during the month of the eclipse was 181 (**3**). In contrast the 1954 eclipse showed a typical minimum corona with a relative number as low as about 0·2 and with the green line hardly visible with the usual coronagraph.

On the day of the 1958 eclipse good observations were obtained at the Climax station of the High Altitude Observatory of the University of Colorado with a Lyot coronagraph. Since the corona lines on our plate extend far beyond the distance covered by the usual routine corona observations it is of interest to show in Fig. 8 our λ 5303 fringe system superimposed on the intensity contours of the Climax station. One must keep in mind that these contours are not isophotes but relate to intensities only, observed at a distance of about 0·03 radii from the centre of the Sun. On the average our fringe intensity follows the coronagraph limb observations fairly well. Our greatest intensities and, as we will see below from Table I, our greatest fringe widths are found around position angle 80°–120°, obviously in connection with the active centre near the spot group Zürich No. 28 and 21 of rotation 1406.

The two exposures of λ 6374 show the fringes in the vicinity of the equatorial belt very well but, as to be expected and in agreement with the Climax observations of the same day, with much lower contrast than for the green line. Our drawings, of fig. 8 for λ 5303 and Fig. 9 for λ 6374, show the orientation of the fringe system with respect to the solar corona and to the solar coordinates.

Reduction.—Our main aim was to derive a number of line profiles and a greater number of line half widths (and therefore temperatures) for as much of the corona

TABLE I

Half widths in angstroms of the green corona line λ 5303 A as measured on plate 2. The uppermost row gives the readings of the radial lines originating in the centre of the fringe system as shown in the sketch of Fig. 8. The first column left indicates the number of the interference fringes as given in the same sketch.

Fringe	−65	−60	−55	−50	−45	−40	−35	−30	−25	−20	−15	−10	−5	0	+5	+10	+15	+20	+25	+30	+35	+40	+45
1	0·93	0·92	0·92	0·77	0·86	0·82	0·85	0·75	0·63	0·65	0·82						0·80			0·80	0·80	0·91	1·00
2	1·20	0·82	0·81	0·99	0·90	0·92	1·10														0·93	0·97	0·95
3	1·00	0·92	0·81	0·94	1·05	0·91	1·19														0·87	0·97	0·82
4		0·75	0·96	0·80	0·86	1·09	1·39														0·89	0·89	0·90
5		0·80	0·89	0·85	0·89	1·03	1·32														0·91	0·85	
6		0·94	0·91	0·88	0·94	1·07	1·12														0·92	0·96	
7			1·08	0·87	0·97	1·08	1·36														0·88	0·79	
8			0·86	0·85	0·92	1·01	1·20														0·82	0·79	
9				0·73	0·86	1·26	1·17														0·80		
10				0·76	1·17	1·01	0·96	1·10												0·90	0·71		
11				0·77	1·04	1·03	0·93	1·07												0·79	0·66		
12				0·75	1·08	0·93	1·12	1·05												0·85	0·82		
13					1·10	0·94	1·05	1·46	1·20										0·97	0·90	0·64		
14					1·03	1·12	1·18	1·02	1·27	0·78									0·95	0·87			
15							1·10	1·00	1·43	1·00									0·76	0·93			
16								0·99	1·31	0·93	1·01							0·89	0·91	1·08			
17								1·09	1·11	—	0·95	0·83					0·99	0·92	0·98				
18										0·99	0·85	0·93	0·90	0·92	1·30	0·82	0·82	0·97	0·85				
19											0·80	0·98	0·98	0·89	1·24	0·87	0·86	0·96					
20												0·90	0·99	0·85	1·22	0·95	0·77	1·04					
21													1·04	0·86	1·24	0·90	0·70	1·10					
22													0·88	1·04	0·81	1·23	0·76	1·08					
23														0·95	0·94	1·19	1·00						
24																	0·78						
25																	0·99						

as was imaged with sufficient intensity on our plates. The procedure was the following:

1. The two Hg 198 test plates, taken immediately before and after totality were carefully examined. Both are of excellent quality and prove that adjustment of the interferometer during totality must have been very good.
2. A number of microphotometer tracings were made in different directions through the whole fringe system of the mercury plates using the same adjustment and slit widths (0·06 × 0·016 mm) as were later used for the photometry of the corona fringes themselves. Using the intensity calibration of the plates the line profiles for the mercury fringes were then drawn for different parts of the fringe system. As to be expected from the good quality of the lines as shown in Fig. 7 these profiles could be determined easily and with great accuracy. Since we know from previous interferometric observations (**10**) that the line widths produced by our water-cooled mercury isotope lamp are of the order of 0·007 A, the observed line profiles as derived here, give the instrumental profile of the interference fringes including the effects of the microphotometer, with all the accuracy we need. All the line profiles for the mercury fringes normalised to unity were found to be very similar, as one might expect. Their form as finally adopted for the subsequent reductions, is shown in Fig. 10a. It could be approximated most satisfactorily by a Voigt function (**11, 12**) with $\beta_1/h = 0{\cdot}25$ which is very nearly a pure Gaussian curve. On the other hand from the well-known intensity formula of the Fabry–Perot interferometer (**13**) one can also calculate a theoretical line profile as a function of reflectivity. Fig. 10 shows such a profile, calculated for reflectivity = 0·80; it is nearly a pure dispersion curve and shows fairly extended wings at the lower intensities. These well-known wings are one of the reasons why we have chosen to use the interferometer with the rather large range of about 4A. The observed mercury fringe profiles and the theoretical profiles for a reflectivity slightly below 80 per cent fit each other very well over a large range, small differences becoming perceptible only at low intensities. This, of course, is to be expected since the lowest part of the wings in our mercury exposures approach the threshold of the photographic plates. A similar situation occurs for the corona lines as well; their fringes are superposed on a background formed from an image of the corona, so that photometrically the lowest part of their wings also becomes increasingly uncertain by merging into the corona.
3. The next step was to determine the centre of the fringe system on each eclipse plate, which could be done very accurately, since many fringes are observable. Microphotometric tracings were then carried out along straight lines radial to the fringe system and at intervals of 5°, or 2°·5 as indicated in Figs. 8 and 8 (*a*). Each intersection of such a straight line with one of the concentric fringes gave a record of a line profile. With the help of the intensity calibration for each plate these records were then reduced to intensities in the usual manner. From the observed profiles true profiles and true half widths were then calculated by correcting for the instrumental profile we have already discussed. By half width we always mean the full width of the line at half peak intensity. For this purpose both profiles were represented by Voigt functions and the corrections were

calculated in the manner explained in (**12**). This could be done quite reliably; Voigt functions represent both the intensity profile and the observed profile very satisfactorily, as can be seen from some examples in Fig. 10.

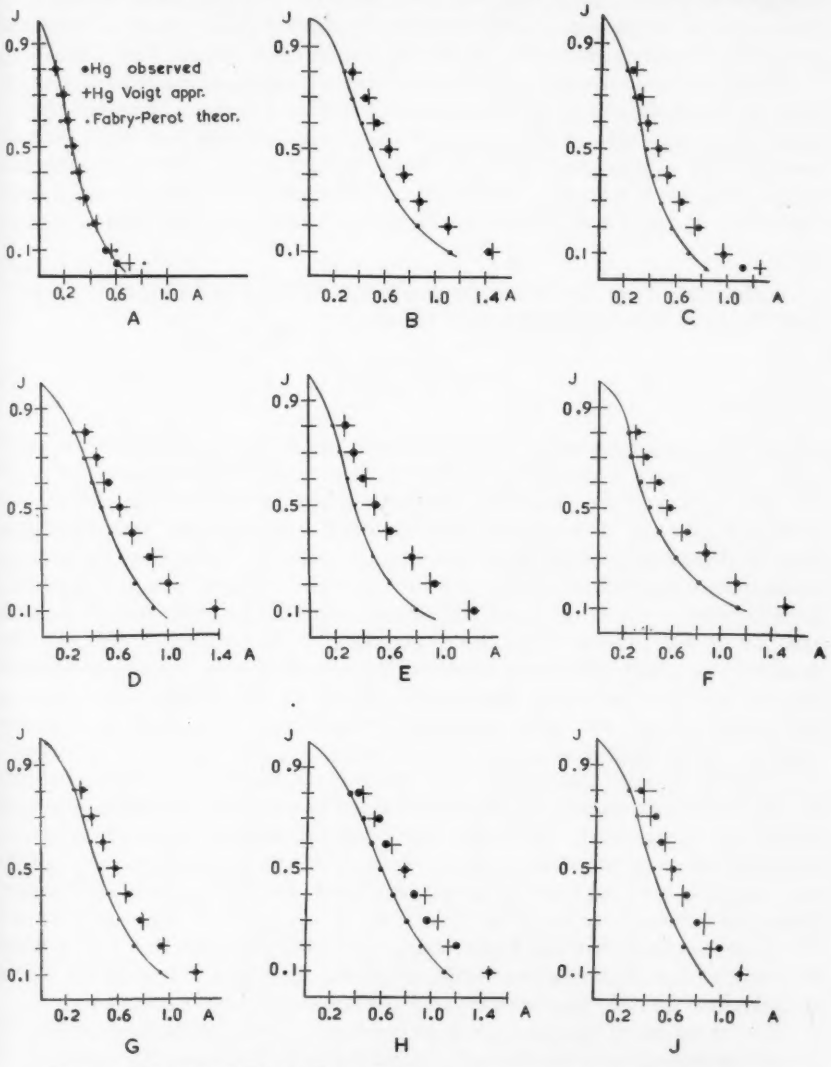

FIG. 10.—*Examples of different line profiles.*

A. *The large dots indicate the observed instrumental line profile for the mercury fringes (including the contribution of the microphotometer), the crosses its representation by a Voigt function and the small dots the profile to be expected from the theory of the Fabry-Perot interferometer (for instance* (**13**)*) accepting a reflectivity of 80 per cent.*

B–G. *Examples of true line profiles for the coronal emission λ 5303 (see Fig. 6). The large dots indicate the observed profiles (including the contribution of the microphotometer), the crosses their representation by a Voigt function and the small dots represent the true line profile expressed also by a Voigt function, after correction has been applied by using the instrumental profile of Fig. 10A according to* (**12**).

H–J. *Same as for* B–G *but for the corona line λ 6374.*

As this is the first time that it has been possible to measure profiles and half widths of corona lines over the whole corona in all position angles simultaneously and to a reasonable distance from the Sun, we believe the results to be valuable enough to be given in some detail in Tables I and II. The location with respect to the corona and to the solar coordinates of each point for which a measurement was obtained can easily be found by combining Tables I and II with Figs. 8 and 9.

The interference fringes could be traced with the naked eye easily to a distance from the Sun indicated by the dotted contour in Figs. 8 and 9. But since photometry gets increasingly unreliable when too low a density on the plate is approached records of the weakest parts of the line have not been used. Photometrically the fringes could be traced to their greatest distance from the Sun's centre near position angle 120°, for 5303 A to a maximum distance $1{\cdot}8\,r$ and for the red line 6374 A to $1{\cdot}7\,r$.

Discussion.—From the half width h given in Tables I and II temperatures T could be derived by the well known formula

$$T = \frac{2 \cdot 10^{12} \cdot h^2 \cdot \mu}{\lambda^2} \qquad (1)$$

where μ is the molecular weight (here 56 for iron) and λ the wave length. These temperatures are found from the half widths of the green line to lie between $1{\cdot}6 \times 10^6$ and about $3{\cdot}2 \times 10^6$ deg. K and in a few cases of obviously high excitation (as near position angles 155° or 250°) rise even to about 8×10^6 degrees. If one excludes some of these exceptionally high values the overall mean value from the present measurement is found to be about $3{\cdot}2 \times 10^6$ degrees. The red line gave temperatures between 2·0 and $3{\cdot}5 \times 10^6$ with some values up to about 6×10^6 degrees and an overall mean value near about $3{\cdot}5 \times 10^6$ degrees. We do not consider the small difference between the overall means for the green and for the red line as being significant. Some of the fringes arise from a corona background with quite steep intensity gradient. Also there is in several regions a good deal of structure in the corona, e.g. near position angle 230°. As is known in other line profile work, there is necessarily some additional uncertainty where the lines are superposed on a rapidly varying or otherwise uncertain continuous background. Although most fringes have been measured on two or more different recordings and in spite of the fact that the internal accuracy usually was very good, we would assume the general accuracy of half widths of these rather broad and diffused lines would be of the order of ± 10 per cent. Since the contrast for the green fringes is much higher than for the red the results for λ 5303 must be considered as much more reliable than those for λ 6374. But on the whole temperatures derived from both lines for the same region agree quite well.

It is of course of special interest to investigate if the line widths or relative intensities depend upon the distance from the centre of the Sun as this would throw some light on the general physics of the corona. For this purpose we have determined the peak intensity of the fringes relative to the coronal background J/J_0. But it must be kept in mind that these intensities are only relative. Further, the corona background in this case is a rather arbitrary one, produced in a somewhat complicated way by the transmission function of the interference filters and of the interferometer. For this reason it appears impracticable to reduce them to absolute intensities.

TABLE II

Half widths in angstroms of the red corona line λ 6374 A as measured on plates 3 and 4. The uppermost row gives the readings of the radial lines originating in the centre of the fringes system as shown in the sketch of Fig. 9. The first column left indicates the number of the interference fringes as given in the same sketch.

Fringe	−47·5	−45·0	−42·5	−40·0	−37·5	−35·0	+15·0	+17·5	+20·0	+22·5	+25·0	+27·5	+30·0	+32·5
5			1·39	1·15	1·35	1·15								
6		1·08	1·20	1·20	1·45	1·25								
7	1·07	1·08	1·14	1·25	1·16									
8	1·10	1·15	1·22	1·20	1·16									
9				1·05	1·25									
10		1·01	1·10	1·10	1·37						1·17			
11		0·96		1·30	1·44					1·05	1·25	1·20		1·20
12										1·05	1·12		1·10	1·10
13									1·15	1·28	1·21		1·15	1·15
14							1·05			1·20			1·16	
15							1·10	1·15		1·17				
16							1·12	0·93		0·90				
17										1·05				
18														

Unfortunately because of the curvature of the fringes for most position angles there are only a few points available along a radial line passing through the centre of the Sun. For several typical position angles where sufficient points were available we have nevertheless plotted line widths in Fig. 11 and relative intensities J/J_0 in Fig. 12 for λ 5303 against distances from the Sun's centre. The measurements show hardly any change in the line width with distance, indicating a rather uniform temperature through the region of the corona covered by our observations.

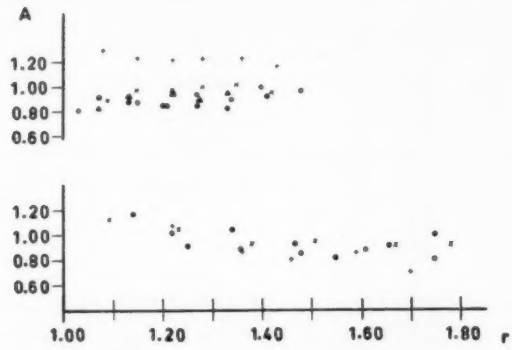

FIG. 11.—*True line half-widths of λ 5303 against distance r from the centre of the Sun.*
Upper sketch: half-widths along 5 radii between −10° and +10° in our arbitrary scale of Fig. 8, i.e. around position angle 230°.
Lower sketch: Half-widths along the fringes 3 to 6, i.e. around position angle 90° (equator east).

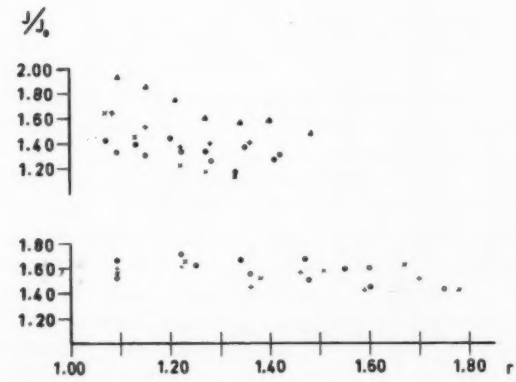

FIG. 12.—*Peak intensities J/J_0 of some fringes for λ 5303, relative to the coronal background (plate 2), against distance r from the Sun's centre.*
Upper sketch: Intensities along 5 radii between −10° and +10° in our arbitrary scale of Fig. 8, i.e. around position angle 230°.
Lower sketch: Intensities on fringes 3 to 6 near position angle 90° (equator east).

While it is known (**14, 15**) that for larger numbers of observations there is statistically a tendency for the equivalent width of the emission lines to decrease with increasing distance from the Sun our measurements show hardly any such effect, presumably because it is masked by the general scatter of the individual values.

As is well known, the intensities and also the widths of the corona lines can vary appreciably for different position angles around the Sun. In Fig. 13 we have plotted our half widths of λ 5303, for three different distances from the Sun's centre, as a function of the position angle. From this figure it becomes clear that there is a good deal of variation of the widths with position angle. The high values between 80° and 180° are certainly connected with the active area around the large spot group mentioned above and similarly the maximum at position angle 240 is probably connected with another photospheric disturbance indicated by a large prominence visible there on the day of the eclipse. It can also be seen from Figs. 11 and 13 that there is hardly any alteration in the width of the line with increasing distance from the Sun.

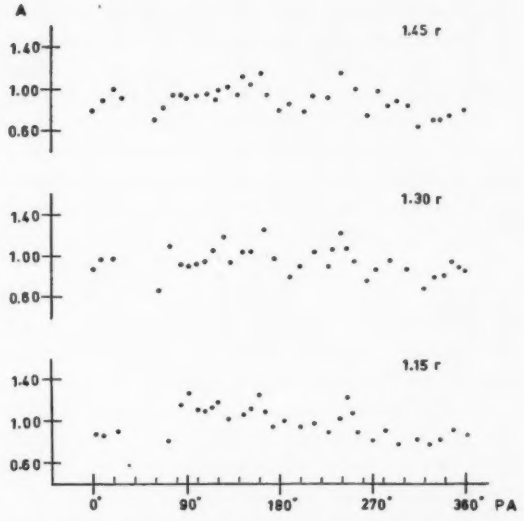

FIG. 13.—*True half-widths of* λ 5303 *plotted against position angle for different distances r from the Sun's centre.*

Further outlook.—The experience gained in this work shows that it is quite possible during a total solar eclipse to obtain a large number of line profiles for λ 5303 over the area of the corona by using modern interferometric techniques. This holds also for the λ 6374 line, if very narrow band filters can be used and if the line at the moment of the observations happens to be not too weak. In our case, admittedly during a period of unusually high solar activity, fringes of λ 5303 could be traced up to 1·8 solar radii from the Sun's centre. This was achieved with an equivalent focal ratio of 5·6, a peak transmission of the interference filter of 40 per cent, a reflectivity of the interferometer of 70 to 80 per cent and with an exposure time of about 20 seconds only. It would be of great interest to obtain line profiles to still greater distances from the Sun's centre and with special equipment this could probably be done quite well. In principle it should be possible to work with special optical equipment at a focal ratio of about 1 : 2. Furthermore one could avoid or reduce the loss of light at several surfaces of the auxiliary filters and lenses and could make use of the full maximal transparency of 70 to 80 per cent of

TABLE III

Line half width in A.U. *and in brackets corresponding temperatures using formula* (1) *in* 10^6 *deg* K.

Number	Year	Author	λ 5303	λ 5694	λ 6374	Res. Power in A.U.	Instrument	Reference
1	1931 1936	Lyot	0·8–1·2 (2·5–5·7)		~1·0 ~(2·8)	0·6	Pic du Midi Coronagraph	20
2	1941 1947	Waldmeier	1·3 (6·8) 0·56–1·08 (1·2–4·5) 0·8–1·3 (2·6–6·8)			0·8	Arosa Coronagraph	21
3	1953	Lyot/Dollfus			0·91–0·97 (2·2–2·5)	0·23	Pic du Midi Coronagraph	22
4	1954	Pecker, Billings, Roberts	0·92–1·19 (3·2–5·7)	1·19–1·48 (3·5–5·5)	1·11–1·47 (3·3–6·0)	0·5	Climax Coronagraph, old	23
5	1955	Jarrett, v. Klüber	0·7–1·1 (2·0–4·8)			0·21	Interferometer during eclipse 1954	1
6	1956	Billings, Hirsch, Varsavsky	~0·6–1·0 ~(1·4–4·0)		~0·7–1·2 ~(1·4–4·0)	0·5	Climax Coronagraph, old	24
7	1957	Billings		1·32 (4·2)		0·15	Climax Coronagraph, new	25
8	1959	Billings	0·78 (2·4)		0·94 (2·4)	0·15	Climax Coronagraph, new	26
9	1960	Jarrett, v. Klüber	0·6–0·9 (1·6–3·2)		0·9–1·2 (2·0–3·5)	0·50	Interferometer during eclipse 1958	present publication

modern interference filters. Furthermore, special plates could give gain in speed by perhaps a factor of 2, and if one is prepared to devote the whole duration of totality, say 200 seconds, to one exposure a further factor of about 10 should be gained. If one takes further into account that the intensity gradient of the corona becomes less steep with increasing distance from the Sun but that the intensity gradient for the corona emission lines seems to be steeper than for the continuum (**16**) we estimate that it should be possible under favourable circumstances and depending upon the properties of the filter, to obtain fringes up to about 2·5 solar radii from the Sun's centre.

If one restricts oneself to a few fringes only photoelectric observations of high accuracy should well be possible with a Fabry–Perot device. Actually such arrangements have alrady been designed elsewhere (**5**).

As has been observed for some time, temperatures within the corona derived from spectrographic observations either with coronagraphs or during a total solar eclipse have a quite obvious tendency to be higher than temperatures derived by other methods (**17, 18, 19**). Table III gives a short summary of most of the spectroscopic temperature determinations available so far, using the simple relation (1) for converting line widths into temperatures. Since different authors have reduced and presented their results in somewhat different ways only average mean values could be given in the Table and to obtain accurate figures the original publications, as quoted, should be consulted. Some local and exceptionally high values are excluded from the Table.

Acknowledgments

The expedition to Atafu Islands was sponsored by the Joint Permanent Eclipse Committee of the Royal Society and Royal Astronomical Society. We are also indebted to Dr B. H. Billings of Baird Atomic Inc., Cambridge, Mass. for the production of the narrow band interference filter for λ 6374 and to the research laboratory of Kodak Ltd., Harrow, for providing several photographic test emulsions as well as the emulsions actually used for our observations. The preparations for our expedition and our work on Atafu Island received much support from Mr G. W. Markham of D.S.I.R., Wellington, N.Z., J. L. Thomsen, Director of the Carter Observatory, Wellington and from the Tokelau Islands Administration in Samoa. The Royal New Zealand Air Force stationed at Lauthala Bay, Suva, Fiji, and its Commanding Officer, then Group Captain A. S. Agar, provided us with transport between Fiji and Atafu by Sunderland flying boat. We should specially thank the Faipule and our many friends of Atafu village for their most friendly hospitality and for their constant helpfulness, given despite the inconvenience and trouble which our presence in their small community must have caused.

The Observatories,
Madingley Road,
Cambridge:
1960 *November.*

References

(1) A. H. Jarrett and H. von Klüber, *M.N.*, **115**, 343, 1955.
(2) H. von Klüber, *Naturwissenschaften*, **42**, 3, 1955.
(3) M. Waldmeier, *Mitteil. Eidgen. Sternwarte*, Zürich No. 149, Abb. 11, 1947.
(4) H. von Klüber, *Sky and Telescope*, **15**, 538, 1956.
(5) ——, *Naturwissenschaften*, **46**, 437, 1959.
(6) ——, *Naturwissenschaften*, **43**, 28, 1956.

(7) Kodak Data Booklet SE 3—*Scientific Plates.*
(8) Kodak Data Booklet GN 5—*Photography in the Tropics.*
(9) *Mitteil. Eidgen. Sternwarte*, Zürich No. 221, 1959.
(10) H. von Klüber, *Nature*, **181**, 1007, 1958.
(11) W. Voigt, *Münchener Berichte*, 1912, p. 603.
(12) H. C. van de Hulst, J. J. M. Reesinck, *Ap. J.*, **106**, 121, 1947.
(13) S. Tolansky, *High Resolution Spectroscopy*, London, 1947.
(14) H. C. van de Hust, *The Sun*, Chicago 1953, p. 271.
(15) M. Waldmeier, *Zeitschr. f. Astrophysik*, **22**, 1, 1942.
(16) C. W. Allen, *M.N.*, **106**, 137, 1946.
(17) C. W. Allen, *Report on Progress in Physics* **17**, 135, 1954.
(18) C. de Jager, *Handbuch der Physik* Bd. **52**, 270, 1959.
(19) A. Unsöld, *Zeitschr. f. Astrophysik* **50**, 48, 1960.
(20) B. Lyot, *C.R.*, **194**, 443, 1942; *C.R.*, **202**, 392, 1936; *M.N.*, **99**, 586, 1939.
(21) M. Waldmeier, *Zeitschr. f. Astrophysik*, **20**, 323, 1941; *Zeitschr. f. Astrophysik*, **21**, 120, 1941 *Astron. Mitteil. Eidgen. Sternwarte Zürich*, No. 149, 1947.
(22) A. Dollfus, *C.R.*, **236**, 996, 1953.
(23) Ch. Pecker, D. E. Billings, W. O. Roberts, *Ap. J.*, **120**, 509, 1954.
(24) D. E. Billings, S. Hirsch, C. Varsavsky, *Ap. J.*, **123**, 532, 1956.
(25) D. E. Billings, *Ap. J.*, **125**, 817, 1957.
(26) D. E. Billings, *Ap. J.*, **130**, 961, 1959.

SPECTRAL CLASSIFICATION AND PHOTOMETRY OF SOUTHERN B STARS

M. W. Feast, R. H. Stoy, A. D. Thackeray and A. J. Wesselink

(Received 1960 November 1)

Summary

248 B stars drawn from the Cape Zone Catalogue of faint stars, from the Tonantzintla lists of OB stars, from Selected Areas 172, 193, 194 and from the Henry Draper Catalogue have been observed for spectral classification. Of these, 184 have been observed photoelectrically in three colours at the Cape or Radcliffe Observatories. Corrected distance moduli (based on MK classes and $B-V$ photometry) are tabulated. Stars with computed distances greater than 3 kpc are plotted on the galactic plane (together with northern stars from Hiltner's list). A considerable concentration of distant supergiants is found in longitudes (l^{II}) 328 to 336°. 46 Tonantzintla OB stars are nearly all classified as B2 or earlier, but only two supergiants are found among them.

1. *Introduction.*—This paper presents spectral classifications of faint southern B type stars based on material obtained with the 2-prism Cassegrain spectrograph attached to the 74-inch Radcliffe reflector, combined with photoelectric observations in three colours made with the 74-inch reflector or with the 24-inch Victoria telescope of the Royal Observatory, Cape. Distance moduli based on MK classes and $B-V$ photometry have been calculated for stars adequately observed.

2. *Selection of stars.*—The object of the investigation has been to improve our knowledge of distant regions in the galactic plane visible from the southern hemisphere. We have therefore been at pains to draw on sources of B stars fainter than the limit of the HD Catalogue, although it is known that the HD Catalogue includes fainter stars in the southern hemisphere than in the northern.

The stars in this programme have been selected from the following sources:

(*a*) All stars classified as " B " or B2 and earlier by Miss Cannon in the Cape Zone Catalogue of Faint Stars ($-40°$ to $-52°$). Many of these are not in the HD or HDE Catalogues.

(*b*) The Tonantzintla lists (**1**) of OB stars in the region 16^h to 19^h R.A. Stars in rich and apparently transparent portions of the Milky Way, judged by examination of Franklin-Adams Charts, were favoured.

(*c*) Stars in Selected Areas 172, 193, 194, classified by the Potsdam workers (**2**) as B2 or earlier. With few exceptions all such stars are included in our tabulation.

(*d*) Miscellaneous stars from the HD Catalogue (B5 and earlier) fainter than 8·5 visual magnitude in the region 14^h to 17^h R.A.

(*e*) A few stars in Hiltner's Catalogue (**3**) were observed photoelectrically for overlap.

Photoelectric observations are available for nearly all stars except those in group (*d*). Stars of group (*a*) are restricted to two regions of R.A.—near 8^h and 16^h—where the Cape Zone cuts the Milky Way. For climatic reasons the 8^h stars were observed photoelectrically by Stoy at the Cape Observatory while the 16^h stars were observed by Wesselink at the Radcliffe Observatory. Stars in

group (*b*) were all observed at the Radcliffe Observatory, while some stars in group (*c*) were observed at the Cape. Group (*d*) was added to the spectroscopic programme as covering longitudes where galactic rotation effects are large; supergiants are scarce in the region 14^h to 16^h R.A. and the discovery of even a few would be of importance.

3. *Spectral classification.*—All programme stars were initially observed at dispersion 86 A/mm at Hγ with projected slit-width 0·027 mm on 103aO emulsion, except that a few stars in group (*c*) have already been classified at the Radcliffe Observatory (**4**) on the basis of plates at 49 A/mm or 29 A/mm at Hγ; these classifications are requoted here for the purpose of coordinating our material on the Selected Areas 172, 193, 194. About half of the stars in groups (*a*), (*c*) and most of those in groups (*b*), (*d*) were classified on the basis of one plate only at 86 A/mm. For the remainder, duplicate plates are available, including some at 49 A/mm at Hγ taken specifically for radial velocity. Spectral classifications were made by comparison with MK standards, usually in duplicate (by Feast and Thackeray).

4. *Photometry.*—The Cape three-colour photoelectric observations (Table I, Nos. 1–103) were made with the 24-inch Victoria Refractor in the usual manner (**5**) and the blue and yellow observations reduced to the standard Johnson V, $B-V$ system using the latest transformation formulae (**6**). It is believed that the systematic deviations from this standard system are now less than the accidental errors of observation. Each star is normally observed at least four times and the standard error of the resulting magnitudes and colours is usually less than $\pm 0^m{\cdot}01$, but because of the richness of the field surrounding many of the present stars and the 45″ diameter of the diaphragm used and also because of possible slight intrinsic variability of many of the stars concerned, the results given in Table I do not always attain this accuracy.

The " refractor " $(U-B)_C$ colours are on the system set out in Cape Mimeogram No. 5. No attempt has been made to convert these colours to the Johnson $(U-B)$ system which refer to observations made with an aluminized reflecting system and thus contain a very much wider band of ultra-violet light. Properties of the V, $B-V$, $(U-B)_C$ system are described in a forthcoming Royal Observatory Bulletin.

For a number of stars which were not observed photoelectrically, magnitudes and colours on the V, $B-V$ system have been extracted from the Cape Photographic Catalogue for 1950.0 (**7**) following the precepts given in the introduction to that catalogue. These magnitudes and colours have a probable error of the order of $\pm 0^m{\cdot}05$; they are distinguished by being given in italics in Table I where the magnitudes have been rounded off to $0^m{\cdot}1$.

For the Radcliffe observations (Table I, Nos. 142–248) the photometric equipment and observational procedure were the same as that previously described (**8**). As before, the diaphragm usually used had a diameter of 18″ of arc. Standards of magnitude and colour as published by the Royal Observatory, Cape, (**9**) have been used throughout. Conversion to Johnson V, $B-V$ was effected by means of the Cape relations (**9**) together with final corrections according to Cousins (**6**). The ultra-violet colours U_R-B_R are on the same system as previously described (**8**) and cannot be converted to the Johnson system. The observations were reduced to the zenith using extinction coefficients of 0·16, 0·33 and 0·50 per atmosphere (for V, B, U respectively) at the zenith in Pretoria.

TABLE I

No.	C.P.D.	H.D.	α (1900)	δ	*l*II	*b*II	*V*	*B*–*V*	(*U*–*B*)$_0$	Sp.	$m_0 - M$	
1	−42°2357		8h15·6	−42°33	260·0	−3·8	9·90	+0·46	+1·30	B2::Vn	10·3:	
2	41 2449		8 19·3	41 52	259·8	−2·9	9·86	0·31	1·30	B1V	11·7	
3	44 2758		8 31·0	44 41	263·3	−2·8	10·33	0·25	1·29	B1V	12·4	
4	45 2718		8 33·6	45 10	264·0	−2·8	9·10	0·19	1·29	B2 III	11·4	
5	44 2824	73568	8 33·9	44 51	263·8	−2·5	8·33	0·31	1·30	Bo·5 III	11·5	
6	−45°2733		8 34·0	−45 46	264·5	−3·0	10·53	+0·11	+1·28	B3 III	12·5	
7	44 2827		8 34·3	44 15	263·3	−2·1	9·89	0·23	1·31	B2 III	12·1	
8	45 2772	73903	8 35·7	45 52	264·8	−2·9	8·96	0·23	1·31	B1V	11·1	R
9	45 2826		8 37·5	45 44	265·1	−2·3	10·16	0·21	1·28	B2:Vne	11·3:	R
10	44 2920		8 37·8	44 55	264·3	−2·0	8·48	0·40	1·36	B2·5 II	11·3	
11	−45°2877	74528	8 39·3	−45 12	264·6	−2·0	8·44	+0·16	+1·30	B2:Vn	9·7:	
12	45 2896		8 40·0	46 05	265·4	−2·4	10·01	0·05	1·29	B2 V	11·6	
13	45 2907	74677	8 40·2	45 44	265·2	−2·2	8·62	0·24	1·31	B1 III	11·6	
14	50 1776		8 42·8	50 36	269·2	−4·9	9·87	0·43	1·40	B3 V	9·7	R
15	46 3039	75465	8 45·0	46 32	266·3	−2·1	9·0:	0·22	1·30	B3 Vn?e	9·4:	R
16	−44 3129		8 46·5	−44 12	264·7	−0·4	9·43	+0·72	+1·42	O9·5 Ib	12·7	
17	45 3131		8 46·8	45 09	265·4	−1·0	8·92	0·38	1·31	Bo·5 V	10·9	
18	45 3145		8 47·1	45 10	265·5	−0·9	9·1	0·40	1·26	B2:Vne	9·7:	R
19	45 3174		8 47·8	45 18	265·7	−0·9	8·97	0·40	1·32	Bo·5 III	11·8	
20	48 1997		8 48·7	48 36	268·3	−2·9	10·78	0·10	1·32	Bp (?shell)		R
21	−47 2857		8 49·3	−47 12	267·3	−1·9	9·66	+0·22	+1·32	B5 V	9·5	
22	45 3218		8 49·9	45 39	266·2	−0·8	8·90	0·78	1·47	Bo·5 III	10·6	
23	47 2896		8 50·9	47 07	267·4	−1·7	9·65	0·49	1·37	B1 III	11·8	
24	46 3272		8 53·5	46 40	267·4	−1·0	9·06	0·81	1·46	Bo·5 Ib	12·2	
25	42 3167		8 54·0	42 19	264·1	+1·9	9·73	0·41	1·40	B1 V	11·3	
26	−47 2976		8 55·1	−47 54	268·5	−1·6	9·79	+0·72	+1·46	Bo IV	11·7	
27	41 3206		8 56·0	42 03	264·2	+2·3	9·84	0·39	1·44	B2·5 V	10·1	
28	47 3067	78344	9 02·4	47 22	268·9	−0·4	8·96	1·10	1·54	O9·5 Ia	11·3	
29	47 3070	78345	9 02·6	47 55	269·3	−0·7	9·36	0·90	1·52	Bo·5 II	11·4	
30	43 3397	78958	9 06·0	43 29	266·5	+2·7	8·97	0·68	1·44	Bo·5 Ib	12·5	

TABLE I (*continued*)

No.	C.P.D.	H.D.	(1900) α	δ	l^{II}	b^{II}	V	$B-V$	$(U-B)_0$	Sp.	m_0-M	
31	−41°3586	80834	9h16·9	−41°45	266·7	+5·4	9·72	+0·26	+1·24	BVnne		R
32	50 2284	298369	9 18·6	50 45	273·2	−0·8	9·95	0·38	1·32	B2:Vne	10·6:	R
33	51 2174	298377	9 20·6	51 32	274·0	−1·2	10·27	0·28	1·29	B3:Vn	10·5:	
34	51 2299	298429	9 27·2	51 13	274·5	−0·2	9·67	0·55	1·33	O9 III	13·2	
35	50 2428	298425	9 27·5	50 59	274·3	0·0	9·67	0·54	1·33	O9 V	11·9	
36	−50 2761	297624	9 45·3	−50 38	276·2	+2·1	10·19	+0·24	+1·32	B2 V	11·2	
37	50 2767	297625	9 45·5	50 41	276·3	+2·0	10·5	0·16	1·3	B5 V:?e	10·5:	R
38	51 2828	298742	9 54·6	51 38	278·0	+2·2	11·01	0·22	1·49	B9 V	9·6	
39	60 2606	97319	11 06·9	60 34	291·1	−0·5	8·5	0·25	1·26	O9·5 Ib	13·2	
40	59 3142	306145	11 07·0	59 23	290·7	+0·5	9·55:	0·37	1·30	B2::Vne	10·2:	R
41	−59 3138		11 07·0	−60 07	291·0	−0·1				G		R
42	60 2613	306097	11 07·1	60 22	291·1	−0·4	8·85:	+0·66	+1·43	O9 III	12·0:	
43	58 3268	97471	11 07·8	58 16	290·4	+1·6	*9·3*	*−0·01*		Bo V	12·8	
44	60 2638	97484	11 07·9	60 33	291·2	−0·5	8·4	+0·32	1·28	B+B		R
45	58 3282	303922	11 08·1	58 40	290·6	+1·3	10·34	+0·53	1·65	F7 V		R
46	−58 3286	97521	11 08·2	−58 18	290·5	+1·7	9·52	+0·04	+1·21	B2 V	11·2	
47	57 4420	97533	11 08·3	58 06	290·5	+1·8	8·28	0·03	1·20	B1:Vn	11·0:	
48	60 2665	97581	11 08·5	60 12	291·3	−0·1	8·82	0·26	1·26	B1 III	11·7	
49	60 2696	306205	11 09·2	60 43	291·5	−0·6	9·94	0·14	1·28	B1·5 Vne	11·8	R
50	59 3216	306157	11 09·3	59 45	291·2	+0·4	10·32	0·50	1·36	B1 V	11·6	
51	−60 2698	97707	11 09·3	−60 12	291·4	−0·1	8·05:	+0·51	+1·36	B2 Ia	13·1:	
52	58 3351	97848	11 10·2	58 29	290·8	+1·6	*8·7*	*−0·02*		O9 III	13·9	
53	60 2718	306196	11 10·2	60 31	291·6	−0·3	9·61	+0·34	1·36	Bo:Vn	12·1:	
54	59 3241	306168	11 10·4	60 07	291·4	+0·1	9·5	+0·22	1·24	B3:V	9·9:	R
55	58 3366	97913	11 10·6	58 38	290·9	+1·5	*8·8*	*+0·08*		B1 V:	11·4:	
56	−58 3372	97966	11 10·9	−58 52	291·1	+1·2	*8·8*	*+0·10*		O7·5	12·9	
57	59 3259	97969	11 10·9	59 37	291·3	+0·6	7·69	0·02	+1·21	B1:Vn	10·4:	
58	58 3406	306234	11 12·4	59 02	291·3	+1·2	10·15:	0·28:	1·31:	B2 V	11·1:	
59	60 2774	98210	11 12·7	60 23	291·8	−0·1	8·79	0·08	1·20	Bo·5 III	12·6	
60	60 2783	98260	11 13·0	60 58	292·0	−0·6	9·69	0·26	1·28	B1·5 III	12·2	
61	−57°4563	98481	11h14·6	−57°40	291·1	+2·5	9·15	+0·01	+1·20	B2 III	12·0	

60	60 2783	98260	11 13·0	60 58	292·0	−0·6	9·69	0·26	1·28	B1·5 III	12·2	
61	−57°4563	98481	11h14·6	−57°40	291·1	+2·5	9·15	+0·01	+1·20	B2 III1	12·0	
62	61 2195		11 14·8	61 30	292·4	−1·0				B5 Ib		
63	60 2829	98624	11 15·7	60 41	292·3	−0·2	9·77:	0·22	+1·22	B1:Vne	11·9:	R
64	60 2842		11 16·5	60 30	292·3	0·0	10·74	0·10	1·24	B2 III	13·3	R
65	60 2857	306387	11 17·6	60 29	292·4	0·0	9·51:	0·16	1·26	B1·5 III	12·3	
66	−60 2867	98927	11 17·9	−60 31	292·4	0·0	*9·3*	*+0·1*		B1·5 Ve	11·3:	R
67	59 3411	99024	11 18·6	59 58	292·3	+0·6	9·65	0·01	+1·21	B2:V	11·4:	
68	60 2893	99160	11 19·5	60 48	292·7	−0·2	*9·2*	*0·2*		O9 II:	13·8:	
69	58 3578	306480	11 20·0	59 03	292·2	+1·5	11·13	0·16	1·35	B5 III:	12·4:	
70	60 2920	99354	11 20·8	60 43	292·8	−0·1	8·95	0·13	1·22	B1 IIIne	12·2	R
71	−58 3620	99546	11 22·0	−58 53	292·4	+1·7	8·29	−0·04	+1·14	O8	12·7	
72	61 2350	99897	11 24·4	62 06	293·7	−1·2	8·32	+0·18	1·23	O6	12·3	
73	62 2075	100199	11 26·6	62 23	294·0	−1·4	*8·1*	*0·0*		B1 III p	11·8:	R
74	61 2541	101794	11 37·7	61 55	295·1	−0·6	8·66:	+0·06	1·22	B1·5:V	10·7:	
75	59 3727	306962	11 37·8	59 25	294·4	+1·8	9·64	+0·20	1·21	Bnnep		R
76	−60 3272	306922	11 37·9	−60 56	294·9	+0·3	10·26	+0·21	+1·25	Bnne		
77	61 2551	101837	11 38·1	61 52	295·1	−0·6	8·5	−0·01	1·20	B2:+B2:		R
78	61 2550	101838	11 38·1	62 00	295·2	−0·7	8·40	+0·02	1·19	B1 III	12·0	
79	P193/1621		11 38·7	59 35	294·7	−1·3				Cluster		R
80	61 2560	101964	11 38·9	61 58	295·3	−0·7	(8·3)			Bo·5 III		
81	−61 2622	102475	11 42·5	−61 52	295·6	−0·5	*8·5*	*−0·03*		Bo·5 II	13·3	
82	61 2636	102567	11 43·2	61 39	295·6	−0·2	*9·1*	*+0·3*		B1 Vne	11·0:	R
83	61 2691	102997	11 46·3	61 17	295·9	+0·2	*6·5*			B3 I		
84	59 4396	110360	12 36·4	60 06	301·8	+2·2	*9·3*	*+0·2*		O7·5	13·2	
85	60 4253	110498	12 37·4	61 06	302·0	+1·2	9·66	+0·49	+1·35	Bo·5 III	12·2	
86	−58 4474	110785	12 39·3	−59 05	302·1	+3·2				B2 V		
87	60 4271	311815	12 39·5	60 42	302·2	+1·6	10·77	+0·47	+1·43	B5 V	9·9	
88	59 4423	110863	12 40·0	60 00	302·2	+2·3	*8·8*	*0·44*		B2 V	9·3	
89	59 4468		12 42·9	59 22	302·6	+3·0	10·26:	0·22	1·32	B2:Vnne	11·4:	R
90	58 4539		12 44·4	58 29	302·8	+3·8	11·21	0·07	1·40	B5:V	11·5:	
91	−58 4589	112147	12 49·2	−58 27	303·4	+3·9	*9·0*	*+0·36*		B3 pe		R
92	59 4580	112181	12 49·5	60 07	303·4	+2·2	8·79	0·11	+1·22	B1 Vn	11·3	
93	57 5810	112484	12 51·8	57 51	303·8	+4·5	9·05	0·04	1·22	B2 V	10·7	
94	59 4654	113012	12 55·6	59 32	304·2	+2·8	8·13	0·11	1·20	Bo Ib	13·3	
95	59 4684		12 56·9	59 39	304·4	+2·6	10·41	0·18	1·28	B2 V	11·6	

TABLE 1 (*continued*)

No.	C.P.D.	H.D.	(1900) α	δ	l^{II}	b^{II}	V	$B-V$	$(U-B)_C$	Sp.	m_0-M	
96	−59°4693	113261	12h57·4	−59°50	304·4	+2·5	8·89	+0·22	+1·36	B5 III	9·9	
97	59 4711	113421	12 58·4	59 18	304·6	+3·0	9·34	0·20	1·26	Bo·5 III	12·8	
98	59 4766	114024	13 02·5	59 08	305·1	+3·1	9·78	0·27	1·26	Bo·5 Ia	15·2	
99	60 4480		13 03·6	60 36	305·2	+1·7	9·55	0·23	1·31	B2 Vn	10·6	
100	60 4485	114213	13 04·0	60 56	305·2	+1·3	8·98	0·91	1·53	B1 I(b)	11·8	
101	−60 4528		13 06·9	−60 34	305·6	+1·7	8·74	+0·23	+1·26	B1 III	11·7	
102	61 3566	115316	13 11·3	61 55	306·0	+0·3	9·32	0·24	1·26	B1 V	11·4	
103	59 4914	115805	13 14·4	59 28	306·6	+2·7	9·71	0·35	1·28	B1:Vnne	11·5:	R
104	56 6153	123113	14 00·6	56 39	313·1	+4·2	*9·5*	*0·0*		B3 V	10·6:	
105	59 5432	123465	14 02·7	59 32	312·6	+1·4	*9·3*	*0·0*		B2 V	11·1:	
106	−61 4385	123609	14 03·5	−61 51	312·0	−0·8	(9·8)			B3 V		
107	64 2785	124300	14 07·5	64 16	311·7	−3·3	(10·0)			B2 V		
108	61 4443	124397	14 08·2	61 45	312·6	−0·9	(9·6)			B1 V:		
109	60 5273	124788	14 10·4	60 19	313·3	+0·3	*9·0*	*+0·28*		B5 V	8·7	
110	60 5276	124909	14 11·1	60 26	313·3	+0·2	*9·0*	*+0·26*		B1 III	11·9	
111	−57 6592	125106	14 12·1	−57 59	314·2	+2·5	(10·5)			B2 V		
112	65 2683	125211	14 12·8	65 52	311·7	−5·0	*9·3*	*0·00*		B2 V	11·0	
113	61 4498	125515	14 14·7	61 57	313·2	−1·4	*9·6*	*+0·3*		B5 V	9·2:	
114	60 5353	126004	14 17·8	60 52	313·9	−0·5	(9·2)			B3 Vne		R
115	54 5991	126114	14 18·4	54 08	316·3	+5·8	*9·1*	*+0·02*		B2 V	10·8	
116	−59 5569	126357	14 19·8	−59 17	314·7	+0·9	*9·15*	*+0·13*		Bo·5 II	13·5	
117	59 5612	126940	14 23·4	59 52	314·9	+0·2	*9·4*	*+0·46*		B1·5 II:	12·4:	
118	64 2891	127061	14 24·0	64 17	313·4	−3·9	(9·6)			B3 V		
119	61 4605	127503	14 26·6	61 57	314·5	−1·8	*9·5*	*+0·2*		B1 V	11·7:	
120	60 5443	127838	14 28·4	60 22	315·3	−0·5	*9·12*	*+0·25*		B1 II:	12·9:	
121	−60 5453	127958	14 29·1	−60 32	315·4	−0·7	(9·3)			B1 V		
122	61 4644	128072	14 29·7	61 16	315·1	−1·4	*9·1*	*−0·04*		B2 V	11·0	
123	57 6712	128089	14 29·8	58 00	316·4	+1·6	*8·7*	*+0·31*		B2 V:	9·5:	
124	64 2955	128348	14 31·1	64 14	314·1	−4·2	*9·51*	*+0·25*		B3 V	9·9	
125	50 7122	128585	14 32·6	50 43	319·6	+8·2	(9·2)			B3 V		
126	−62°4246	128842	14h34·2	−62°36	315·1	−2·8	*9·6*	*+0·3*		B7 III:	9·9:	

125	50 7122	128585	14 32·6	50 43	319·6	+8·2	(9·2)		B3 V		
126	−62°4246	128842	14h34·2	−62°36	315·1	−2·8	*9·6*	*+0·3*	B7 III:	9·9:	
127	62 4263	129225	14 36·2	62 51	315·2	−3·1	*9·6*	*+0·4*	B1 III	12·0:	
128	59 5734	130437	14 43·1	59 52	317·2	−0·8	(10·8)		Bnne		
129	51 7214	130534	14 43·7	51 51	320·8	+6·4	*8·8*	*+0·40*	B5 V:	8·1:	
130	59 5739	130612	14 44·0	60 05	317·2	−1·0	*9·0*	*+0·46*	B3 V	8·7	
131	−59 5775	132320	14 53·3	−59 30	318·5	−1·0	*9·42*	*+0·40*	B2 III	11·1	
132	53 6354	134783	15 06·6	53 46	322·9	+3·1	(9·2)		B2:Vp		R
133	57 6957	134844	15 06·9	57 59	320·8	−0·5	*9·2*	*+0·29*	B2 V	10·1	
134	58 5910	136471	15 15·7	58 47	321·4	−1·8	*8·9*	*+0·97*	B1·5 II:	10·4:	
135	49 8031	136556	15 16·2	49 46	326·3	+5·7	(9·7)		Bnne		
136	−60 5814	137405	15 20·7	−60 27	321·0	−3·6	*9·3*	*+0·2*	B2 II	12·9:	
137	58 5962	137603	15 21·8	58 14	322·4	−1·8			WC8+Bo:		R
138	52 8437	137937	15 23·8	52 33	325·8	+2·8	*8·6*	*+0·01*	B5 V:	9·1:	
139	60 5926	138679	15 28·4	60 13	321·9	−3·9	*8·9*	*−0·04*	B2 III	11·9	
140	58 6089	138729	15 28·7	58 15	323·1	−2·3	*9·0*	*+0·38*	B2 V:	9·6:	

TABLE I (*continued*)

No.	C.P.D.	H.D.	(1900) α	δ	l^{II}	b^{II}	V	$B-V$	U_R-B_R	Sp.	m_0-M	
141	−57°7133	139314	15h32·3	−57°44	323·8	−2·2	(10·6)			B2:Ve		
142	45 7545		15 33·4	45 27	331·2	+7·6	10·74	−0·01	+0·52	Bo III	15·3	
143	58 6277	140336	15 37·9	58 38	323·8	−3·4	*9·7*	*+0·3*		B pe		R
144	44 7577		15 38·8	44 11	332·7	+8·1	10·86	+0·05	+0·51	B1·5 V	13·0	
145	48 7958	329905	15 40·7	48 19	330·4	+4·6	10·44	+0·66	+0·61	O9 I	13·8	
146	−59 6394	141522	15 44·4	−59 48	323·8	−4·8	(9·7)			Bo·5 Ia		
147	T13 3 17		15 48·6	54 21	327·6	−0·9	9·93	+0·45	+0·50	Bo·5 III	12·6	
148	T13 3 18		15 50·1	54 16	327·9	−1·0	10·35	0·46	0·49	Bo III	13·5	
149	50 8850		15 52·0	50 41	330·4	+1·6	10·46	0·48	0·60	B1·5 Ve	11·3	R
150	50 8854		15 52·2	50 09	330·7	+2·0	10·23	0·55	0·74	B2 V	10·4	
151	T13 3 19		15 54·0	−53 52	328·5	−1·0	9·75	+0·52	+0·50	O9·5 II	13·2	R
152	−49 8908	330345	15 56·6	49 36	331·6	+2·0	10·27	0·65	0·63	Bo·5 V	11·5	
153	49 8958	144647	16 01·9	49 20	332·5	+1·6	9·97	0·66	0·61	O8	12·3	
154	50 8985		16 02·2	50 49	331·5	+0·4	10·46	0·83	0·81	B2·5 V	9·4	
155	48 8194	144900	16 03·0	48 42	333·0	+1·9	9·66	0·73	0·65	O9 V	11·3	

TABLE I (*continued*)

No.	C.P.D.	H.D.	(1900) α	δ	l^{II}	b^{II}	V	$B-V$	U_R-B_R	Sp.	m_0-M	
156	−48°8196	144918	16h03·1	−48°47	333·0	+1·8	9·97	+0·79	+0·65	O7	12·1	
157	48 8197	144970	16 03·4	48 46	333·0	+1·8	9·74	0·82	0·63	Bo Ve	10·8	R
158	46 7857	144966	16 03·4	46 43	334·4	+3·3	10·01	0·60	0·63	O9·5 V	11·9	
159	T13 3 23	145217	16 04·5	50 03	332·3	+0·8	9·96	0·85	0·68	O8	11·7	
160	50 9059		16 06·2	50 51	332·0	+0·0	10·69	0·56	0·67	B1 III	12·6	
161	−50 9109	145828	16 07·9	−50 44	332·3	−0·1	(10·3)			Bo·5 III:		
162	51 9170		16 09·0	51 47	331·6	−1·0	9·87	+0·85	+0·75	Bo Ia	13·3	
163	51 9171		16 09·0	51 54	331·6	−1·1	9·79	0·85	0·73	Bo Ia	13·2	
164	42 7329		16 09·2	42 55	337·7	+5·4	10·32	0·38	0·80	B8 III	9·9	
165	51 9193		16 09·7	51 31	331·9	−0·9	9·87	0·94	0·80	Bo·5 Ia	13·2	
166	−51 9232		16 10·8	−51 12	332·2	−0·8	10·30	+0·40	+0·58	Bo·5 III	13·2	
167	49 9157	146628	16 12·0	49 31	333·5	+0·3	9·98	0·64	0·64	O9·5 I (a)	13·7	
168	50 9233		16 12·3	50 12	333·1	−0·2	10·17	0·73	0·79	B3 III	10·3	
169	T13 3 38	146955	16 13·8	52 20	331·8	−1·9	9·65	0·18	0·56	B3:V	10·2:	
170	49 9238	330695	16 15·2	49 52	333·7	−0·3	10·42	0·60	0·73	B3 V	9·7	
171	−44 7860	328050	16 16·0	−44 34	337·5	+3·4	10·38	+0·32	+0·61	B3 III	11·7	
172	51 9449	147318	16 16·1	51 54	332·3	−1·8	(9·3)			Bo Ib		
173	46 7948	330587	16 16·7	46 52	336·0	+1·7	9·67	1·17	1·43	G8 III:		R
174	48 8430	330643	16 16·7	48 28	334·8	+0·6	10·71	0·39	0·74	B6: III:	11·0:	
175	T13 3 40	330652	16 17·1	48 35	334·8	+0·4	9·85	0·49	0·63	B2 III	11·3	
176	−48 8443	330642	16 17·3	−48 29	334·9	+0·5	10·37	+0·54	+0·65	B2 III	11·6	
177	T13 3 42	147617	16 17·8	51 48	332·6	−2·0	9·79	0·27	0·39	O9·5 III	13·8	
178	T13 3 44		16 18·7	51 36	332·8	−1·9	9·64	0·24	0·49	B2 III	11·8	
179	48 8499	330806	16 21·6	48 11	335·6	+0·2	9·89	0·33	0·71	B6: III:	10·4:	
180	44 7916	328209	16 22·2	44 15	338·5	+2·8	9·77	0·83	0·69	O9·5 I (a)	12·9	
181	−48 8536	330938	16 24·5	−48 46	335·5	−0·6	10·44	+0·52	+0·64	B2 Vn	10·7	
182	T13 3 51	330950	16 27·1	49 19	335·4	−1·3	9·68	0·46	0·56	B1 Vne	11·1	R
183	49 9449	149298	16 28·7	49 03	335·8	−1·3	9·94	0·45	0·60	B1:Ve	11·4:	R
184	41 7521	149313	16 28·8	41 55	340·9	+3·5	(9·4)			B1:Ve		R
185	47 7793	331003	16 30·6	48 00	336·8	−0·8	10·01	0·53	0·65	B2·5 V	9·9	

186	T13 3 68	328686	16h34·3	−46°42	338·2	−0·4	10·44	+0·47	+0·63	B2 Vn	10·8	
187	T13 3 72	150373	16 35·6	47 21	337·8	−1·0	9·92	0·33	0·52	B3 V	10·0	
188	−47°7883		16 38·3	47 45	337·8	−1·6	9·79	0·67	0·65	Bo·5 Ia	13·9	
189	47 7900	328857	16 39·7	47 08	338·4	−1·4	9·96	0·57	0·60	Bo·5 I (a)	14·3	
190	46 8228N	329034N	16 40·2	46 57	338·6	−1·3	10·33	0·46	0·63	B3 V	9·3:	R
191	−46 8228S	329034S	16 40·2	−46 57	338·6	−1·3				B3 V	9·3:	R
192	46 8232	329033	16 40·6	47 02	338·6	−1·4	10·01	+0·52	+0·62	Bo·5 III	12·5	
193	51 9952		16 41·4	51 42	335·2	−4·6	10·74	0·12	0·58	B2 V	12·2	
194	40 7526	151458	16 42·3	40 38	343·6	+2·5	9·58	0·18	0·60	B5 V	9·6	
195	46 8260	329027	16 43·1	46 59	338·9	−1·7	9·85	0·83	0·69	O9·5 I	13·0	
196	−41 7657	326176	16 43·7	−41 34	343·1	+1·7	9·13	+0·71	+0·62	B1 IV	10·3	
197	42 7539	326364	16 45·6	42 07	342·9	+1·1	9·58	0·35	0·55	Bo IV	12·6	
198	52 10300	151990	16 45·6	52 28	335·0	−5·5	*9·4*	*0·2*		O9 III	14·0:	R
199	41 7683	152060	16 46·0	41 14	343·7	+1·6	9·56	0·07	0·52	B2 IV	11·9	
200	41 7687	326306	16 46·3	41 19	343·6	+1·5	9·82	0·11	0·54	B1 V	12·3	
201	−41 7686	326348	16 46·3	−41 53	343·2	+1·2	9·92	+0·39	+0·57	B1 IV	12·1	
202	41 7697	326327	16 46·6	41 38	343·3	+1·2	9·75	0·27	0·55	B2 IV	11·5	
203	43 7736	326450	16 47·5	43 50	341·8	−0·3	10·13	0·59	0·74	B3 V	9·5	
204	41 7759	326296	16 47·7	41 11	343·9	+1·4	9·82	0·25	0·56	B2 V	10·8	
205	42 7573	152742	16 50·0	42 47	343·0	+0·1	(8·9)			B3 V:		
206	−46 8329	153159	16 52·6	−46 55	340·0	−2·9	9·65	+0·83	+0·80	B3 V	8·3	
207	45 8251	329379	16 53·8	45 33	341·2	−2·2	9·65	1·05	0·95	B1: V	9·3	
208	49 9731		16 55·9	49 54	338·0	−5·2	10·27	0·39	0·56	O9·5 I (a)	14·7	
209	42 7632	326823	16 59·8	42 28	344·3	−1·2	9·00	0·86	0·68	Pec		R
210	50 9971		17 11·0	50 26	339·0	−7·4	10·55	0·01	0·49	Bo·5 III	14·6	
211	−44 8362	329804	17 12·7	−44 38	344·0	−4·3	10·35	+0·51	+0·61	B2 II	13·1	
212	42 7748	323484	17 17·2	42 06	346·5	−3·5	10·08	0·48	0·60	B1 III	12·3	
213	40 7903	323815	17 26·9	40 39	348·7	−4·2	10·21	0·55	0·65	B3 II	12·4	
214	29 4867	316232	17 39·4	29 11	359·8	−0·2	10·25	0·67	0·61			R
215	28 5849	316311	17 41·2	28 55	0·2	−0·4	10·21	0·91	0·75			R
216	−29 4892	316326	17 41·7	−29 18	0·0	−0·7	10·01	+0·62	+0·66			R
217	27 5773	316274	17 42·0	27 43	1·3	+0·1	10·37	0·71	0·83			R
218	T13 3 95	316585	17 46·4	29 48	0·0	−1·8	10·88	0·44	0·52	B1 II:	14·1:	
219	29 5040	316729	17 51·0	29 34	0·8	−2·6	9·90	0·32	0·46			R
220	T13 12 10	314854	17 52·8	26 16	3·8	−1·2	10·68	0·53	0·67	B3: V	10·2:	

TABLE I (*continued*)

No.	C.P.D.	H.D.	(1900) α	δ	l^{II}	b^{II}	V	$B-V$	U_R-B_R	Sp.	m_0-M	
221	T13 12 18	315101	$17^h57{\cdot}9$	$-26°13$	4·4	−2·1	10·41	+0·63	+0·87	B5 III	10·2	
222	T13 12 28	315057	17 59·5	25 20	5·4	−2·0	11·04	0·38	0·54	B1 V:	12·7:	
223	T13 12 33	315181	18 02·1	25 29	5·5	−2·6	10·73	0·24	0·52	B5 V::	10·5:	
224	T13 12 49	167611	18 10·9	18 35	12·5	−1·0	9·45	0·19	0·49	B1 III	12·5	
225	−19°6745	T13 13 20	18 11·3	19 03	12·2	−1·3	9·83	0·27	0·61	B2 V	10·8	
226	−19 6752	T13 13 21	18 11·5	−19 07	12·1	−1·4	9·56	+0·54	+0·63	B1·5 III	11·2	
227	19 6757		18 12·1	19 09	12·2	−1·6	8·94	0·98	0·79	B1·5 Ib	11·6	R
228	18 4892	T13 13 23	18 12·1	18 39	12·6	−1·3	10·02	0·38	0·55	B2 III	11·8	
229	13 4912	T13 13 24	18 12·2	13 53	16·8	+1·0	10·00	1·18	0·96	B2 III	9·3:	
230	12 4975	T13 13 26	18 12·4	12 18	18·2	+1·7	10·46	0·77	0·70	Bo V	11·6	
231	−12 4973	T13 13 25	18 12·4	−12 14	18·3	+1·7	10·82	+0·89	+0·72	B1 III:	11·8:	
232	T13 18 61		18 18·3	13 34	17·8	−0·2	10·51	0·67	0·65	B1 V:	11·3:	
233	−12 5039	T13 13 33	18 19·1	12 08	19·2	+0·3	10·77	1·18	0·91	O6:	11·8	
234	T13 18 71		18 21·1	14 31	17·3	−1·2	9·26	0·52	0·54	Bo III	12·2	
235	T13 18 72		18 21·4	14 22	17·5	−1·2	11·07	0·39	0·59	B2 IV	12·5	
236	−13 4990	T13 13 38	18 22·7	−13 10	18·7	−0·9	10·62	+0·46	+0·56	Bo V:	12·7:	
237	9 4742	T13 13 39	18 22·9	9 39	21·8	+0·7	10·43	0·73	0·69	B2 V:	10·0:	
238	T13 18 78		18 23·9	13 09	18·8	−1·2	11·35	0·58	0·58	B1 III	13·2	
239	9 4748	T13 13 40	18 24·1	9 16	22·3	+0·6	10·83	0·94	0·79	B3 Vn:	9·1:	
240	12 5074	T13 13 41	18 24·5	12 54	19·1	−1·2	10·33	0·57	0·60	B1 V	11·4	
241	T13 18 81		18 25·0	−12 16	19·7	−1·0	11·06	+0·65	+0·77	B5 V:	9·6:	
242	−9 4754	T13 13 43	18 25·4	9 07	22·5	+0·4	10·40	0·83	0·77	B2 III	10·8	
243	6 4787	T13 13 44	18 27·2	6 22	25·2	+1·3	10·22	0·98	0·80	O8: n	11·6	
244	11 4674	T13 13 45	18 28·2	11 16	21·0	−1·2	10·18	1·11	0·89	O9·5 I	12·4	
245	13 5039	171344	18 29·3	13 57	18·7	−2·7	9·52	0·29	0·48	Bo·5 III	12·7	
246	−6 4891	T13 13 49	18 41·2	−6 11	27·0	−1·7	10·49	+0·39	+0·56	B1 V	12·1	
247	6 4903	173820	18 42·2	−6 25	26·9	−2·0	9·89	0·28	0·38	O9 I	14·4	
248	T13 18 98		19 02·6	+3 27	31·9	−5·1	10·84	0·65	0·76	Bo·5: Vp	12·0:	R

Remarks on stars in Table I

9. Hβ, γ emission.
15. Cape observations suggest variability. Hβ probably washed out by emission The HD classification is Fo, Potsdam Bo: (F?).
18. Cape observations suggest variability. Hβ, ?γ, emission.
20. B type spectrum represented by diffuse He and winged H lines. Sharp Fe II lines and very strong sharp H cores may represent a shell spectrum. Mg II 4481 and perhaps He I were stronger in 1957 than in 1960.
31. Hβ, γ emission. Diffuse He probably present.
32. Hβ, γ emission.
37. Cape observations suggest variability. Hβ probably emission. Hγ sharp absorption core.
40. *S* component of double. Hβ, γ emission.
41. In cluster y Car. Potsdam classification as B2 may refer to CPD −59°3133.
44. EM Carinae. Eclipsing binary. Double lines appear on one available plate.
45. Potsdam classification (Bo) is erroneous. HDE gives F8.
49. Hβ emission.
54. GL Car. Eclipsing binary.
63. Hβ, ?γ, emission.
64. Potsdam 193/458, classified B2:, apparently refers to −60°2842; −60°2841, 1′ South of this star is type A.
66. Double Hβ emission.
70. Hβ weak, perhaps filled in by emission.
73. Double Hβ emission.
75. Strong Hβ, γ emission. ?Fe II emission, He I and ?O II absorption.
77. V 346 Cen eclipsing binary.
79. Potsdam classification Bo. No spectra available, but visual examination reveals a small cluster.
82. Double Hβ emission.
89. Hβ emission.
91. Hβ emission.
103. Weak Hβ emission on absorption.
114. Hβ emission.
132. Possibly composite and variable spectrum. Of two spectra one shows a sharp Hγ absorption core and suspected He II 4686 emission.
137. Also discussed by H. J. Smith. Harvard thesis, 1955, p. 133.
143. Hβ emission. Almost pure continuum.
149. Hβ, ?γ, emission.
151. Follows a supergiant M star in a small cluster.
157. Hβ emission is possibly variable.
173. −46°7948 coincides with 330587 as marked on HDE charts but the HD classification as Bo is wrong.
182. Hβ, γ emission on absorption.
183. H emission on broad absorption, He I fairly narrow.
184. Hβ, γ, δ emission on absorption.
190. Photometric data based on one measure of combined light of CZf 15489, 15490. The distance modulus is derived on the assumption of equality of the two stars.
191. CZf 15490. See 190 above.
198. Interstellar K strong. HD has Hβ suspected bright.
209. Peculiar emission line object. H, He I, Fe II, Mg II are main emission contributors. Ca II interstellar lines strong. He I 3888 has strong sharp central reversal (? shell). Spectrum suspected to be variable. A long series of plates to be discussed separately.
214. Hiltner (No. 657) gives: $V=10{\cdot}30$; $B-V=+0{\cdot}68$; $U-B=-0{\cdot}37$.
215. Hiltner (No. 660) gives $V=10{\cdot}24$; $B-V=+0{\cdot}92$; $U-B=-0{\cdot}14$.
216. Hiltner (No. 663) gives $V=10{\cdot}08$; $B-V=+0{\cdot}62$; $U-B=-0{\cdot}32$.

217. Hiltner (No. 664) gives $V=10{\cdot}41$; $B-V=+0{\cdot}72$; $U-B=-0{\cdot}14$.

219. Hiltner (No. 685) gives $V=9{\cdot}94$; $B-V=+0{\cdot}33$; $U-B=-0{\cdot}59$.

227. Hiltner (No. 736) gives $V=8{\cdot}90$; $B-V=+0{\cdot}96$; $U-B=-0{\cdot}05$.

248. Si II suspected to be present as well as Si IV. Si III not seen.

The number of observations per star has usually been three, and sometimes more. We find the following standard errors for the values of V, $B-V$, U_R-B_R:

$$\pm 0{\cdot}016;\ \pm 0{\cdot}011;\ \pm 0{\cdot}014.$$

The present list has six stars in common with Hiltner's list (**3**). We find for the average difference Radcliffe–Hiltner $-0{\cdot}03$ in V and $0{\cdot}00$ in $B-V$.

5. *Description of Table I.*—Table I presents the observations in the following form:

(1) Serial number.

(2) CPD number, when star is in $-19°$ zone or more southerly. BD number when star is north of $-19°$. Tonantzintla stars designated in the form T 13 *mn* where *n* is the Tonantzintla number on page *m* of Bulletin 13. In an isolated instance (No. 79) the Potsdam numbering in Selected Area 193 is given.

(3) HD number. Towards the end of the table this column alternatively gives the Tonantzintla numbering for CPD or BD stars too faint to appear in the HD catalogue.

(4), (5). Right ascension and declination for epoch 1900. These positions are based as far as possible on the CPD or CZf positions. It has been found at the telescope that some Tonantzintla positions are subject to errors, but no attempt has been made to correct these errors unless the star is also in one of the Cape catalogues.

(6), (7). Galactic longitude and latitude on the new system recommended by the I.A.U. (**10**). Most of these co-ordinates have been kindly computed at our request by Miss Torgard of the Lund Observatory, based on our 1900 positions. In a few cases the tabulated coordinates are based on our interpolated corrections to the Ohlsson (**11**) coordinates.

(8), (9) V, $B-V$ on the Johnson system converted from observations made with the 24-inch Cape refractor (1 to 103) or with the 74-inch Radcliffe reflector (142 to 248). Figures in italics (V, $B-V$) represent Cape photographic observations (**7**) converted to the Johnson system. Stars without such photoelectric or photographic observations have their HD photometric magnitudes entered *in brackets* in column (8).

(10) $(U-B)_C$ with the 24-inch Cape refractor (1 to 103) unconverted to the Johnson system. U_R-B_R (142 to 248) Radcliffe ultra-violet colours with silvered primary, unconverted to the Johnson system.

(11) Radcliffe spectral classification on the MK system.

(12) Computed distance moduli $V-A_v-M_v$, after correction for absorption ($A_v=3{\cdot}0\ E_{B-V}$); intrinsic colours and M_v as function of Spare taken from Johnson (**12**).

(13) R draws attention to a special remark at the end of the table.

6. *Distribution of distant B-type stars.*—In Fig. 1 are plotted O–B stars with distance moduli $(m_0 - M) \geq 12{\cdot}4$ (or $r > 3{\cdot}0$ kpc), projected on the galactic plane. Besides the stars of Table I we have plotted a few additional southern stars drawn from various sources (e.g. E. Smith (**13**) and photometric data by Morgan *et al.* (**14**) combined with Radcliffe spectral classifications). The northern stars are exclusively drawn from the extensive list of Hiltner (**3**).

These stars are, of course, very closely confined to the galactic plane. Four stars with $|b| > 6°$ are designated by open circles (lying between longitudes 330 and 10°). The very few other instances, falling in densely populated regions of the diagram, are not separately distinguished.

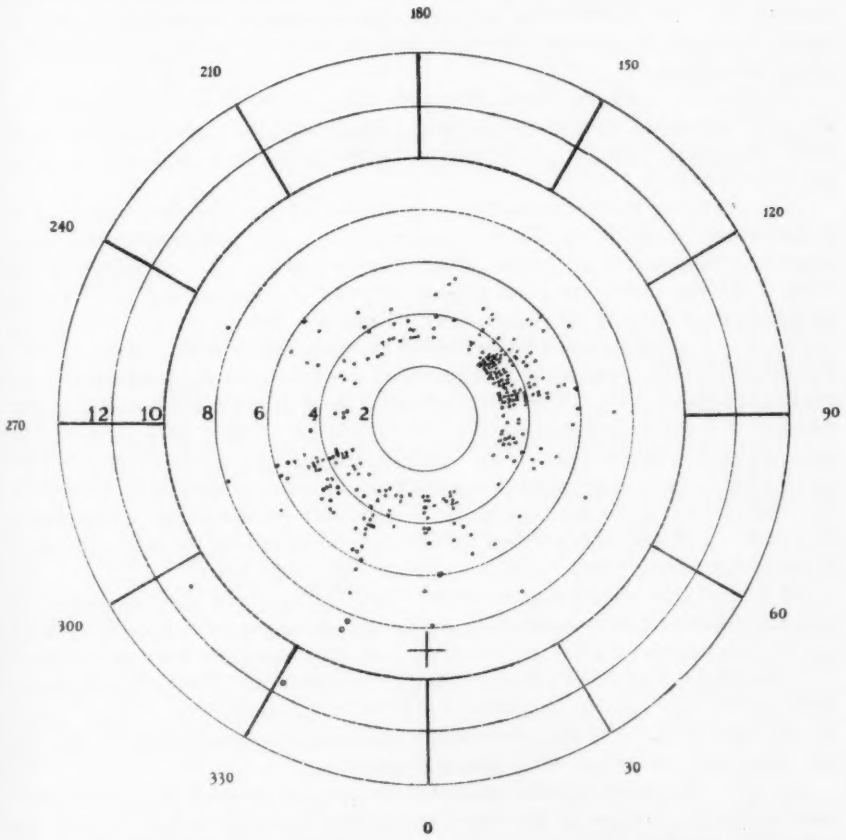

FIG. 1.—*Distribution of B stars in the galactic plane with computed distances greater than 3·0 kpc. Longitudes are on the new (III) system. The cross indicates roughly the location of the galactic centre* (**17**).

Owing to the patchy distribution in longitude of dense absorbing clouds, to selection effects and to inaccuracies of the distances it is not possible to draw any very firm conclusions regarding spiral structure from this figure. However, some interesting comparisons can be made with the 21 cm observations; reference

should be made to the combined north and south plot by Oort, Kerr and Westerhout (**15**).

(*a*) *The Perseus Arm.*—The very dense clustering of stars between 3 and 4 kpc and longitudes 97 and 137° is presumably associated with this arm (see Hiltner's discussion, p. 436 of (**3**)). It is interesting to note that this clustering lies at nearly twice the distance of Morgan's (**16**) string of associations but coincides fairly closely with a maximum of H I density according to the 21 cm observations. The Perseus arm appears to be of considerable thickness (nearly 2 kpc) in this direction. Morgan's approach is likely to select the nearest associations, which are easiest to detect and to measure, and thus to delineate the nearer edge of such an arm. On the other hand, our optical approach is likely to overestimate distances of the most distant stars, since the observations are necessarily limited by apparent magnitude and from the stars observed we are selecting those apparently most distant (**17**).

(*b*) *Carina-Centaurus-Norma* (*longitude* 286–340°).—It is well known that towards Carina and portions of Centaurus we observe numerous distant B stars and Cepheids. Further observations would doubtless add many more points in the figure.

The relatively heavy concentration of B stars with computed distances 4 to 6 kpc in the direction of Norma (longitudes 328–335°) is perhaps the most important outcome of the investigations of this paper. The 16^h region of the Cape Zone has shown far more supergiants than the corresponding 8^h region (with identical criteria for selection) in Table I. Moreover, the gap in the region $l^{II} = 314$–$328°$ cannot be attributed to lack of photometric data, for consultation of Table I will show that there are hardly any supergiants among the stars investigated here. The HD Catalogue itself shows a marked rise in the number of B stars when passing from $l^{II} = 320$–$330°$. Fig. 1 does seem to give some support to the idea that at $l^{II} = 328°$ we are suddenly beginning to view an inner spiral arm of the Galaxy tangentially. This has already been suggested by observations of double interstellar K (**18**) and by the 21 cm observations (**15**), (**19**). It is also noteworthy that the 3·5 m observations by Mills (**20**) show a more pronounced " step " at this longitude than at any other.

It is true that in the region of the " gap " (314–328°) there is a lane of obscuring clouds clearly visible on small-scale photographs of the Milky Way (and to the naked-eye), but the few distant B stars that have been investigated here have failed to show doubling of interstellar lines even though the separation expected for this galactic longitude should be easily detectable. The " gap " is well reflected in the 21 cm observations which are of course entirely freed from the difficulties associated with optical obscuration.

(*c*) It is of interest to point out that there are more stars in Fig. 1 with computed distances $\geqslant 5$ kpc in the inner hemisphere ($l^{II} = 270$ to 90°) than in the outer ($l^{II} = 90$–$270°$), despite the obvious fact that the latter has been far more intensively surveyed with northern telescopes. Actual counts give 31 such stars in the inner hemisphere, 17 in the outer.

(*d*) *The need for radial velocities.*—All the stars of Fig. 1 could be observed for radial velocity with large telescopes without undue difficulty. Many of those in Table I are in fact being currently observed at the Radcliffe Observatory. When one compares this figure with that showing distant B stars with known radial velocities (**17**) it will be obvious that motions of distant regions of the

Galaxy could be studied optically, and with great profit for comparison with the 21 cm observations. At the same time it is clear that much effort is needed to strengthen the accuracy of the stellar distances.

7. *Remark on the Tonantzintla OB stars.* We have identified 46 of the stars in Table I with stars classified as " OB " at Tonantzintla including 7 listed by L. Münch (**21**). In the majority of cases the Radcliffe slit spectra have confirmed this classification, when taken to indicate a star of type B2 or earlier. Only 8 out of the 46 have Radcliffe classifications B3 or later, and in 6 of these 8 the classifications are necessarily doubtful on account of diffuse lines.

On the other hand, these 46 stars contain only two stars with luminosity class I. The distribution among the MK classes (omitting three O6 to O8 stars without luminosity classes) is shown below:

Luminosity class	I	II	III	IV	V
Number of stars	2	3	17	1	20

8. *Acknowledgment.* We are deeply indebted to Dr I. H. M. Torgard of the Lund Observatory for her cooperation in supplying computed galactic coordinates (l^{II}, b^{II}) for most of our stars.

Radcliffe Observatory,
Pretoria:
1960 *October*.

Royal Observatory,
Cape.

References

(1) G. Gonzalez *et al.*, *Tonantzintla & Tacubaya Obs. Bull*, **13**, 3–18, 1955.
(2) F. Becker, *Potsdam Obs. Publ.*, Nos. 89, 90, 1930.
(3) W. Hiltner, *Ap. J. Supp.*, **2**, 389, 1956.
(4) M. W. Feast, A. D. Thackeray & A. J. Wesselink, *Mem. R.A.S.*, **68**, Pt. 1, 1957.
(5) R. H. Stoy, *M.N.A.S.S.A.*, **17**, 142, 1958.
(6) A. W. J. Cousins & R. H. Stoy, *M.N.A.S.S.A.*, **19**, 52, 69, 1960.
(7) *Cape Obs. Ann.*, **17** to **21**.
(8) M. W. Feast, A. D. Thackeray & A. J. Wesselink, *M.N.*, **121**, 387, 1960.
(9) *Cape Obs. Mimeograms*, Nos. 3 & 5.
(10) *Trans. I.A.U.*, **10**, 525, 531, 1958.
(11) J. Ohlsson, *Lund Obs. Ann.*, **3**, 1932.
(12) H. L. Johnson, *Lowell Obs. Bull.*, Nos. 90 & 91, 1958.
(13) E. Smith, *Harvard Thesis*, 1955.
(14) W. W. Morgan, A. D. Code & A. E. Whitford, *Ap. J. Suppt.*, **2**, 41, 1955.
(15) J. H. Oort, F. J. Kerr & G. Westerhout, *M.N.*, **118**, 382, 1958 (Plate 6).
(16) W. W. Morgan, A. E. Whitford & A. D. Code, *Ap. J.*, **118**, 318, 1953.
(17) M. W. Feast & A. D. Thackeray, *M.N.*, **118**, 125, 1958.
(18) A. D. Thackeray, *Nature* (*Lond.*), **178**, 1458, 1956.
(19) F. J. Kerr, J. V. Hindman & C. S. Gum, *Aust. J. Phys.*, **12**, 270, 1959.
(20) B. Y. Mills, *P.A.S.P.*, **71**, 267, 1959.
(21) L. Münch, *Ap. J.*, **113**, 309, 1951.

REDUCTION OF METEOR VELOCITIES FROM CONTINUOUS-WAVE RADIO RECORDS

D. W. R. McKinley and E. L. R. Webb

(Communicated by C. S. Beals)

(Received 1960 November 7)

Summary

Mainstone has suggested that there may be a large negative bias, averaging −5 per cent or more, in meteor velocities which are reduced from continuous-wave records of meteor diffraction echoes by means of the Ottawa velocity formula. An analysis of the particular reduction technique employed to reduce the Ottawa records shows that the statistical bias, if any, was positive, and was probably less than 1 per cent.

In a recent paper Mainstone (**1**) has examined some interesting aspects of the rather complicated records of radio diffraction echoes which are obtained from meteors when the continuous-wave or the coherent-pulse technique is employed. Mainstone has suggested that an indiscriminate application of the approximate velocity reduction formula (**2**), proposed by the Ottawa meteor group some time ago, could lead to appreciable errors and, more important, to systematic negative errors in the deduced velocities of the order of −5 per cent or more. It is true that our original paper (**2**) dealt at length with the results of the Ottawa observing programme, and it did not go very deeply into the actual reduction procedure. It is therefore understandable that Mainstone's conclusion, in so far as it can be presumed to apply to the Ottawa experiments, may have been based on our rather abbreviated account of this part of the work. The problems are not new—as far back as 1949 the Stanford workers (**3**) pointed out some of the pitfalls that await the unwary analyst of continuous-wave records—and both the Ottawa and the Stanford groups have developed practical methods to minimize the errors, though little seems to have been published on the mechanical details. In this paper we shall explain why we believe that the mean velocity errors in our method are neither as great as Mainstone suggests nor are they biased to yield low velocities.

The theoretical expression for the resultant received power, P_{r+d}, due both to the meteor echo and to the direct ground wave, was given in our earlier paper (**2**) in terms of the conventional Fresnel integrals, C and S, as follows,

$$P_{r+d}=(F_r C+F_d\cos\psi)^2+(F_r S-F_d\sin\psi)^2.$$

The parameters F_r and F_d have the dimensions of field strength; F_r refers to the wave reflected from the meteor and F_d to the direct wave received from the transmitter. The phase difference between the direct and reflected waves is $\psi=2\pi(2R_0-D)/\lambda$, where λ is the radio wavelength, D is the separation between transmitter and receiver, and $2R_0$ is the distance travelled by the reflected wave at

XUM

the time t_0 of closest approach of the meteor. The expression for P_{r+d} may be evaluated by means of tables of Fresnel integrals (the reader may find that the available tables are inadequate), or by a graphical method based on a drawing of Cornu's spiral. A third approach, which we shall follow here, is to substitute Cauchy's approximations for the Fresnel integrals. This yields two analytical expressions involving only ordinary algebraic and trigonometrical functions.

Before the t_0 point we have

$$P_{r+d}(-s) = \frac{F_r^2}{\pi^2 x^2} + F_d^2 + \frac{2F_r F_d}{\pi x} \sin\left(\frac{\pi x^2}{2} + \psi\right). \tag{1}$$

Here, $\pi x^2/2 = 2\pi s^2/R_0\lambda$, where the distance s is measured along the meteor path relative to the t_0 point and is negative prior to t_0. The approximations used are valid for $|x| > 1$, and the resultant analytical expressions are very precise representations for $|x| > 2$.

In equation (1) the absolute angle ψ is very large indeed and cannot be determined by the simple continuous-wave methods. However, since ψ appears in the equation as the argument of a trigonometric function which is cyclic with a period 2π, we may write $\psi = 0$ whenever $\psi = 2N\pi$, where N is a large but unknown integer, of the order 10^4 to 10^5. It is important to note that, to an extremely good approximation, the diffraction echo waveform for any given angle ψ is identical to each of those for $\psi \pm 2p\pi$, where the integer $p \ll N$.

After the t_0 point the echo power is defined by

$$P_{r+d}(+s) = \frac{F_r^2}{\pi^2 x^2} + E^2 + \frac{2EF_r}{\pi x} \sin\left\{\frac{\pi x^2}{2} - \tan^{-1}\left(\frac{F_r - F_d \sin\psi}{F_r + F_d \cos\psi}\right)\right\} \tag{2}$$

where

$$E^2 = F_d^2 - 2\sqrt{2}F_d F_r \sin\left(\psi - \frac{\pi}{4}\right) + 2F_r^2. \tag{3}$$

We may observe in passing that equation (3) shows there will be a translation up or down of the mean power level after t_0, relative to the power level F_d^2 prior to t_0. In particular, when $\psi = 0$ the post-t_0 level will be higher. Let $2F_r^2 = k^2 F_d^2$, where k is usually less than unity, though it may exceed unity for a few very strong echoes. As ψ increases from zero the post-t_0 level will cross the pre-t_0 level when $\sin(\psi - \pi/4) = k/2$. When $k = 1$ the translation occurs for values of ψ between $5\pi/12$ and $13\pi/12$, or in one-third of the cases (see Fig. 1). When $k < 1$, as it is for most echoes, the post-t_0 level will be lower for phase angles ranging between slightly greater than $\pi/4$ and slightly less than $5\pi/4$, that is in nearly half of the cases (see Fig. 2). It should be noted that the smaller the value of k the more closely the inverted waveform for $\psi \pm \pi$ approaches the waveform for ψ (see Fig. 2). If the records are transparencies or photographic negatives, one has only to turn over one record, rotating it about the time axis, and to look at it from the other side in order to match the other waveform.

The Ottawa formula for rapid reduction of the meteor velocity V is

$$V = \sqrt{R_0\lambda}\left(\frac{\sqrt{n} - \sqrt{m}}{\Delta t}\right) \tag{4}$$

where Δt is the time interval between the mth and the nth cycles, counting cycles backward in time form the t_0 point. When the quality of the record permitted we made the measurements not at the maxima or minima but at the cross-over points

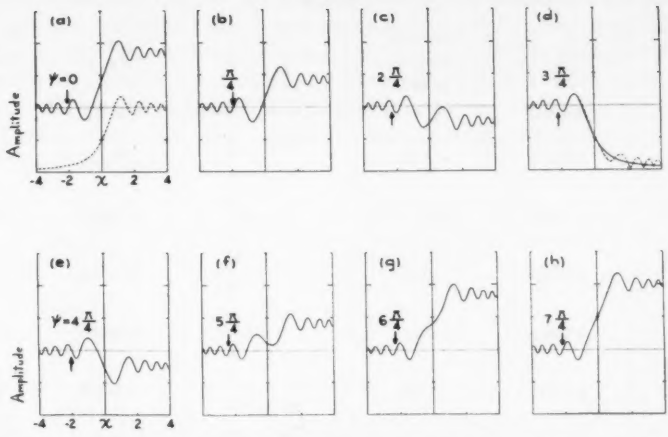

FIG. 1.—*Theoretical amplitude-time continuous-wave records of meteor echoes, plotted for* $k=1$. *The amplitude, or receiver output voltage, is proportional to* $P_{T+d}^{1/2}$. *The arrows indicate the zero-crossings selected to represent* $n=1$ *in the velocity formula.*

In (d) the solid curve is obtained only when $k=1$ *and* $\psi=3\pi/4$, *since* $E=0$ *for this case. Slight variations in either parameter will cause post-*t_0 *oscillations to appear—see the dashed curve in (d) for* $\psi=141°$.

The dashed curve in (a) represents the incoherent pulse radar case, which is independent of ψ.

where the slope is steepest and the measurements most accurate. (If the resolution of the record was poor, due to noise or interference, we measured Δt at the maxima—this will be considered later.) For $\psi=0$, the first complete cycle prior to t_0 is thus defined by the *second* downward crossing of the axis, as indicated by the arrow in Fig. 1 (*a*). In general, the x value which defines the nth complete cycle (see equation 1) is given by

$$\frac{\pi x_n^{\,2}}{2} \pm \psi = 2n\pi$$

$$x_n = \left(4n \mp \frac{2\psi}{\pi}\right)^{1/2}. \qquad (5)$$

To illustrate, we shall use the values $m=4$ and $n=9$, which were adopted for the bulk of the Ottawa observations in order to simplify the calculations. When $\psi=0$ in equation (5), we have $\nabla_{4,9}=x_9-x_4=6{\cdot}0000-4{\cdot}0000=2{\cdot}0000$, where we have adopted Mainstone's convenient symbol ∇. Since $x=2s/\sqrt{R_0\lambda}=2Vt/\sqrt{R_0\lambda}$, we have $\nabla_{4,9}=2V\Delta t_{4,9}/\sqrt{R_0\lambda}=2{\cdot}0000$; this, of course, is the same as the formula (4) and yields the correct value of V when $\psi=0$. When $\psi\neq 0$, the measured Δt (or ∇) will be too small or too large because, for convenience, we still measure Δt at the nearest zero-crossing points, whereas the points that should be used to define Δt will now be displaced from the zero-crossing points. (The displacement of a given point is very nearly proportional to $\psi/2\pi$ multiplied by the mean period at that point.) For example, when $\psi=\pi/4$, the zero-crossing value of $\nabla_{4,9}$ is $5{\cdot}9582-3{\cdot}9370=2{\cdot}0212$, and when $\psi=-\pi/4$, $\nabla_{4,9}=6{\cdot}0415-4{\cdot}0620=1{\cdot}9795$. Table I lists these readily-computed values of $\nabla_{4,9}$ for $\pm\pi/4$ increments in ψ. The same percentage error will appear in the calculated velocity, though with reversed sign (see Table I).

TABLE I

ψ	$\nabla_{4,9}$	Per cent velocity error	ψ	$\nabla_{4,9}$	Per cent velocity error
0	2·0000	0	0	2·0000	0
$\frac{\pi}{4}$	2·0212	−1·06	$-\frac{\pi}{4}$	1·9795	+1·03
$2\frac{\pi}{4}$	2·0431	−2·15	$-2\frac{\pi}{4}$	1·9597	+2·02
$3\frac{\pi}{4}$	2·0658	−3·28	$-3\frac{\pi}{4}$	1·9404	+2·98
$4\frac{\pi}{4}$	2·0893	−4·47	$-4\frac{\pi}{4}$	1·9218	+3·91
$5\frac{\pi}{4}$	2·1137	−5·68	$-5\frac{\pi}{4}$	1·9037	+4·82
$6\frac{\pi}{4}$	2·1390	−6·95	$-6\frac{\pi}{4}$	1·8861	+5·70
$7\frac{\pi}{4}$	2·1653	−8·27	$-7\frac{\pi}{4}$	1·8690	+6·55
$8\frac{\pi}{4}$	2·1928	−9·64	$-8\frac{\pi}{4}$	1·8524	+7·38

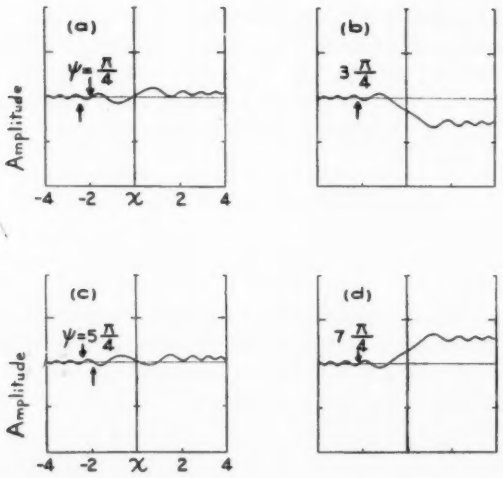

FIG. 2.—*Theoretical amplitude-time continuous-wave records of meteor echoes, plotted for* $k=0{\cdot}25$. *The arrows indicate the selection of* $n=1$. *The two arrows on* (*a*) *show the possible uncertainty which may result in practice in these particular cases.*

Mainstone suggests that the progressive error in V, as ψ increases, will follow a curve similar to the curve AB shown in Fig. 3—this is plotted directly from Table I for positive values of ψ. Note, however, that the waveform for $\psi=2\pi$ (or -2π) is identical to that for $\psi=0$. To get a velocity bias error of $-9{\cdot}64$ per cent at either $\psi=0$ or 2π our analyst would have to make the mistake of counting the zero-crossing

point which is marked with the arrow in Fig. 1 (*a*) as the *second*, not the first cycle. In effect, our analyst would have measured the interval $\nabla_{3,8}$ and used this value erroneously in the $\nabla_{4,9}$ formula. He could equally likely slip in the other direction and measure the interval $\nabla_{5,10}$, which would result in the bias curve shown as CD on Fig. 3. Misinterpretations like this can only be regarded as gross operator errors—fortunately rather rare. There is therefore no intrinsic bias error for $\psi = \pm 2\pi$ in our analysis.

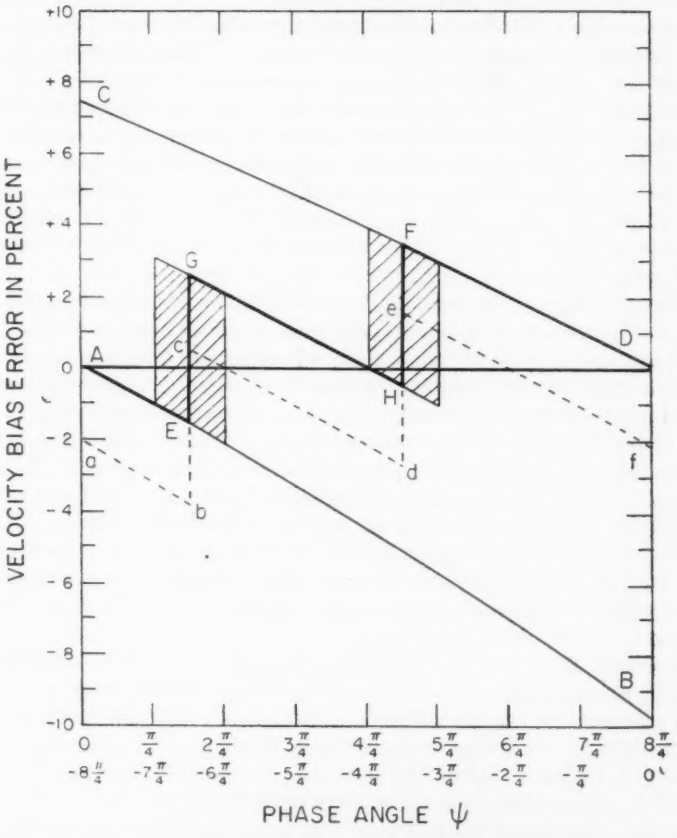

FIG. 3.—*The theoretical variation of the velocity bias error with the phase angle* ψ.

The waveforms for $\psi = \pi/4$, $6\pi/4$ and $7\pi/4$ differ only slightly from each other and from that for $\psi = 0$, and there is no difficulty in deciding which zero-crossing may best be used to represent $n = 1$ in the formula. These points are marked on Fig. 1 (*b*), (*g*) and (*h*) with downward arrows. There is now, however, an intrinsic velocity error in each case when the simple formula is applied directly. For $\psi = \pi/4$ the error is $-1{\cdot}06$ per cent, in agreement with Mainstone, but for $\psi = 7\pi/4$ the error is $+1{\cdot}03$ per cent, not $-8{\cdot}27$ per cent, since this case is identical

to $\psi = -\pi/4$, and the analyst will surely not have erred in his count by nearly one complete cycle. In Fig. 3 the segments of the curve AE and FD show the intrinsic bias errors over these particular ranges of ψ.

As ψ departs more and more from the value zero, the displacement of the zero-crossings becomes increasingly apparent, and in the neighbourhood of $\psi = \pm\pi$ it will amount to about one half-cycle. Fortunately, the depression of the post-t_0 signal level is a clear indication that the phase angle in these cases lies somewhere between $\pi/4$ and $5\pi/4$. The analyst was instructed to turn the waveform over (mentally) whenever the post-t_0 level was below the pre-t_0 level, and then to continue as before. See the upward-going arrows on Fig. 1 (*c*), (*d*) and (*e*) which denote the zero-crossings selected to represent $n = 1$. This procedure is equivalent to insertion of a phase shift of 180°, and results in the velocity formula yielding zero bias at $\psi = \pm\pi$. The complete error curve is therefore given by AEGHFD in Fig. 3. The hatched areas denote regions of uncertainty where the analyst may have had understandable difficulty in deciding whether or not to invert the waveform. We concede that in these regions he may make a mistake of one-half cycle but not one whole cycle, see Fig. 2 (*a*) and (*c*). The overall mean bias amounts to slightly less than + 1 per cent for the curve AEGHFD, including the areas of uncertainty.

Weak echo records, obscured by interference or excessive noise, were difficult to read at the zero-crossing points. In these cases we were forced to measure Δt between maxima. A given maximum is closer to t_0 by about one-quarter cycle than is the corresponding zero-crossing point. In effect, we measured $\nabla_{4-1/4,\,9-1/4}$ in these cases. Since $\nabla_{4-1/4,\,9-1/4}$ is always greater than $\nabla_{4,\,9}$ the resultant velocities will be lower, by approximately 2 per cent. The mean bias curve for these echoes measured at the maxima is shown as *abcdef* in Fig. 3. The overall mean bias error is just over − 1 per cent for this curve. It may be parenthetically noted that the mean theoretical bias is close to zero for the interval $\nabla_{4-1/8,\,9-1/8}$, as a direct consequence of the $\pi/4$ phase shift in equation (3). In practice, though, the points corresponding to this interval are more difficult to determine accurately than are either the zero-crossings or the maxima, and the resultant spread of individual velocities might be greater.

If we could have asserted that there were equal numbers of good records (measured at zero-crossings) and poor records (measured at maxima) in the original observations we could logically have concluded that the residual bias errors cancelled. After a lapse of ten years, though, we are unable to say with certainty what the ratio might have been. A re-examination of the notebooks does suggest that the number of good records outweighed the poor ones that were actually used by perhaps two to one. This would leave us with a small positive bias, probably less than + 0·5 per cent, in contrast to the − 5 per cent bias suggested by Mainstone. It happens that some of the conclusions of the original paper, regarding the incidence of hyperbolic velocities, would be strengthened, not weakened, by a *post hoc* reduction of the observed velocities, but a correction this small would be of little consequence, even if we were sure of the exact value to apply.

For the average meteor the period of the "body-Doppler" beat frequency due to radial wind drift is considerably longer than the time taken for the meteor to cross the first Fresnel zone. (The reader may refer to Fig. 3 of reference (2)—not reproduced here—which illustrates records of both the diffraction echo and the "body-Doppler" echo. Fig. 4 of reference (1) also shows this clearly.)

Therefore, most of the records show negligible distortion of the waveform in the vicinity of t_0, and there is usually no difficulty in assessing the value of ψ within limits of $\pm\pi/2$ or smaller. For the better specimens, ψ can be determined to within a few degrees. Only for slow meteors and strong radial winds does the "body-Doppler" effect interfere with the interpretation of the records. We concede that application of the simple velocity formula in these cases may yield unnecessarily large errors. It happened that interest in the original paper was focussed on the moderate to high velocity range, where radial wind drifts are not bothersome. The radial component of the wind does create a small velocity error owing to a phase shift of a few degrees between the Δt segment and the t_0 point. These errors should average out to zero during a statistical survey employing an omnidirectional antenna, as in the Ottawa programme, although they will naturally increase the spread of velocity errors. At the time the survey was conducted we did not have adequate wind-drift measuring equipment of a kind similar to the apparatus which has been used to good effect by Mainstone and others at Adelaide. The Ottawa continuous-wave records did yield the magnitude but not the sign of the wind drift, provided that the meteoric ionization lasted long enough to show a few cycles of "body-Doppler"—many echoes did not. Only in a few cases were we able to derive the direction of drift from the change of range of the radar echo. In general, the velocities were not corrected for wind drifts, but the corrections are small (as Mainstone pointed out) and their omission does not result in a systematic bias.

To sum up, we believe that the overall average error in the velocity measurements made on the Ottawa programme was about ± 5 per cent, as stated in the original paper. This included the reading error in measuring Δt, the two errors due to wind drift and to the finite displacement of transmitter and receiver which both average to zero in an omnidirectional system, the error in range measurement, and finally the error caused by applying the simple velocity formula which has been discussed at length above. We do not believe the reduced velocities contain any serious bias error—certainly not on the low side. Perhaps the best confirmation is the excellent agreement in the values obtained for the major meteor shower velocities by the Ottawa continuous-wave method, the Jodrell Bank radar method, and the Harvard photographic method. Some of these shower velocity reductions (**4**, **5**, **6**, **7**) were made from the basic Ottawa data long after the latter were published. If a bias of -5 per cent had been present in the Ottawa data it should have been quite evident. In this same connection it is of interest to refer to a summary comparison by Millman (**8**) of the Ottawa and the Jodrell Bank data (the latter obtained by the incoherent pulse radar method (**9**) which is independent of ψ). Not only are the mean velocities identical, but the two frequency distributions of velocities, when superposed, show a remarkable similarity in every aspect.

The simple velocity formula given by equation (4) is quite adequate for the rapid reduction of thousands of velocities in a statistical programme. Even when the 4th and 9th cycles only are used the resultant error is small in comparison with other errors of the observations. One can, of course, use the formula with higher values of m and n to attain more precision and less bias error, though the number of useable records will be fewer. However, we agree with Mainstone that the rapid reduction technique should not be employed when the velocities are to be used in orbital calculations. It would be a poor balance to spend only a few

minutes in obtaining an approximate velocity for a meteor when the radiant determination and other aspects of the data processing, not to mention the orbital calculation, may take many hours. Where great precision is required one should use all the information in the continuous-wave record, not just a two-point sample. We have developed more accurate measuring methods, and applied them in certain cases where we desired the best possible accuracy (**10**), but the procedures are naturally more tedious and time-consuming.

The continuous-wave method is capable of yielding more accurate velocities than the radar method, since a typical meteor will show several times more readable cycles prior to t_0 (by the continuous-wave or coherent-pulse radar method) than after t_0 (by the incoherent-pulse radar method). When corrected for wind drift, a correction that is equally applicable to the post-t_0 radar diffraction records, the continuous-wave records should produce velocities with accuracies not greatly inferior to the photographic methods. Incidentally wind drifts have little or no effect on velocities computed from meteor head-echo records, which are obtained with a high-resolution pulse radar (**10**). The echo from any point of the path is independent of the echoes from other points which differ in range by more than one-half of the pulse length. In this respect the head-echo and the photographic techniques are similar. Unfortunately, so far only the brighter meteors have produced acceptable head-echo records. Higher transmitter power will be needed to delineate the head-echoes from fainter meteors.

Up to the present the radio diffraction echo methods have utilized the diffraction echo only in the immediate vicinity of t_0, and have failed to tell us much about another very important parameter of the meteor, namely the deceleration the meteor has suffered prior to reaching the small segment of its path near t_0. (Approximate decelerations can sometimes be deduced by the head-echo method (**10**) but, to date, the number of suitable records has been few.) The observed velocity may be several per cent lower than the true no-atmosphere velocity, and until we can evaluate the deceleration accurately by radio methods it seems unrewarding to strive for a fractional percentage error in the observed velocity at one point only on the path. Fortunately, the deceleration problem is not insoluble, only more difficult, and current attacks on it appear quite promising.

Radio and Electrical Engineering Division,
National Research Council,
Ottawa 2,
Canada:
1960 *October* 19.

References

(1) J. S. Mainstone, *M.N.*, **120**, 517, 1960.
(2) D. W. R. McKinley, *Ap. J.*, **113**, 225, 1951.
(3) L. A. Manning, O. G. Villard and A. M. Peterson, *J. App. Phys.*, **20**, 475, 1949.
(4) B. A. Lindblad, *Trans. Chalmers Univ. Technol. Gottenburg*, No. 129, 1952.
(5) Peter M. Millman and D. W. R. McKinley, *J.R.A.S.C.*, **47**, 237, 1953.
(6) D. W. R. McKinley, *Ap. J.*, **119**, 519, 1954.
(7) D. W. R. McKinley, *Ap. J.*, **112**, 513, 1955.
(8) Peter M. Millman, *Science*, **120**, 325, 1954.
(9) J. G. Davies and C. D. Ellyett, *Phil. Mag. Ser.* 7, **40**, 614, 1949.
(10) D. W. R. McKinley, *J. App. Phys.*, **22**, 202, 1951.

THE GALAXIAN LUMINOSITY FUNCTION

T. Kiang

(Communicated by the Director of the University of London Observatory)

(Received 1960 November 18)

Summary

The discordant results reached by Hubble (1936 a) and Zwicky (1957) on the *form* of the galaxian luminosity function are shown to be due to observational selection. In a sample of some 600 *field galaxies*, regarded as coming from a selection according to the apparent magnitude, the distribution of the residuals from the redshift-magnitude relation is shown to be consistent with a luminosity function that varies as x^3 (the *cubic*) for $0 < x < 3$, and as $10^{0 \cdot 2x}$ (the *exponential*) for $2 \cdot 5 < x < 8$, x being the magnitude from the brightest limit M_0. The cubic law is also found to hold among *bright cluster galaxies* from analyses of "mean clusters" and on the magnitude differences among the 10 brightest members in each of 18 clusters; while the exponential law, originally suggested by Zwicky, is re-affirmed among *faint cluster galaxies*.

The limit M_0 is estimated to be $-22^{\mathrm{m}} \cdot 0 - 5 \log (H/100)$; the number of galaxies in the first 8 magnitudes of the luminosity range is estimated to be $0 \cdot 46\ (H/100)^3$ per cubic megaparsec; the light emission near 4300 A throughout the luminosity range is estimated to be the equivalent of $3 \cdot 7\ (H/100)$ galaxies of $M_{pg} = -15$ per cubic megaparsec, or $7 \cdot 6 \times 10^{-38}\ (H/100)$ ergs^{-1} cm^{-3}A^{-1}; the ubiquitous H being Hubble's constant in km/sec/Mpc. These density estimates are uncertain by $\pm 0 \cdot 15$ dex.

Introduction.—The present work was prompted by the wide divergence of results on the form of the luminosity function of galaxies. According to Hubble (1936a, b), the luminosity function is approximately a normal curve with a standard deviation of 0·85 mag., whereas according to Zwicky (1957) it is a monotonic function over the entire observed range (of some 7–8 magnitudes), increasing exponentially with decreasing luminosity. Hubble's data refer to the more or less isolated, relatively near "field galaxies", while Zwicky's data refer to the more distant clusters of galaxies. Does the difference in their results indicate then a real difference in the statistical make-up of these two classes of objects, or is there simply something wrong in the analyses?

Field Galaxies

Selectional bias in Hubble's data.—If the frequency distribution of absolute magnitudes M in a certain sample of galaxies is to be taken as the luminosity function, then we must see that the sample is a representative one from a certain volume of space. This follows from the definition of luminosity function. The question to be asked is then: do the samples analysed fulfil this condition? The answer is obviously "No" for Hubble's (1936 b) sample of redshifts. While the

selection of galaxies for redshift observation may have been subject to various criteria, it seems true to say that the overriding consideration must have been the apparent brightness. Accordingly, rather than equating the observed frequency distribution directly to the luminosity function, as did Hubble, we should equate it to the luminosity function times $\text{antilog}_{10}(-0{\cdot}6M)$. This would of course greatly alter the result. As for Hubble's (1936a) sample of *resolved* galaxies, selected mainly according to the apparent magnitude of the brightest member star, it appears at first sight that the sample does fulfil the condition of being a fair space-sample. (That the brightest stars have been shown to be mostly H II-regions (Sandage 1958) has no bearing on the statistical problem and we shall for convenience continue to refer to these as stars). However, there is good evidence that the luminosity of the brightest star in a galaxy is correlated with the total luminosity of the galaxy: the mean relation between the absolute magnitudes is, according to Hubble (1936a, p. 166), M (star) $= 0{\cdot}222\ M$ (galaxy) $- 2{\cdot}97$, or, according to Holmberg (1950, p. 41), $M(\text{star}) = 0{\cdot}60\,M(\text{galaxy}) + 2{\cdot}4$. Also, the collection of photographs from which Hubble took the sample was incomplete in the apparently faint galaxies (Hubble 1936a, p. 166). Both factors conspire to suggest that the less luminous galaxies were increasingly under-represented in the sample. For lack of more precise information these factors cannot be evaluated quantitatively at the present. The following re-determination was therefore based on redshift data only.

A re-determination of the luminosity function.—The catalogue of Humason and Mayall (1956), representing a five-fold increase in the number of measured redshifts over Hubble's original data, provides excellent material for a re-determination of the luminosity function of field galaxies. Under the fundamental assumption of an exact proportionality between distance and redshift (in other words, neglecting peculiar motions), the absolute magnitude M is given by

$$M = m - 5\log cz + 5\log H - 25 \qquad (1)$$

where m is the apparent magnitude, cz is the redshift in units of km/sec, and H is Hubble's constant in km/sec/Mpc. As far as the *form* of the luminosity function is concerned, a correct value of H is not essential, and we shall adopt $H = 100$. Then

$$M = m - 5\log cz - 15. \qquad (2)$$

From the above catalogue, galaxies in the Virgo Cluster (taken to be the rectangle $12^h\,8^m < \alpha < 12^h\,48^m$, $+2°{\cdot}5 < \delta < +18°{\cdot}5$) were excluded because of their well-known excessive peculiar motions; also excluded were those galaxies with observed red shifts less than + 100 km/sec (they are more or less synonymous with members of the Local Group within which the red shift-distance relation is known to fail). Galaxies fainter than 15th mag. or south of declination $-30°$ were further excluded to enhance the homogeneity of the data. 563 galaxies remained; these will be referred to as Data I. For each galaxy of Data I the right hand side of (2) was calculated. Values of cz (corrected for solar motion) were taken from the above catalogue. Apparent magnitudes were taken, in order of preference, from Holmberg (1957), Sandage (1956), de Vaucouleurs (1953) with a correction of $-0{\cdot}12$ mag. (de Vaucouleurs 1957), and Holmberg (1937) with a correction of $-0{\cdot}1$ mag., derived from a comparison with Sandage's values for galaxies common to both lists. Two corrections were made to the apparent magnitude. First the following correction for the *total* galactic obscuration: $0^m{\cdot}25\,\text{cosec}\,b$ for

$90° > b > 20°$, $0^m.73$ for $20° > b > 17°$, $0^m.21$ cosec b for $17° > b > 0°$, b being the galactic latitude taken without regard to sign. The coefficient for high-latitudes is the generally adopted value (Hubble 1934) and the smaller coefficient for low-latitudes was deemed appropriate because of an obvious selection effect (cf. Holmberg 1957, p. 58). The second correction was the reduction to zero inclination (i.e. the *differential* correction for internal obscuration) for spiral galaxies, and was made according to the mean curves given by Holmberg (1957, p. 43); the diameter ratios necessary for applying the correction were taken from the various catalogues listed by de Vaucouleurs (1959), with micrometric ratios converted into photometric ratios according to Holmberg's (1946) precepts. No correction for redshift (K-correction) was made, as it was generally small compared with the corrections for galactic obscuration and the inclination effect.

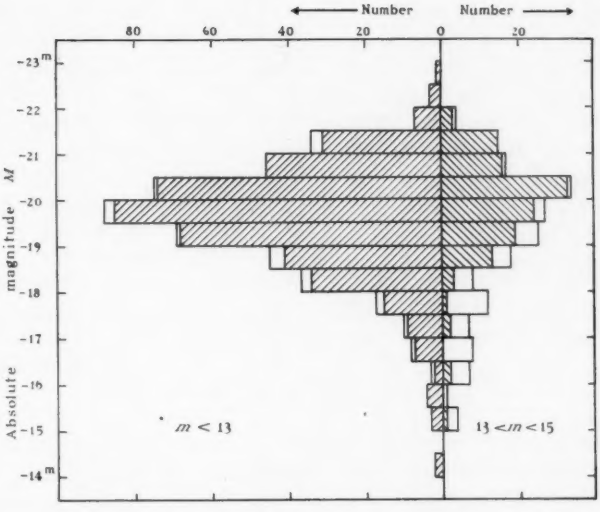

FIG. 1.—*Distributions of absolute magnitudes for* $m < 13$ *and* $13 < m < 15$ *separately. Filled part* ≡ *Data I; unfilled part* ≡ *Data II.*

For a general luminosity function to be meaningful, it should be independent of the distance, hence of m; and the independence is preserved in any sample selected according to m only. The values of M calculated above were examined in this regard, and it was found that the distribution of M for given m remained sensibly the same down to $m = 13$, while for $13 < m < 15$ there was a relative abundance of more luminous objects (Fig. 1, filled histograms). A similar phenomenon was observed before by Hubble (1936 b, p. 283) who attributed it to a tendency to select brighter members of small groups of faint galaxies. The unwelcome feature could be avoided by restricting the material to $m < 13$, but, since the accuracy of the final result depends very much on the sizes of the observed class frequencies and very little on the individual accuracy of the M-values, the following procedure was preferred. Those galaxies in Data I which belonged to known double or multiple systems in Holmberg's (1937) catalogue were singled out, and

the absolute magnitudes of their mates were estimated on the assumption that all the components of such systems have the same redshift. 75 galaxies brighter than the 15th mag. had their absolute magnitudes estimated this way; these will be referred to as Data II. As may be expected, compared with Data I, Data II showed a preponderance of (both apparently and intrinsically) faint galaxies (Fig. 1, unfilled histograms). If full weight were given to Data II then the trend which was to be avoided would reverse in direction; if half weight were given to Data II, then there would be no systematic trend one way or the other. (These statements can be made more precise in terms of standard statistical tests, which were performed.) The combination Data I + ½ Data II was adopted as the observed data n.

The errors in the individual M-values were compounded of the peculiar motions and the errors in the observed apparent magnitudes and in the corrections for galactic obscuration and inclination effect. The dispersion in the logarithm of the peculiar motion was estimated from 17 groups of galaxies having 3 or more members with known redshifts in the Humason–Mayall catalogue. It showed considerable variation with distance, but for the present purpose it was deemed sufficient to consider the straight mean of $\pm 0{\cdot}086$ (corresponding to $\pm 0{\cdot}43$ mag.). The standard errors of the apparent magnitudes from the four sources were $\pm 0{\cdot}05$ mag. for Holmberg (1957), $\pm 0{\cdot}18$ mag. for Sandage, $\pm 0{\cdot}30$ mag. for de Vaucouleurs and $\pm 0{\cdot}30$ mag. for Holmberg (1937). The standard error in the corrections for galactic obscuration and inclination was estimated to be somewhat under $\pm 0{\cdot}30$ mag. (cf. Holmberg 1957, Table 9). These led to an adopted mean standard error in M of $\pm 0{\cdot}57$ mag.

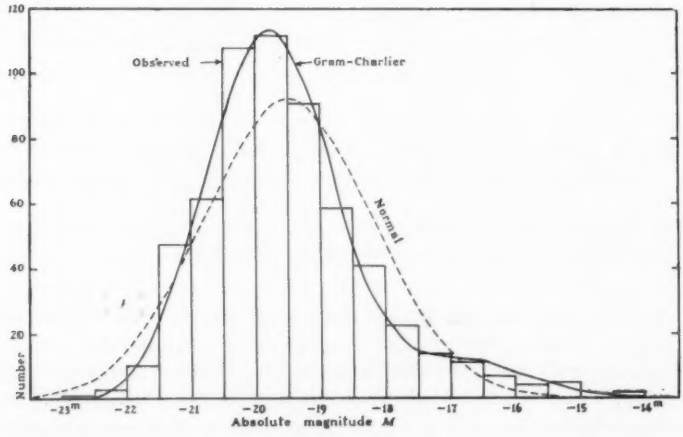

FIG. 2.—*Histogram shows the finally adopted observed frequencies n. Broken curve is the "best-fitting" normal curve; solid curve is the associated Gram-Charlier series (first 3 terms).*

Following Jeffreys's (1938) recommendation, a smooth curve was fitted to the observed frequencies before applying the correction for the standard error. It was found that the observed frequencies n could not be satisfactorily represented by a normal curve ($\chi^2 = 76{\cdot}5$ on 10 degrees of freedom !). An attempt was then made to represent n by a Gram–Charlier series (see Trumpler and Weaver 1953

pp. 24–27, 123), because of the ease with which the correction could be made if such a representation was feasible. It was then found that a good fit could be achieved by the first 3 terms of the series (see Fig. 2), i.e. by

$$\frac{\mathcal{N}}{\sigma}\{\Phi(t)+A_3\,\Phi^{\mathrm{III}}(t)+A_4\,\Phi^{\mathrm{IV}}(t)\} \tag{3}$$

where $\Phi(t)$ is the normal curve of the standardized variable $t=(M-\bar{M})/\sigma$, $\Phi^{\mathrm{III}}(t)$, $\Phi^{\mathrm{IV}}(t)$, its third and fourth derivatives, and the constants $\mathcal{N}$, $\bar{M}$, σ, A_3, A_4, calculated from the observed distribution, were:

$$\begin{aligned}\mathcal{N}&=600{\cdot}5=\text{total number}\\ \bar{M}&=-19^{\mathrm{m}}{\cdot}52\\ \sigma&=\pm 1^{\mathrm{m}}{\cdot}30\\ A_3&=-0{\cdot}9298/3\,!\\ A_4&=(4{\cdot}415-3)/4\,!\end{aligned} \tag{4}$$

To obtain the corrected frequencies n_0 it was only necessary to substitute in (3) for σ the corrected dispersion $\sigma_0=(1{\cdot}30^2-0{\cdot}57^2)^{1/2}$, both explicitly and implicitly through t, while retaining all other constants. This assumes that the error in M is at least approximately normally distributed, which is at variance with the view (Hubble 1936 b, p. 272) that the peculiar motions, and not their logarithms, are symmetrically distributed. However there does not seem to be much empirical evidence for this view: for example the distribution of the *logarithms* of the 25 measured redshifts in the Ursa Major Cloud shows no greater asymmetry than the distribution of the redshifts themselves.

The corrected frequencies n_0 (shown in Fig. 3) can now be compared with theoretical expectations. The present sample is taken to be selected with the apparent magnitude as the sole criterion, and the theoretical expectations are, therefore, of the form

$$\text{constant}\times 10^{-0{\cdot}6M}\times\phi(M)\,dM, \tag{5}$$

$\phi(M)$ being the luminosity function. Hubble's suggestion that $\phi(M)$ is a normal curve means that (5) is also a normal curve, but we have already seen that the fit of a normal curve to n was extremely poor, so the fit to n_0 would be somewhat poorer still. It may be noted that in Hubble's original distribution there was already a significant departure from normality, but the asymmetry had increased to such an extent in the present distribution as to render a normal curve for $\phi(M)$ altogether unlikely. On the other hand, with Zwicky's suggestion that

$$\phi(M)=\text{constant}\times 10^{0{\cdot}2M}, \tag{6}$$

(5) becomes constant $\times\,10^{-0{\cdot}4M}\,dM$. This is a monotonic, decreasing function of M, and obviously cannot fit the whole observed range either. In fact it proved to be not possible to achieve a good fit (as judged by χ^2) to the whole range by any *one* sufficiently simple formula. For the fainter 2/3 of the range, Zwicky's formula applies (Fig. 3). For the brightest 3 magnitudes a power law of the form

$$\phi(M)=\text{constant}\times(M-M_0)^j \tag{7}$$

with exponent j and an upper limit to luminosity M_0, was tried. (The many advantages of the power law will become manifest in the sequel.) As an indication

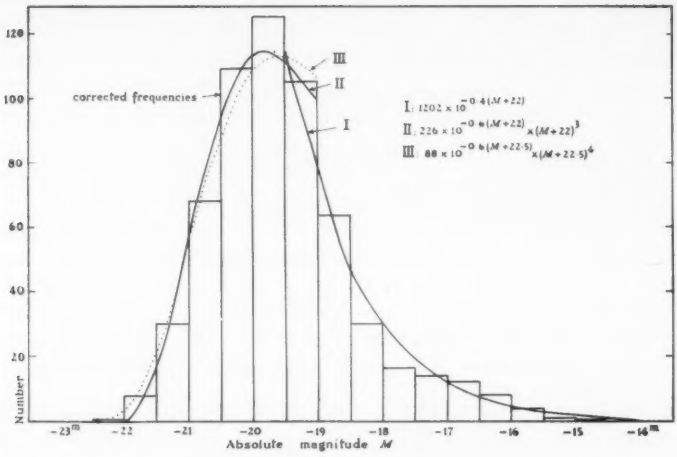

FIG. 3.—*The corrected frequencies n_0 (histogram) are seen to be consistent with the exponential law (curve I) for $M > -19{\cdot}5$, and with the cubic law (curve II) or the quartic law (curve III) for $M < -19{\cdot}0$.*

of the goodness of fit to the range $M < -19$ made by various combinations of M_0 and j, we have

TABLE I

Values of χ^2 on 5 degrees of freedom

$M_0 =$	$-22^{m}{\cdot}75$	$-22{\cdot}50$	$-22{\cdot}25$	$-22{\cdot}00$	$-21^{m}{\cdot}75$
$j=2$				91·8**	29·9**
$j=3$			26·0**	3·39	19·1**
$j=4$	29·5**	5·84	9·52	38·6**	

Here, as in the sequel, single and double asterisks will denote significance at 5 per cent and 1 per cent respectively. It appears that the combinations ($M_0 = -22{\cdot}0$, $j=3$) and ($M_0 = -22{\cdot}5$, $j=4$) each gives a satisfactory fit (Fig. 3).

The conclusion to be drawn from the present redetermination is that the form of the luminosity function for field galaxies is *not* a normal curve; it is representable by a power law (7) in the brighter portion ($M < -19$) and by Zwicky's exponential law (6) in the fainter portion ($M > -19{\cdot}5$).

CLUSTER GALAXIES

The exponential law, which Zwicky originally inferred from a study of 704 clusters, was seen to apply to the fainter portion, but not the brighter portion of the luminosity range among field galaxies. Possible selection effects in Zwicky's data will be discussed later; meanwhile other available data on bright galaxies in clusters will be analysed to see whether they, like their counterparts in the general field, also prefer the power law (7) to the exponential law (6).

The 10 brightest members.—Sandage (1956, p. 146) gave the apparent magnitudes m_r ($r = 1, 3, 5, 10$) of the rth brightest members in 18 clusters. We shall call the difference $m_s - m_r$ ($s > r$) the interval $[r, s]$; it is of course equal to the difference in *absolute* magnitude between the rth and the sth member. To

infer something about the luminosity function from the observed intervals, the following conceptual background $\mathscr{H}$ will be adopted. The n brightest members of a cluster are to be regarded as a random sample from a population conforming exactly to the power law (7), the sampling being done with replacement and restricted to a certain range R at the bright end. It is convenient to consider as variate

$$x = M - M_0. \tag{8}$$

The probability that a sampled value ξ will be less than x is then

$$P(\xi < x \,|\, \mathscr{H}) = (x/R)^k, \tag{9}$$

where k is related to j in (7):

$$k = j + 1. \tag{10}$$

Following Pearson (1932), who examined the statistics of ranked individuals in great detail, we shall put

$$(x/R)^k = \alpha(x), \tag{11}$$

then the probability that the rth rank in a sample of n will be found in an interval $d\alpha_r$ is

$$P(d\alpha_r \,|\, nR\mathscr{H}) = \frac{n!}{(r-1)!\,(n-r)!}\,\alpha_r^{r-1}(1-\alpha_r)^{n-r}\,d\alpha_r, \tag{12}$$

and the joint probability that the rth rank will be in $d\alpha_r$ and the sth rank in $d\alpha_s$ is, $s > r$.

$$P(d\alpha_r d\alpha_s \,|\, nR\mathscr{H}) = \frac{n!}{(r-1)!\,(s-r-1)!\,(n-s)!}\,\alpha_r^{r-1}(\alpha_s - \alpha_r)^{s-r-1} \times (1-\alpha_s)^{n-s}\,d\alpha_r\,d\alpha_s. \tag{13}$$

From these the formulae (Pearson's formulae lxxxvi, lxxxvii, lxxxix, p. 240) for the expectations of the rth rank, of its square, and of the product of the rth and the sth rank follow:

$$\langle x_r \rangle = R\left\{\left(1 + \frac{1}{n}\frac{1}{k}\right)\left(1 + \frac{1}{n-1}\frac{1}{k}\right)\cdots\left(1 + \frac{1}{r}\frac{1}{k}\right)\right\}^{-1}, \tag{14}$$

$$\langle x_r^2 \rangle = R^2\left\{\left(1 + \frac{1}{n}\frac{2}{k}\right)\left(1 + \frac{1}{n-1}\frac{2}{k}\right)\cdots\left(1 + \frac{1}{r}\frac{2}{k}\right)\right\}^{-1}, \tag{15}$$

$$\langle x_r x_s \rangle = R^2\left\{\left(1 + \frac{1}{n}\frac{2}{k}\right)\left(1 + \frac{1}{n-1}\frac{2}{k}\right)\cdots\left(1 + \frac{1}{s}\frac{2}{k}\right)\right\}^{-1}\left\{\left(1 + \frac{1}{s-1}\frac{1}{k}\right) \times \left(1 + \frac{1}{s-2}\frac{1}{k}\right)\cdots\left(1 + \frac{1}{r}\frac{1}{k}\right)\right\}^{-1}. \tag{16}$$

Formula (14) shows that the ratio $\langle x_s \rangle : \langle x_r \rangle$ is a function of s, r and k only, hence the ratio of the expectations of any two intervals $\langle x_s - x_r \rangle : \langle x_q - x_p \rangle$ is also independent of n. These ratios can therefore be calculated for a given k with any convenient value of n, and then compared with observed ratios. For the latter, mean values must be used, and the question of the spread in richness arises, for, as is obvious from (14), $\langle x_s - x_r \rangle$ decreases as n increases. Sandage's clusters were therefore segregated according to richness groups, as given in Abell's (1957) catalogue. The data were supplemented with estimates made from Shapley's (1933) observations on southern clusters. No significant differences were found

between Sandage's mean intervals and Shapley's mean intervals for the same richness groups, nor were there any significant differences among the richness groups 0, 1, 2, while 5 very rich clusters (of groups 3–5) on Shapley's list had significantly smaller intervals. The richness groups 0, 1, 2, were then pooled together and the overall means calculated. These values are shown in Table II (column O), followed by their standard errors e (calculated from observed dispersion), followed by the number ν of intervals used in calculating the mean (the first number refers to Sandage's data, independent photographic and photometric measurements being counted separately; the second number refers to Shapley's data).

TABLE II

Interval	Observed			Calculated ($k=4$)			
	O m	e m	ν	$\langle x_s - x_r \rangle$	C m	ϵ m	χ^2
[1, 3]	0·473	0·051	24+15	0·204 R	0·505	0·048	0·45
[3, 5]	0·312	0·033	24+15	0·107 R	0·264	0·027	3·06
[5, 10]	0·389	0·034	20+15	0·163 R	0·404	0·028	0·29
[1, 10]	1·171	0·071	20+15	0·474 R	1·173		3·80

The intervals [1, 3], [3, 5], [5, 10], were then compared with theoretical expectations calculated from (14) with $n=10$ for $k=2(1)7$. Sample calculation for $k=4$ is shown. The theoretical values $\langle x_s - x_r \rangle$ in units of R were normalized so as to have the observed sum of 1·173 mag. (column C). χ^2 were then calculated with standard errors ϵ given by

$$\epsilon = \frac{C}{\nu^{1/2}} \frac{\sigma_{rs}}{\langle x_s - x_r \rangle}, \tag{17}$$

where σ_{rs} is the standard error of unit weight of the interval $[r, s]$ on $\mathscr{H}$, i.e. given by

$$\sigma_{rs}^2 = \langle x_s^2 \rangle - 2\langle x_r x_s \rangle + \langle x_r^2 \rangle - \langle x_s - x_r \rangle^2, \tag{18}$$

the right hand terms having been calculated according to (14), (15), (16) with $n=10$. The ratio $\sigma_{rs}: \langle x_s - x_r \rangle$ can be shown to be quite insensitive to n, the adoption of a particular value of n in the calculation of ϵ should cause no misgivings. The results are as follows:

$k=j+1=$	2	3	4	5	6	7
χ^2 on 2 d.f. $=$	17·3**	5·09	3·80	4·43	5·60	6·96*

(19)

From this it appears that the observed intervals among the brightest galaxies in clusters are consistent with the luminosity function being a power law with exponent (j) between 2 and 5, the preferred value being 3.

The zero-points (values of M_0) corresponding to the several powers will now be sought. This can be done by evaluating, on one hand, $\langle x_r \rangle$ from the observed intervals, and on the other, the mean absolute magnitude $\bar{M}_r$ of the rth brightest member from (2). A comparison between the dispersions in M_r and x_r also offers some hope of restricting our choice of the exponent. Clearly the first rank ($r=1$) is the best for this purpose.

In evaluating $\langle x_r \rangle$ only the interval [1, 10] will be used because of all the mutually independent intervals it is the best determined by observations. It

follows from (14) that the ratio $\langle x_r \rangle : \langle x_{10} - x_1 \rangle$ is independent of n, and we have, from the previous calculation for $k = 4$ (and $n = 10$),

$$\begin{aligned} \langle x_1 \rangle &= 0{\cdot}502\, R \pm 28{\cdot}0 \text{ per cent} \\ \langle x_3 \rangle &= 0{\cdot}706\, R \pm 14{\cdot}9 \text{ per cent} \\ \langle x_5 \rangle &= 0{\cdot}813\, R \pm 11{\cdot}1 \text{ per cent} \\ \langle x_{10} \rangle &= 0{\cdot}976\, R \pm 7{\cdot}7 \text{ per cent} \\ \langle x_{10} - x_1 \rangle &= 0{\cdot}474\, R \pm 28{\cdot}5 \text{ per cent.} \end{aligned} \tag{20}$$

The fractional errors of x_r,

$$\frac{\sigma_r}{\langle x_r \rangle} = \frac{\{\langle x_r^2 \rangle - \langle x_r \rangle^2\}^{1/2}}{\langle x_r \rangle},$$

given in (20), however, were calculated from (14), (15) with $n = 100$. The reason is that they become insensitive to n only when n is as large as about 100, especially the one with $r = 10$. The fractional error in the *interval* [1, 10], being as already mentioned, insensitive to n, was taken directly from the previous calculation. The observed mean interval [1, 10] is (Table II) 1·171 mag., the mean being taken over 35 values. Equating it to the expected value, we have

$$R = 2{\cdot}47 \text{ mag.} \pm 4{\cdot}8 \text{ per cent},$$

and hence,

$$\begin{aligned} \langle x_1 \rangle &= 1^{\mathrm{m}}{\cdot}24 \pm 0^{\mathrm{m}}{\cdot}35 \\ \langle x_3 \rangle &= 1{\cdot}74 \pm 0{\cdot}27 \\ \langle x_5 \rangle &= 2{\cdot}01 \pm 0{\cdot}24 \\ \langle x_{10} \rangle &= 2{\cdot}41 \pm 0{\cdot}22. \end{aligned} \tag{21}$$

These values were calculated for $k = 4$. The variation of $\langle x_r \rangle$ with k was found to follow approximately the following rule:

$$\langle x_r \rangle_{k+1} = \langle x_r \rangle_k + 0^{\mathrm{m}}{\cdot}41, \quad k = 3, 4, 5. \tag{22}$$

That the variation was independent of r was to be expected since the differences $\langle x_3 \rangle - \langle x_1 \rangle$ say, for all these values of k must be mutually comparable, each being comparable to the mean observed interval [1, 3].

To evaluate $\bar{M}_1$, the photographic magnitudes of the brightest galaxies in 13 clusters given by Sandage (1956, p. 146) were used. Each of these magnitudes, after corrections for *total* galactic obscuration (= the listed *differential* correction augmented by 0·25 mag.) and redshift (= the listed K-correction), was entered together with the listed redshift in the right hand side of (2). The resulting values of M_1 were found to have the following mean and standard deviation (unbiassed estimate).

$$\begin{aligned} \bar{M}_1 &= -21^{\mathrm{m}}{\cdot}18 \pm 0^{\mathrm{m}}{\cdot}12 \\ \sigma &= \pm 0^{\mathrm{m}}{\cdot}43. \end{aligned} \tag{23}$$

The dispersion is compounded of the measuring error in the magnitude ($\sim 0{\cdot}18$ mag.), of negligible errors in the redshift measurement, and negligible effect due to random motions, of errors in the two corrections (estimated to be about 0·20–0·25 mag.) and the sampling error s, which will be about 0·29–0·33 mag., after deducting the foregoing from the observed value. On the other hand the standard error σ_1 of x_1 can be calculated in the model $\mathscr{H}$. For $k = 2(1)7$ the ratios $\sigma_1 : \langle x_1 \rangle$ were calculated for $n = 100$, and then using (21) and (22), it was found that

$k = j + 1 =$	2	3	4	5	6	7
$\sigma_1 =$	$0^{\mathrm{m}}{\cdot}21$	0·29	0·35	0·38	0·41	0·45

(24)

It appears that, of the four values of j which were found to be consistent with the observed ratios of intervals, the dispersion in M_1 rather favours the smallest two ($j=2, 3$).

If $j=3$, ($k=4$), then (21) and (25) will combine to place M_0 at $-22{\cdot}4$ mag.; if $j=2$, then M_0 will be at $-22{\cdot}0$ mag. Comparing this with results shown in Table I, it appears that, if we impose the same zero-point on both field and cluster galaxies, then the exponent must differ by 1, while if we impose the same exponent 3, the zero-points will differ by 0·4 mag. The latter procedure leads to a somewhat more convenient description, and will be adopted. The difference could have resulted if the 10 brightest members in these clusters were generally brighter than the corresponding true averages by a few tenths of a magnitude, and this contingency is not unlikely in view of the almost unavoidable tendency of including richer-than-average clusters containing brighter-than-average members in a sample selected for redshift observations (cf. Scott 1957).

Mean clusters.—The cubic law $\phi(M)\propto(M-M_0)^3$ was seen in the last section to apply to the range occupied by the ten brightest members of a cluster. How much further does its applicability extend? To answer this question a fuller use was made of Shapley's (1933) data, together with the observed luminosity functions of 5 clusters given by Abell (1957, p. 220), and those for the Virgo Cluster by Shapley and Ames (1929), and for the Coma Cluster by Hubble and Humason (1931). The combined data were first segregated according to Abell's richness groups, and "lined-up" at the third brightest member. Mean luminosity functions were formed for the groups 0, 1, and separately for the group 2. These are shown in Table III; the numbers of clusters used in forming the means are shown in brackets.

TABLE III

Mean luminosity function

$m-m_3$	Richness groups	
m	0 and 1	2
<0·8	12·6 (14)	21·7 (7)
0·8–1·6	17·1 (14)	47·4 (7)
1·6–2·4	28·9 (7)	90·6 (5)
2·4–3·2	35·0 (3)	56·5 (4)

Simple calculations will show that the cubic law applies to the first three frequencies in each case. Since, from (21), $\langle x_3\rangle=1{\cdot}74$ mag., this means that the cubic law applies to a range of $1{\cdot}74+2{\cdot}40=4{\cdot}14$ mag. among cluster galaxies.

Cubic law versus exponential law.—Because of its particular form the exponential law (6) is not amenable to the same sort of tests that have been performed on the power law (7). So, instead of examining whether the observations on the bright galaxies in clusters are consistent with the exponential law, we shall consider the question whether the observations are of sufficient size to distinguish between the cubic law and the exponential law. The cubic law was seen to apply to the first 4 magnitudes, within which range a cluster of richness group 0 or 1 may have about 60 members, and a cluster of richness group 2 may have 130 members (cf. Table III). Let us then consider a cluster with 100 members in its brightest 4 magnitudes. In this case the expected frequencies in successive

magnitudes are 1, 6, 25, 68, on the cubic law, and 11, 17, 28, 44, on the exponential law. The two runs are so different that it does not seem possible to have an observational run consistent with them both. It is therefore inferred that the observations on the bright galaxies in clusters do in fact reject the exponential law.

Exponential law for faint cluster galaxies.—The conclusion just reached says nothing about the applicability of the exponential law among *faint* cluster galaxies. On this point, rather surprisingly, misgivings were expressed by Zwicky (p. 174), originator of the law. Zwicky inferred the law from the observation that the mean number of discernible galaxies per cluster for a given angular diameter γ of the cluster varied approximately linearly with γ, (the fundamental assumption being that all clusters are alike), and his misgivings arose from the fact that there were large deviations from the linear relation at large values of γ.

It will now be shown that there is really no ground for the misgivings. Deviations have significance only when they are compared with standard errors, and the standard errors corresponding to these large deviations were themselves very large. This is shown in Table IV. In constructing the table, Zwicky's data given on p. 172 of *Morphological Astronomy* were combined into intervals of 0·5 in 5 log γ. The successive columns show, for each interval, the mean diameter $\bar{\gamma}$, the number of clusters ν, the mean number of galaxies per cluster $\bar{N}$,

TABLE IV

$\bar{\gamma}$	ν	$\bar{N}$	ϵ	χ	χ_1	$\Delta \log N$
2·2	4	21	0·50	+34	+38	0·04
3·3	20	29	0·22	+73	+86	0·43
4·5	14	34	1·75	+ 5·7	+ 8·0	0·26
5·6	27	44	2·76	+ 3·6	+ 5·4	0·53
6·7	42	47	2·38	+ 1·3	+ 3·8	0·41
8·4	79	·58	1·63	− 0·6	+ 4·3	0·57
10·6	81	74	2·97	− 1·7	+ 2·4	0·73
13·3	111	93	2·27	− 4·4	+ 1·3	0·46
16·8	96	118	3·19	− 5·0	0·0	0·75
20·9	88	153	4·53	− 4·0	+ 0·4	0·57
26·5	64	194	11·0	− 2·5	− 0·2	0·98
33·5	30	243	15·8	− 2·5	− 0·6	0·68
42·3	27	351	30·3	− 0·4	+ 1·0	0·69
53·4	11	333	45·8	− 2·8	− 1·7	0·79
69·3	5	890	218·0	+ 1·3	+ 1·6	0·63
81·7	5	664	129·0	− 0·3	+ 0·2	0·48

the standard error ϵ in $\bar{N}$, ($\epsilon = s/(\nu-1)^{1/2}$, s being the observed root-mean-square deviation), and the ratio $\chi = (\bar{N} - N_0) : \epsilon$, N_0 being the number expected according to Zwicky's straight line (his eqn. 136).

$$N_0 = 8{\cdot}93(\gamma - 1{\cdot}79), \quad \gamma \text{ in minutes of arc.} \tag{25}$$

We note that the χ-values for large γ are actually among the least. Taken as a whole the χ-values are generally too large (even if we ignore the two enormous values at the small end of γ) and the run of the sign too systematic for (25) to be considered as a good fit to the observations. Now it is known (Zwicky p. 169)

that the data are increasingly incomplete with diminishing γ, appreciable incompleteness setting in at about $\gamma = 15'$. For $\gamma > 15'$, the points follow a somewhat different line:

$$N_1 = 8{\cdot}0(\gamma - 2{\cdot}0), \quad \gamma \text{ in minutes of arc,} \tag{26}$$

The residuals from (26), divided by ϵ, are the values χ_1 shown, from which it appears that (26) in fact fits the observations well down to $\gamma = 10'$. This in turn reaffirms that the exponential law (6) holds for cluster galaxies fainter than the limiting luminosity corresponding to $\gamma = 10'$.

The correspondence between the limiting luminosity and γ can be established using clusters with both diameter measurements and photometric data on members of known ranks. Of the 54 clusters described on pp. 160–1 in *Morphological Astronomy*, 20 can be found in Abell's (1958) catalogue. Fig. 4 shows a plot of 5 log γ (from Zwicky) against m_{10} (from Abell) for these 20 clusters; the solid line is the mean relation

$$m_{10} + 5 \log \gamma = 24{\cdot}13. \tag{27}$$

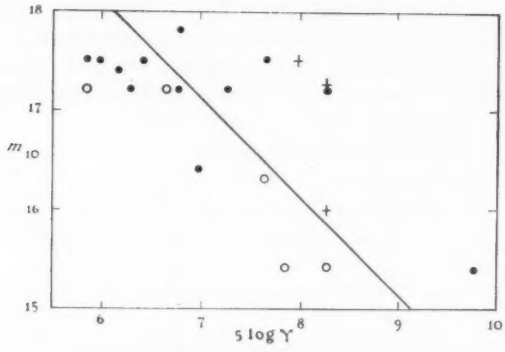

FIG. 4.—*Abscissa is 5 log γ, γ being the angular diameter in minutes of arc; ordinate is the apparent magnitude of the tenth brightest member.*

Clusters of richness groups, 2, 1, 0, are shown respectively as crosses, dots and circles. Diagram suggests a positive correlation between richness and linear diameter. The large scatter can only be accounted for by an appreciable spread in the linear diameter and/or large measuring error of γ.

Let x correspond to the limiting absolute magnitude. Then

$$x - x_{10} = m_l - m_{10}, \tag{28}$$

where m_l is the limiting apparent magnitude. The descriptions given in the book indicate that the plate on which Zwicky found those clusters was taken with the same instrumentation as Palomar Sky Survey plates, for which Abell (p. 214) quotes a limiting magnitude of 20·0. Putting in (28) this value for m_l, the expected value of x_{10} as given in (21), and taking account of (27), we arrive finally at the required relation:

$$x = 5 \log \gamma - 1{\cdot}7. \tag{29}$$

Accordingly we conclude that the exponential law holds for $3^{m}{\cdot}3 < x < 8^{m}{\cdot}1$ (corresponding to $10' < \gamma < 90'$) among cluster galaxies. This result is not affected by selectional bias which, as will be shown in the following section, is important only for $\gamma < 10'$ or so.

XUM

Selectional bias in Zwicky's data.—Two factors will be considered which probably have produced bias in Zwicky's data. The first factor is associated with the phenomenon of segregation. It was repeatedly pointed out by Zwicky (1957) that the ratio of bright-to-faint members invariably decreases outwards from the centre of a cluster. This means that the diameter of a cluster as defined by its bright members is smaller than the diameter as defined by its faint members. From the information given (Zwicky 1957, pp. 157 and 169) regarding the observational procedures it appears that clusters with *less* than 50 recognizable members in Zwicky's data were probably affected by the phenomenon, while those with *more* than 50 recognizable members were not, because the measured diameters for the latter objects apparently refer to members within a standard range of luminosity (3 magnitudes from the brightest member). Zwicky's Table XLIV (p. 172) shows that clusters with *less* than 50 recognizable members begin to be included in the data at $\gamma = 11'{\cdot}2$ and become increasingly common with diminishing γ. The effect produced is that a unit interval in the observed 5 log γ would correspond to less than a unit interval in the limiting absolute magnitude. The following consideration suggests that this is indeed the case: the range in γ in which the data are incomplete is at least as wide as from $\gamma = 15'$ to $\gamma = 2'{\cdot}2$, corresponding to a range of at least 4 in 5 log γ, but a range of 4 magnitudes of incompleteness on plates taken with every effort to uniformity seems quite unlikely.

The second factor is suggested by a joint consideration of the incompleteness of data already mentioned, and the observed dispersion in N for given γ. The dispersions in N in small intervals of γ, as recorded by Zwicky (p. 172) are much larger than their natural uncertainties (of the order of $N^{1/2}$), and should presumably be attributed to an intrinsic spread in the linear diameters and measuring errors of γ, (these, and these only, would also account for the large scatter about the mean relation in Fig. 4). Now for any reasonable luminosity function the increase of log N with magnitude is always steeper at the bright end (the small end in γ) than at fainter parts, any dispersion in log N arising from the above cause should therefore not be smaller for small γ than for large γ. However the observed range $\Delta \log N$ (shown in Table III) betrays a general decrease with decreasing γ (the decrease is the more convincing when the varying number of clusters in each interval is taken into consideration). The decrease rather significantly starts at about the same place when the data become appreciably incomplete. The incomplete data are thus also biassed in the sense that only part of the true spread in log N is represented. It seems natural to suppose that the observed portion comprises the richer part of the spread.

The probable existence of these factors has now been demonstrated. Both produce spurious effects in the same sense. At present any corrections we might make for these factors would be more or less arbitrary. We are therefore forced to admit that Zwicky's data for small clusters ($\gamma < 10'$ or so) cannot be reliably used at present for the determination of the luminosity function

Conclusions

The form of the galaxian luminosity function.—The several results obtained in this paper on the form of the galaxian luminosity function will now be summarized, and it is convenient to do so in terms of x, the absolute magnitude counted from

the brightest limit M_0. It has been shown that the observed frequencies in a sample of some 600 *field galaxies* (the sample being regarded as resulting from a selection according to the apparent magnitude) are consistent with a luminosity function that varies as x^3 for $0{\cdot}0 < x < 3{\cdot}0$, and as $\text{antilog}_{10}(0{\cdot}2\,x)$ for $2{\cdot}5 < x < 8{\cdot}0$. The cubic law was then found to hold also among *cluster galaxies* for $0{\cdot}0 < x < 4{\cdot}1$ from analyses on the 10 brightest members in each of 18 clusters and on "mean clusters". The exponential law was re-affirmed for clusters observed by Zwicky with apparent diameter γ in the range $10' < \gamma < 90'$ corresponding to $3{\cdot}3 < x < 8{\cdot}1$. Thus it appears that different observations relating to the field galaxies on the one hand and cluster galaxies on the other are all consistent with *one and the same form* of luminosity function The difference between Hubble's and Zwicky's results, referred to at the beginning of the paper, is due to the neglect of selectional effects. These are the main conclusions of the present investigation.

With the cubic law reigning in the brighter portion and the exponential law in the fainter portion, the point of demarcation will now be fixed by the condition that the two laws give the same value at the junction. If this point is taken to be at $x = 2{\cdot}5$, then the above condition requires that, for a sample selected according to the apparent magnitude, the numbers in the ranges $0 < x < 2{\cdot}5$ and $2{\cdot}5 < x < 8{\cdot}0$ should be in the ratio of 747 : 533 (see (32)), which is quite close to the observed ratio of 340 : 257 in our corrected data n_0 of field galaxies.

We shall therefore adopt

$$\begin{aligned} \phi(M) &= ax^3 && \text{for} \quad 0{\cdot}0 < x < 2{\cdot}5 \\ &= a\,.\,10^{0{\cdot}2x}\,(2{\cdot}5^3/10^{0{\cdot}5}) && \text{for} \quad 2{\cdot}5 < x < 8{\cdot}0 \\ x &= M - M_0 \end{aligned} \tag{30}$$

as the final form of the galaxian luminosity fuction, a being an adjustable constant.

Number of galaxies per cubic megaparsec and space density of photographic emission.—As Hubble's constant H will enter in all our absolute values, these will be calculated for $H = 100$ km/sec/Mpc. Their dependence on H will be shown explicitly in the final presentation (Fig. 5).

Recall first that, if the cubic law is adopted, then the observations on the field galaxies require

$$M_0 = -22^{\text{m}}{\cdot}0, \tag{31}$$

(see Table I). We shall now evaluate the constant a in (30). The number of galaxies with apparent magnitudes brighter than m and absolute magnitudes in the range $0 < x < 8$ is, according to (30).

$$a\,.\,\frac{4\pi}{3}\,.\,10^{-15+0{\cdot}6m-0{\cdot}6M_0}\left(\int_0^{2{\cdot}5} x^3\,10^{-0{\cdot}6x}\,dx + \frac{2{\cdot}5^3}{10^{0{\cdot}5}}\int_{2{\cdot}5}^{8{\cdot}0} 10^{-0{\cdot}4x}\,dx\right)$$

$$= a\,.\,\frac{4\pi}{3}\,.\,10^{-15+0{\cdot}6m-0{\cdot}6M_0}\,(0{\cdot}747 + 0{\cdot}533) \tag{32}$$

if a is in $\text{Mpc}^{-3}\,\text{mag}^{-1}$. On the observational side, the frequency distribution of m' (= observed apparent magnitude corrected for inclination in case of a spiral galaxy) in our sample of redshifts (Data I) indicates that the sample is complete down to $m' = 11{\cdot}0$, (incidentally, the brightest galaxy in Data II has $m' = 11{\cdot}3$), and there are 119 galaxies with $m' < 11{\cdot}0$. Of these, 59, 34, 26, respectively are situated in the zones $+90° > \delta > +30°$, $+30° > \delta > 0°$, $0° > \delta > -30°$; this well known anisotropy will contribute an uncertainty of $\pm 0{\cdot}15$ dex in our numerical

estimates. Correction will now be made for the effect of galactic obscuration. For this purpose Hubble's (1934) reduced count of galaxies ($\log \overline{N}$ in his Table 1) were used to form $\overline{N}$, the mean number for a given latitude b, and a cosecant relation fitted to $\log \overline{N}$, with the result: $\log \overline{N} = \text{constant} - 0{\cdot}164 \operatorname{cosec} b$. All Hubble's survey fields except the one at $b = +50°$, $l = 10°$, were used in a least-square solution. The correction factor is, accordingly,

$$\left\{\int_0^{\pi/2} 10^{-0{\cdot}164 \operatorname{cosec} b} \cos b \, db\right\}^{-1} = 2{\cdot}47. \tag{33}$$

The sky coverage is 3/4. The number of galaxies in the entire sky which would appear brighter than the 11th magnitude (inclination effect being allowed for) if there were no galactic obscuration is therefore $119 \times 2{\cdot}47 \times 4/3 = 391$. Equating this to (32), with $m = 11{\cdot}0$, and M_0 as given by (31), we have

$$a = 10^{-2{\cdot}94} \text{ Mpc}^{-3} \text{ mag}^{-1}. \tag{34}$$

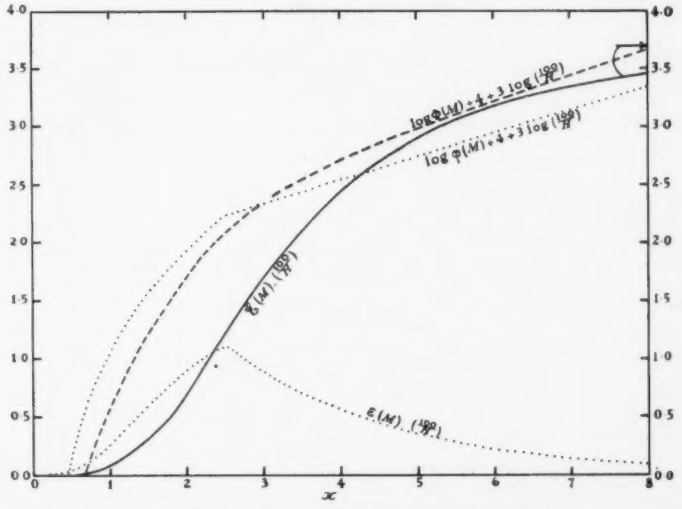

FIG. 5.—*Showing the variation with absolute magnitude M of:* (i) $\phi(M)$ = *number of galaxies per unit of absolute magnitude per cubic megaparsec;* (ii) $\Phi(M)$ = *number of galaxies brighter than M in one cubic megaparsec;* (iii) $\epsilon(M)$ = *photographic emission per unit of absolute magnitude per cubic megaparsec; and* (iv) $\mathscr{E}(M)$ = *photographic emission of all galaxies brighter than M in one cubic megaparsec.* $\epsilon(M)$ *and* $\mathscr{E}(M)$ *are expressed as number of galaxies of* $M_{pg} = -15$.
Abscissa $x = M - 22{\cdot}0 + 5 \log (100/H)$. *H is Hubble's constant in km/sec/Mpc.*

Integrating (30) with this value of a, we have the following estimates for space densities of galaxies:

$$\begin{aligned} &0{\cdot}011 \text{ Mpc}^{-3} \text{ in the range } 0 < x < 2{\cdot}5 \\ &0{\cdot}45 \text{ Mpc}^{-3} \text{ in the range } 2{\cdot}5 < x < 8{\cdot}0 \\ \text{giving} \quad &0{\cdot}46 \text{ Mpc}^{-3} \text{ in the range } 0 < x < 8{\cdot}0. \end{aligned} \tag{35}$$

The luminosity function $\phi(M)$, given by (30) and (34), and its integral $\Phi(M)$ over all magnitudes brighter than M, are shown in *logarithmic* form in Fig. 5. The space density of photographic emission $\epsilon(M)$ corresponding to $\phi(M)$, expressed as number of galaxies with $M_{pg} = -15$ per cubic megaparsec per

magnitude, and *its* integral $\mathscr{E}(M)$ over all magnitudes brighter than M are also shown. Their dependence on Hubble's constant H is made explicit, which is to be expressed in km/sec/Mpc. The relation between M, H, and the abscissa x is

$$M = x - 22{\cdot}0 + 5 \log \frac{H}{100}. \tag{36}$$

The asymptotic value of $\mathscr{E}(M)$, indicated by an arrow in Fig. 5, is

$$3{\cdot}7 \times \frac{H}{100}\ \mathrm{Mpc}^{-3} \quad \text{"galaxies of } M_{pg} = -15\text{"}, \tag{37}$$

or

$$7{\cdot}6 \times 10^{-36} \times \frac{H}{100}\ \mathrm{erg\ s^{-1}\ cm^{-3}\ A^{-1}} \text{ near } 4300\,\mathrm{A}, \tag{38}$$

using constants given by Allen (1955). Also, taking account of the dependence on H, (35) now reads: there are

$$0{\cdot}46 \times \left(\frac{H}{100}\right)^3 \text{ galaxies in the range } 0 < x < 8 \text{ per cubic megaparsec.} \tag{39}$$

The estimates (37), (38), (39), as all values of $\phi(M)$, $\Phi(M)$, $\epsilon(M)$, $\mathscr{E}(M)$, read from Fig. 5, are uncertain by $\pm 0{\cdot}15$ dex due to the already mentioned uncertainty in the evaluation of a. The value (37) differs from Oort's (1958) estimate of the space density of luminosity by just the stated uncertainty.

University of London Observatory,
Mill Hill Park,
London, N.W.7:
1960 *November.*

References

Abell, G. O., 1957, *Ap. J. Suppl.*, **3**, 211.
Allen, C. W., 1955, *Astrophysical Quantities*, The Athlone Press, p. 174.
Holmberg, E., 1937, *Lund Annals*, no. 6.
——1946, *Lund Medd.* II, no. 117.
—— 1950, *Lund Medd.* II, no. 128.
—— 1957, *Lund Medd.* II, no. 136.
Hubble, E., 1934, *Ap. J.*, **79**, 8.
—— 1936 a, *Ap. J.*, **84**, 158.
—— 1936 b, *Ap. J.*, **84**, 270.
Hubble, E., and Humason, M. L., 1931, *Ap. J.*, **74**, 67.
Humason, M. L., and Mayall, N. U., 1956, *A.J.*, **61**, 97.
Jeffreys, H., 1938, *M.N.*, **98**, 190.
Oort, J. H., 1958, Solvay Report, Bruxelles, p. 180.
Pearson, K., 1932, *Biometrika*, **24**, 240.
Sandage, A. R., 1956, *A.J.*, **61**, 155.
—— 1958, *Ap. J.*, **127**, 522.
Scott, Elizabeth, L., 1957, *A.J.*, **62**, 248.
Shapley, H., 1933, *Harvard Reprint* I, no. 92.
Shapley, H., and Ames, Adelaide, 1929, *Harvard Bull*, no. 865.
Trumpler, R. J., and Weaver, H. F., 1953, *Statistical Astronomy, Univ. Calif. Press*, pp. 24–27, 123.
de Vaucouleurs, G., 1953, "*A Revision of Harvard Survey of Bright Galaxies*", *Australian Nat. Univ. Mimeograph*, Canberra.
—— 1957, *Ann. Obs. Houga*, **2**, fasc. 1, 43.
—— 1959, *A.J.*, **64**, 400.
Zwicky, F., 1957, *Morphological Astronomy*, Springer, pp. 166–176, 222–228.